



TAMPEREEN TEKNILLINEN YLIOPISTO  
TAMPERE UNIVERSITY OF TECHNOLOGY  
*Julkaisu 762 • Publication 762*

Antti-Jussi Romppanen

## **Inverse Load Sensing Method for Line Load Determination of Beam-Like Structures**



Tampereen teknillinen yliopisto. Julkaisu 762  
Tampere University of Technology. Publication 762

Antti-Jussi Romppanen

## **Inverse Load Sensing Method for Line Load Determination of Beam-Like Structures**

Thesis for the degree of Doctor of Technology to be presented with due permission for public examination and criticism in Festia Building, Auditorium Pieni Sali 1, at Tampere University of Technology, on the 31st of October 2008, at 12 noon.

Tampereen teknillinen yliopisto - Tampere University of Technology  
Tampere 2008

ISBN 978-952-15-2053-2 (printed)  
ISBN 978-952-15-2379-3 (PDF)  
ISSN 1459-2045

## **Abstract**

In this thesis, an inverse load sensing method is developed and investigated. Accordingly, it is found that strain measurements of a beam-like structure can be utilized in order to solve the actuating line load distribution. The feasibility of the method, especially for rotating beams is evaluated.

The main applications of the method are in paper manufacturing processes, in which the paper web is pressed between rotating rolls and a line load distribution is created in the cross direction of the contact zone. The line load is particularly important, since it controls the surface properties of the paper, and is typically very difficult to measure accurately. In the contact zone, not only the paper, but also the rolls, are significantly influenced by the line load and experience considerable bending and flattening deformations. Thus, based on measurement of the strain of one of the rolls, the proposed method could be used to determine the governing line load distribution. Furthermore, the method could also be applied to other types of beam-like structures, for which the loading has to be determined.

The strain-force relationship of the given structure is described by an influence coefficient matrix, which is formed by means of an appropriate unit load procedure. Since the loading input of the structure is determined on the basis of the strain response it produces, the proposed method is inverse. As is often the case in inverse problems, the system equations are found to be ill-posed, therefore, small errors in the measured input cause large deviations in the solution. Thus, the quality of the solution is improved by introducing a suitable regularization technique.

The feasibility of the inverse load sensing method is first verified in two experimental cases of static point forces acting on beam-like structures. Then, two different approaches and the applicability of the method are evaluated with a purely computational analysis of a case, in which the line load distribution acts on a static beam-like roll structure. Finally, the feasibility of the method is tested on a real dynamic application of a pilot roll press. Strain gages are installed onto the inner surfaces of one of the rolls to give the needed strain data during a run. With appropriate conditions and adaptations, the proposed load sensing method can be utilized. The results were promising, although the implementation of the method should be carefully evaluated according to the requirements of the application.



## Preface

The work presented in this study was carried out in the Department of Mechanics and Design at Tampere University of Technology during 2003-2008. The research was initiated and done for the most parts in the projects funded by the Technology Development Agency TEKES, which is gratefully acknowledged. I am also grateful to the Paper Manufacturing Graduate School for accepting me to the PhD program as a graduate school student and funding the work, as well as for the support of the Graduate School of Concurrent Engineering. My thanks are also due to the research partners of the TEKES projects, Metso Corporation and ABB. Financial support of the Finnish Foundation for Technology Promotion and the Foundation of Walter Ahlström are also gratefully acknowledged.

I wish to express my gratitude to Professor Erno Keskinen for the inspiration and guidance for this study. I want to thank him for the encouragement and support during the work, and especially for helping to create a flexible and productive working environment during the latter stages of writing the manuscript. I would also like to thank Docent Juha Miettinen for his effort and participation as well as motivation and important advice during the work. I am grateful to Mr. Pekka Salmenperä for his help with the measurements, and for Dr. Veli-Matti Järvenpää for his advice concerning the computational procedures. In addition, my warmest thanks go to the staff of the Department of Mechanics and Design for having a nice and supportive working environment.

The assessors of the manuscript, Professor Gary Marquis from the Helsinki University of Technology, and Professor Uwe Hanebeck from the University of Karlsruhe, are kindly acknowledged for their valuable comments to improve the manuscript. I am also grateful to Professor Robert Hildebrand, for revising the language of the manuscript.

I wish to express my warmest gratitude to my dear wife for the love, support, patience and understanding during the course of the work. Finally, the steady support and encouragement from my family, especially my parents, has been helpful and important during the work.

Turku, October 2008  
Antti-Jussi Romppanen

# Contents

<b>Abstract</b> .....	<b>i</b>
<b>Preface</b> .....	<b>iii</b>
<b>Contents</b> .....	<b>iv</b>
<b>Nomenclature</b> .....	<b>vi</b>
<b>1. Introduction</b> .....	<b>1</b>
1.1 Background and motivation .....	1
1.2 Inverse problems in general .....	3
1.3 Approaches for the inverse load sensing method .....	5
1.3.1 Influence coefficients and FEM .....	5
1.3.2 Applications of the influence coefficient method .....	7
1.3.3 Force identification .....	9
1.4 Other interesting inverse problems .....	11
1.5 Objective and scope of the study .....	11
1.5.1 Scope of the study .....	12
1.5.2 Initial assumptions .....	12
1.6 Contributions of the thesis .....	12
<b>2. Description of the operational environment</b> .....	<b>13</b>
2.1 The problem environment: rolls and roll pair applications in paper machines .....	13
2.1.1 Surface sizing using film size press .....	13
2.1.2 Calendering .....	14
2.1.3 Techniques for controlling the CD nip load .....	15
2.2 The pilot roll press .....	19
2.2.1 The rolls and the loading mechanism .....	20
2.2.2 The roll drives .....	21
<b>3. Inverse load sensing method and formulation</b> .....	<b>24</b>
3.1 The Formulation of ICM .....	24
3.2 FEM and ICM .....	28
3.2.1 The Mathematical connection of FEM and ICM .....	29
3.2.2 Using FEM as an external tool .....	31
3.2.3 Discussion about forward solution .....	32
3.3 Errors in the solution .....	33
3.3.1 Modelling and measurement error .....	33
3.3.2 Errors in the inverse procedure .....	34
3.3.3 Handling of the error .....	34
3.4 Inverse problems: ill-conditioning and regularization .....	34
3.4.1 Regularization .....	35
3.4.2 The regularization parameter $\delta$ .....	37
3.4.3 The effect of matrices D and H .....	39
3.4.4 Inverse crime .....	40

3.5 Determination of influence coefficients of a roll structure.....	41
3.5.1 Unit point force approach.....	42
3.5.2 Unit loading function approach.....	43
<b>4. Dynamics of a flexible rotor.....</b>	<b>46</b>
4.1 Equations of motion for a flexible continuous rotor.....	46
4.2 Solving the equations of motion for typical loading cases.....	50
4.2.1 Response to gravity.....	51
4.2.2 Response to unbalance force.....	52
4.2.3 Response to lateral line loading.....	53
4.2.4 Other components affecting the deformations in rotation.....	54
4.3 Balancing of flexible rotors.....	55
<b>5. Analysis of the accuracy and sensitivity issues of the inverse load sensing method 58</b>	
5.1 Preliminary analysis of the strain set-up and the unit point force cases.....	58
5.2 Preliminary analysis of the unit loading function cases.....	64
5.3 Considerations on strain.....	66
5.3.1 Strain calculation of FEM.....	66
5.3.2 Mapping of strain.....	67
<b>6. Analysis of the inverse load sensing method in different static loading cases .....</b>	<b>69</b>
6.1 Using inverse load sensing method for solving point forces on beam-like structures ..	69
6.1.1 Case study 1, a simply supported prismatic beam.....	69
6.1.2 Case study 2, a tubular roll structure.....	73
6.2 Using inverse load sensing method for solving distributed loading profile on a roll structure.....	76
6.2.1 Analysis of the method when unit point force approach is used.....	76
6.2.2 Analysis of the method when unit loading function approach is used.....	89
<b>7. Analysis of the inverse load sensing method in a dynamic case, case study: pilot roll press .....</b>	<b>95</b>
7.1 Strain measurements of the pilot roll press.....	95
7.1.1 Dynamical considerations.....	95
7.1.2 Adapting the measurements.....	98
7.2 Calculating the loading profile based on strain measurements.....	99
7.2.1 Results when unit point force approach is used.....	99
7.2.2 Reference results from the nip paper measurements.....	103
<b>8. Conclusions .....</b>	<b>105</b>
<b>9. References .....</b>	<b>108</b>



## Nomenclature

$\mathbf{A}, \mathbf{A}(t)$	Transformation matrix between fixed and rotating coordinates
$A$	Area
$a$	A dimension of the roll structure
$\mathbf{B}$	Strain-displacement matrix of the displacement method
$\mathbf{B}_f$	Strain-displacement matrix of the force method
$\mathbf{C}$	Damping matrix
$c$	Damping
$\mathbf{D}$	Linearization matrix
$\mathbf{D}_0$	Zeroth-order linearization matrix
$\mathbf{D}_I$	First order linearization matrix
$d_5, d_{10}, \dots$	Length of a line load segment on which unit point forces act
$E$	Young's modulus
$\mathbf{F}$	Loading vector
$\mathbf{F}_g$	Gravitational force vector
$\mathbf{F}_q$	Line loading vector
$\mathbf{F}_{ub}$	Unbalance force vector
$F_{\text{bearing}}$	Equivalent bearing loading
$F_i$	Unit point force
$F_i$	Generalized loading components (Lagrange)
$F_X(t), F_Y(t)$	Force component
$\mathbf{f}$	Loading vector
$\tilde{\mathbf{f}}$	Vector containing loading case factors
$\mathbf{f}_{calc}$	Calculated load
$\mathbf{f}_e$	Loading vector in the element level
$\mathbf{f}_{orig}$	Original known load
$\mathbf{f}^*$	Typical loading vector according to <i>a priori</i> knowledge
$\mathbf{f}_\delta$	Regularized loading vector
$f_i$	Loading factors, unit loading functions
$\mathbf{G}$	Gyroscopic matrix
$\mathbf{g}$	Gyroscopic matrix (2)
$g$	Gravity

<b>H</b>	Positive definite matrix
<b>H<sub>0</sub></b>	Positive definite matrix in the case of zeroth-order linearization
<i>I<sub>d</sub></i>	Diametrical moment of rotor (roll)
<i>I<sub>p</sub></i>	Polar moment of rotor (roll)
<i>I<sub>z</sub></i>	Second moment of area (cross section)
<b>K</b>	Stiffness matrix
<b>K<sub>f</sub></b>	Flexibility matrix
<b>k<sub>e</sub></b>	Stiffness matrix of an element
<b>k<sub>fe</sub></b>	Flexibility matrix of an element
<i>k</i>	Number of eigenfunctions
<i>k<sub>ω</sub></i>	Number of rotational speeds in rotor balancing procedure
<i>L</i>	Length of the roll shell
<i>L<sub>X</sub>, L<sub>Y</sub>, L<sub>Z</sub></i>	Angular moment of rotor (roll)
<b>M</b>	Mass matrix
<b>M<sub>tr</sub></b>	Mass matrix, translational degrees-of-freedom
<b>M<sub>rot</sub></b>	Mass matrix, rotational degrees-of-freedom
<i>M<sub>GYRO</sub></i>	Gyroscopic moment
<i>M<sub>RI</sub></i>	Rotary inertia
<i>M<sub>b</sub>, M<sub>X</sub>, M<sub>Y</sub></i>	Bending moment of a beam
<i>m</i>	Number of measurement points
<i>m̂</i>	Trial mass
<b>N</b>	Transformation matrix of modal/principal coordinates
<b>n</b>	Basis function vector
<i>n<sub>i</sub>(ξ)</i>	Basis function
<i>n</i>	Number of loading factors
<b>P</b>	Orthogonal projection matrix
<b>Q</b>	General loading vector in modal/principal coordinates
<b>Q<sub>g</sub></b>	Gravitational force vector in modal/principal coordinates
<b>Q<sub>q</sub></b>	Line loading vector in modal/principal coordinates
<b>Q<sub>ub</sub></b>	Unbalance force vector in modal/principal coordinates
<i>q(x), q(z)</i>	Line loading
<i>q<sub>X</sub>(z), q<sub>Y</sub>(z)</i>	Line loading in the X-direction and Y-direction respectively
<i>q<sub>i</sub></i>	General coordinate (Lagrange)
<i>R</i>	Outer radius of roll

$\mathbf{r}$	Local position vector of rotor (roll)
$r$	Inner radius of roll
$\mathbf{S}$	Translation displacement vector of bending in fixed coordinate reference
$\mathbf{S}_g$	Translation displacement caused by gravity in fixed coordinate reference
$\mathbf{S}_q$	Translation displacement caused by line loading in fixed coordinate reference
$\mathbf{S}_{ub}$	Measured displacements caused by initial unbalance in fixed coordinate reference
$\mathbf{s}$	Translation displacement vector of bending in rotating coordinate reference
$\mathbf{s}_{ub}$	Translation displacement caused by unbalance in rotating coordinate reference
$T, T_{tr}, T_{rot}$	Kinetic energy, translational and rotational respectively
$t$	Time
$\mathbf{U}$	Displacement vector
$U$	Translation displacement of bending in fixed coordinate reference in the X-direction
$U_{pot}$	Potential energy
$\mathbf{u}$	Local displacement vector of an element
$u$	Translation displacement of bending in rotating coordinate reference in the x-direction
$V$	Translation displacement of bending in fixed coordinate reference in the Y-direction
$V_X, V_Y$	Shear force of a beam
$v$	Translation displacement of bending in rotating coordinate reference in the y-direction
$\mathbf{W}$	Weighting matrix
$w$	Deflection of a beam
$\mathbf{X}$	General displacement vector in modal coordinates
$\mathbf{X}_g$	General displacement caused by gravity in modal coordinates
$\mathbf{X}_{ub}$	General displacement caused by initial unbalance in modal coordinates
$X$	Direction in the fixed coordinate system
$x$	Direction in the rotating coordinate system
$x_s$	Coordinate on the axial/cross direction of roll shell
$Y$	Direction in the fixed coordinate system
$y$	Direction in the rotating coordinate system

$\mathbf{Z}$	The influence coefficient matrix, the system matrix
$\tilde{\mathbf{Z}}$	The system matrix in the stacked form of regularization
$\mathbf{Z}_e$	The influence coefficient matrix in the element level
$\mathbf{Z}_{5A}, \mathbf{Z}_{10A}, \dots$	Influence coefficient matrices determined from axial strains
$\mathbf{Z}_{5B}, \mathbf{Z}_{10B}, \dots$	Influence coefficient matrices determined from axial and tangential strains
$\mathbf{Z}_X$	Trial weight relation in the X-direction
$\mathbf{Z}_Y$	Trial weight relation in the Y-direction
$\mathbf{z}_i$	Influence coefficient matrix column vector
$Z_{ij}$	Element of the influence coefficient matrix
$z$	General coordinate in the z-direction (axial/cross direction of roll)

### Greek Symbols

$\alpha$	Angle of line loading of roll
$\beta$	Variable for the eigenfrequency
$\delta$	Regularization parameter
$\boldsymbol{\varepsilon}$	Strain data vector
$\tilde{\boldsymbol{\varepsilon}}$	The strain response vector in the stacked form of regularization
$\boldsymbol{\varepsilon}_e$	Strain data vector of an element
$\boldsymbol{\varepsilon}_i$	The strain response of a unit loading case
$\boldsymbol{\Theta}$	Angular displacement vector of bending in fixed coordinate reference
$\theta_X$	Angular positive direction in the fixed coordinate system, angular displacement of bending in fixed coordinate reference
$\theta_Y$	Angular positive direction in the fixed coordinate system, angular displacement of bending in fixed coordinate reference
$\kappa$	Magnitude of error
$\boldsymbol{\Lambda}$	Load case matrix
$\boldsymbol{\mu}$	Correction weight vector in rotor balancing
$\boldsymbol{\mu}(z)$	First mass moment with respect to neutral axis
$\mu_X$	Unbalance in the x-direction
$\mu_Y$	Unbalance in the y-direction
$\zeta$	Coordinate
$\rho$	Density

$\sigma, \sigma_{min}, \sigma_{max}$	Singular value of the matrix, minimum and maximum respectively
$\phi(z)$	Eigenmode function, natural mode function
$\phi(z)_{SS}$	Eigenmode function, natural mode function, simply supported beam
$\phi(z)_{FF}$	Eigenmode function, natural mode function, free-free beam
$\phi(z)_{r1}$	Eigenmode function, natural mode function, 1 <sup>st</sup> rigid mode
$\phi(z)_{r2}$	Eigenmode function, natural mode function, 2 <sup>nd</sup> rigid mode
$\psi$	Coefficient
$\chi$	Condition number of the matrix
$\chi_{5A}, \chi_{10A}, \dots$	Condition number of the influence coefficient matrices determined from axial strains
$\chi_{5B}, \chi_{10B}, \dots$	Condition number of the influence coefficient matrices determined from axial and tangential strains
$\omega$	Rotational speed of the rotor (roll)

### Acronyms

CD	Cross direction
DE	Drive end
dof	degree-of-freedom
FEM	Finite element method
FF	Free-free eigenfunctions (functional basis)
ICM	Influence coefficient method
MD	Machine direction
PC	Personal computer
SS	Simply supported eigenfunctions (functional basis)
TE	Tending end
WLAN	Wireless local area network
2-D	2-dimensional
3-D	3-dimensional

# 1. Introduction

## 1.1 Background and motivation

Paper manufacturing is a fairly complex process and the production line consists of a large number of different elements. One of the most significant elements of the paper production line is the presence of beam-like roll structures. The paper web is typically led through different unit processes using guiding rolls and roll pairs, where the paper is run between the rolls. In some of the unit processes the paper web is manipulated by compressing it against the rolls. Naturally, the paper web is very sensitive to the compressive forces and loading, which are in some cases considered and used as important control parameters. To enable the control of these types of loadings accurately enough, one has to be able to somehow measure or calculate them.

The conventional way to compress the web is to lead it through the contact zone of a roll pair, where the rolls are pressed together. The unit processes where this kind of loading typically plays a very important part are pressing, surface sizing, coating, calendering and winding processes. In this study, the main interests are in surface sizing and calendering. Both of these unit processes seek to improve the printing properties of the paper. The paper production line where the sizer and calender processes are highlighted is illustrated in figure 1, and examples of the two unit processes are presented in figure 2.

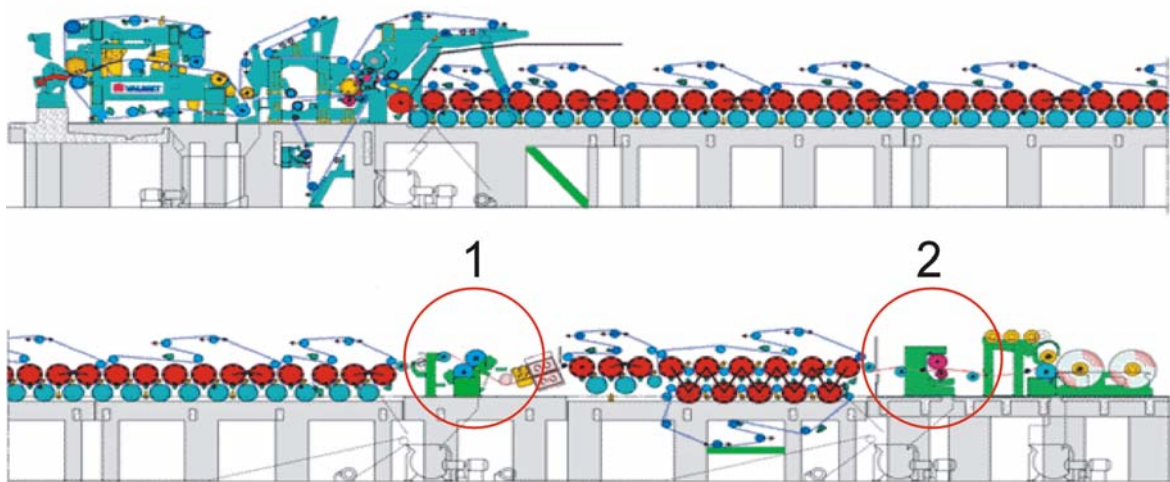


Figure 1. A paper production line, (1) sizer, (2) calender [Knowpap 2007].

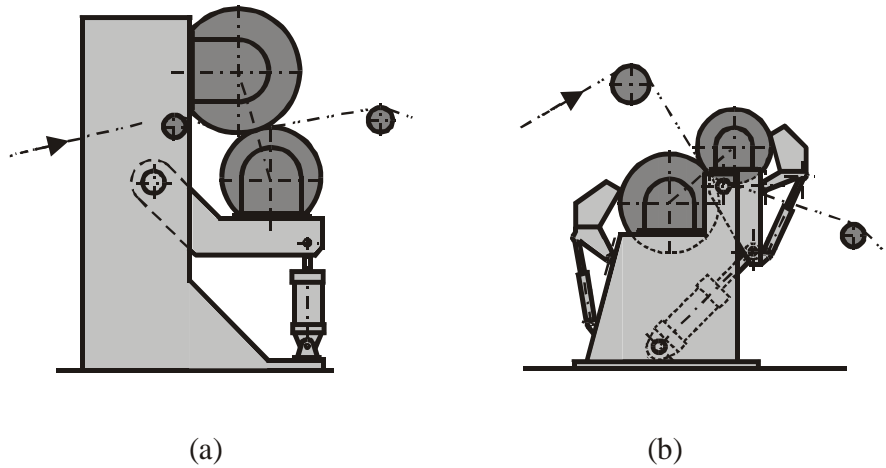


Figure 2. A calendering unit (a) and a size press unit (b) [Kivinen 2001].

The force for the compression is typically generated by using hydraulic actuators at both ends of the rolls. The contact zone of the roll pair is called a nip, and in the nip there are both axial and tangential loading distributions which correspond to the cross direction (CD) and the machine direction (MD) respectively. The typical loading distributions in both the axial and the tangential directions are presented in figure 3. In the tangential direction, the load distribution and the length of the nip are mainly affected by the pressure, the roll materials and the design of the nip, which are not of interest here [Paulapuro 2000]. This study aims to investigate the load distribution of the nip in the axial direction, i.e., the line load.

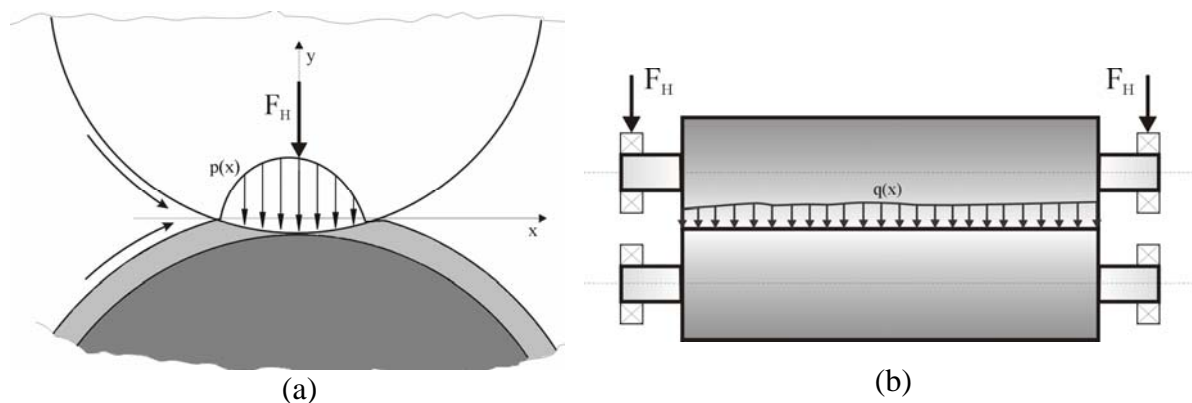


Figure 3. Typical tangential (a) and axial (b) loading distributions in the nip.

In the unit processes mentioned above, the line load distribution is one of the main control parameters influencing the paper quality. In order to operate these processes as well as possible, the line load distribution has to be accurately controlled for uniform CD quality. The conventional methods for achieving this are not adequate in many cases. For instance,

deflection compensation, which is fixed in design of the rolls, and loading actuators at both ends of the roll, are really not accurate enough to control the axial loading distribution of the nip. The most effective tool in this case is the use of a zone controlled roll, in which small ring sectors of the roll shell are individually controlled by hydraulic actuators. They are used locally to repair the incorrect line load distribution. Evidently, the input for the zone controls comes from the quality scanning measurements of the paper at the end of the production line. If one wants to further improve the control of the process, a real online system to measure the loading distribution right at the spot should be applied.

A closer look at the roll pair and the contact zone leads to a significant notion. In these roll pair contacts not only the paper web but also the rolls are significantly influenced by the loading. As flexible beam-like structures the rolls experience notable bending and flattening deformations caused by the loading in the nip contact. Thus the information needed to achieve better line load distribution could be found by measuring the deformations of one of the rolls in contact and thereafter applying an inverse method, idea of which is patented [Pat. FI 114413 B 2004]. Accordingly, one has to form a reliable connection between the deformations and the unknown loading distribution. For the purpose of doing that, a suitable method is introduced herein.

In conclusion, the goal of this study is to develop and study a method with which one is able to measure the CD line load distribution of a roll pair contact zone (nip). The deformations of one of the rolls of the nip caused by the unknown line loading are measured. And, based on the measurement data, the actual magnitude and profile of the loading distribution is calculated with a suitable computational procedure. Actually, the procedure can be characterized as inverse. Roughly speaking, one could simplify the underlying idea to the concept of using the beam-like roll structure itself as a force sensor. The feasibility of this inverse load sensing application is thoroughly evaluated. Moreover, the method introduced here could also be applied to other types of flexible beam-like structures which are affected by loading, such as wings and bridges for example.

## **1.2 Inverse problems in general**

Before examining the problem more closely, one has to understand the predominant concept of an inverse problem, which is described in figure 4. In a forward system, one can



calculate the unknown response directly by knowing the system matrix and the input, whereas in an inverse problem, this configuration is turned around. Only the system matrix and the response are assumed to be known, while the actual input of the system is unknown. According to this definition of inverse problems, all experimental problems could be regarded as inverse [Doyle 2004].

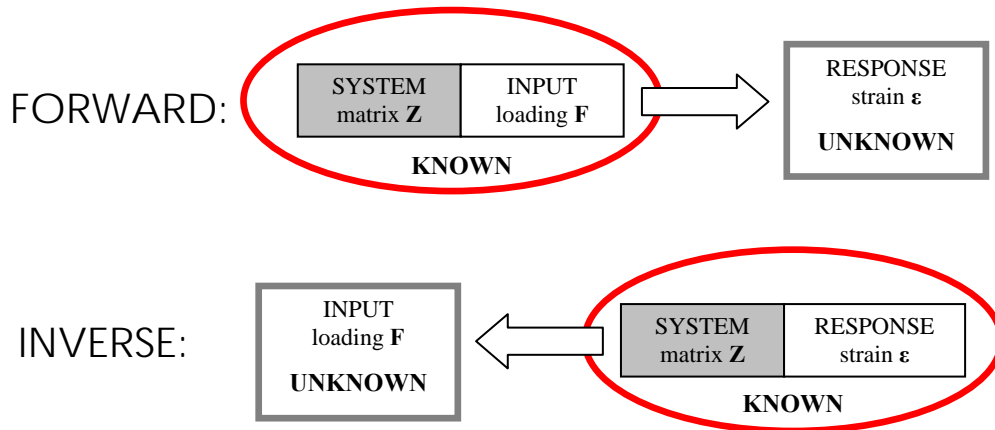


Figure 4. The concept of forward and inverse problems.

The investigated load sensing problem is clearly an inverse problem, since the loading is determined indirectly utilizing measured deformations, the response of the structure. Here, the main application is a paper machine roll, which can be equipped with strain gage sensors that express the roll deformation information directly as strain. This strain response can then be substituted into an inverse equation, in which an appropriately constructed system matrix describes the strain-force behaviour of the system. As a result, one is able to obtain the actual loading input, which caused the measured strain response in the first place. This is also presented in figure 4. Actually, by following this approach, it is possible to determine the system matrix in a direct way as a forward problem.

Once the system matrix is formed and the response strain vector is known, one is faced with an inverse equation. The linear matrix equation has to be inverted in order to obtain the influential input, the loading. This generates and also describes the root of the difficulties that typically occur with inverse problems. Namely, the linear matrix equation does not always behave in a stable manner as it is most likely to be ill-posed. In other words, it does not fulfil the mathematical conditions of a well-posed equation as defined by Hadamard (see for example [Engl et al. 1996, p. 31]). In practice, it means that small errors

in the strain data cause large deviations in the loading solution. Fortunately, there are mathematical means, such as different regularization techniques, to overcome these problems. Thus, regularization is utilized to enhance the inverse solution quality.

### **1.3 Approaches for the inverse load sensing method**

In this study, the inverse load sensing method that is used to solve the unknown line load distribution is the influence coefficient method (ICM), i.e., the required system matrix is formed from influence coefficients. It is a widely known method, and has been used in many applications and subject areas. In fact, in the recently published book by Doyle [Doyle 2004], which covers the modern experimental stress analysis of partially specified problems, a method called the sensitivity response method (SRM) is used, and is a very similar method to the influence coefficient method. The finite element method (FEM), which is the usual method used in structural analysis, is not directly applicable, but it can be useful as a tool in this load sensing problem.

In addition, the problem at hand could very much be categorized as a force identification problem, which is in some references called a force reconstruction problem. Indeed, from the published research on force identification, one can find similar structural problems, in which static, or more typically, dynamic force/loadings are calculated inversely based on structural measurements. As structural data, both acceleration and strain measurements have been used, of which the former is more common in dynamic cases. The system matrices of these problems are basically formed and used in the same way as they are here, but because their main focus is typically in dynamic interactions, such as vibrations, impacts, moving loads or sound, the approach and the equations are somewhat different. In any case, these types of inverse force identification problems give good ideas about the measurements, and moreover, the treatment of inverse equations in the case of structural problems.

#### **1.3.1 Influence coefficients and FEM**

In structural analysis, a connection between the known and the unknown quantities has to be determined. The typical method used in such cases is the finite element method, which is fast and easy to use. FEM is based on specified discrete elements, with which the given

structure is described and meshed. Elements are idealized parts of the structure, which behave according to some known laws or equations. But sometimes the idealization of the given structure with elements is not possible, because of the nature of the problem. This might be the case, for example, when real measurements, which consist of a discrete number of data points, are used to calculate some additional data. The information needed for a full FE analysis is imperfect: thus new ways of handling the problem have to be found. In this type of situation, the influence coefficient method is an advantageous and applicable way of connecting the unknowns to the known quantities. In the method, the connection is established by forming a matrix that can be applied to the partially defined case. The matrix consists of influence coefficients, which are either determined experimentally based on measurements, or theoretically based on computations.

Characteristically, the basic concept of the influence coefficient method is general and versatile. Influence coefficients can be determined to describe the behaviour and relationship of almost any combination of two quantities. When structural analysis is considered, the concept of the influence coefficients lies in the theory of matrix structural analysis discussed by Przemieniecki [Przemieniecki 1968]. The actual continuous system is formulated for a discrete system of a finite number of degrees-of-freedom (dof's), upon which matrix algebra operations can be performed. Accordingly, the force-strain relationship is described by a system matrix, which is the influence coefficient matrix.

In the typical idealized discrete-element treatment of structural problems with FEM, the force-displacement relationship is described with stiffness or flexibility matrices as the system matrices. These generate the basis for the displacement or force methods of FEM, respectively [Bathe 1982; Przemieniecki 1968]. Evidently, a definite relation can be obtained between the influence coefficient matrix and the matrices of FEM. However, using this kind of straightforward approach would signify that the nodes (measurement points) considered ought to be congruent, and, in principle, determined by the FE model mesh. Hence, the advantage of using ICM is that the conditioning of the structure is not as strict as in the idealized FEM. ICM is based on the direct relationship of the known and the unknown quantities, and it is fairly easy to apply to practical measurements. One could limit the computations to only the interesting or measurable degrees-of-freedom and treat them in a suitably enhancing way. Naturally, this raises the questions concerning the accuracy of the method, and, must therefore be investigated. Basically, one could regard

the influence coefficient method as a special case of FEM, because ICM is more direct and fairly easy to utilize with actual measurements. Alternatively, FEM is a special could be regarded as a special case of ICM, because it is an idealized presentation of the force-deformation relationship of a structure.

The influence coefficient matrix can either be formed experimentally or theoretically on the basis of computations. In the latter case, one can use known analytical solutions appropriate to the given structure, or, with more complicated structures, FEM. The influence coefficients are determined with a forward unit loading procedure, in which the unit loadings consist of point forces or a proper functional basis. The influence coefficient matrix is then formed of the influence coefficients. Thus, it can be utilized to solve a system of linear equations concerning the force-deformation behaviour of the structure.

### **1.3.2 Applications of the influence coefficient method**

In structural analysis, there are lots of areas where influence coefficients are used. The common feature of these applications is the mathematical formulation of the system or the model. The influence coefficient method offers an alternative for determining the required system equations.

The utilization of structural measurements in the experimental analysis of structures is discussed in the book by Doyle [Doyle 2004], where a method similar to the influence coefficient method, called the sensitivity response method, is introduced, as previously mentioned. It is shown that the method can be applied to different structures utilizing strain gage measurements, whole-field strain measurements, as well as acceleration measurements. The sensitivity responses of a particular structure can be determined with the help of an adequate FE model, and the method is applicable even if the system is partially specified. When utilizing strain measurements, the focus of the book is in the whole-field strain measurements. Nevertheless, it is shown that strain gages are also a good way to measure the loading of a structure in specific cases, such as when measuring the magnitude of a point force or a force pair, or separate parameters of a structure. Similar results are also obtained in this study. When it comes to measuring traction loads or other continuous loading distributions, whole-field strain data and the Tikhonov regularization technique are utilized [Doyle 2004]. In the present study, the objective is to measure

distributed loads and concentrate on the application, which is set up with strain gages, and to further develop the method to suit strain gage measurements better.

A very popular application, in which the influence coefficients are used, is rotor dynamics, or to be more exact, the procedure of balancing rotors. Rotors are typically either balanced by modal balancing [Bishop & Gladwell 1959; Kellenberger 1972] or by influence coefficient balancing with trial weights [Ehrich 1992; Goodman 1964; Lund & Tonnesen 1972; Tan & Wang 1993; Tessarzik et al. 1972], of which the latter method is of obvious interest here. In fact, the process of balancing a flexible rotor by trial weights is an ISO standard [ISO 11342:1998]. There are various ways to apply the method: for instance, one could make use of semidefinite modal coordinates [Keskiniva 1997], or apply the balancing procedure to unsymmetrical continuous rotors such as crank shafts, utilizing an FE model in the process [Kang et al. 1995]. Recently, an interesting approach for continuous real-time balancing was introduced [Keskinen & Kivinen 2002]. In addition, the utilization of regularization and conditioning in influence coefficient balancing is discussed by Kang et al. [Kang et al. 2006]. Since it has been proven that the balancing of continuous rotors, such as rolls, is efficient with the influence coefficient method, it raises one's confidence to successfully use the method for measuring the line loading of a rotating roll. Furthermore, the applications of rotor dynamics are important, because the main element of this study, a rotating paper machine roll, is a continuous flexible beam-like rotor. The rolls of a roll pair are in a dynamic environment, which means that there are not only static, but also dynamic, interactions, which have to be taken into account with appropriate actions.

In aeroelasticity, the influence coefficients have been utilized for measuring wing loads during flights. In the 50's and 60's, when the simulational and the computational methods of calculating the loads and stresses of aeroplanes were not feasible by numerical computations, measurements were used to test and monitor wing structures. At that time, strain gages were used to calculate individual loading quantities such as bending moments, torsional moments and shear forces on a wing, as originally proposed by Skopinski and Aiken [Skopinski & Aiken 1954]. In addition, strain information was used for calculating the deflection and the forces acting on a wing [Bisplinghoff 1955]. Since then, on one hand, the aeroplane wing structures have become more complex, and, on the other hand, the measurement methods and computational tools have developed considerably. This has

led to advancements to the method, as has been reported [Jenkins & Kuhl 1977; Allen 2003, Lokos 2004]. However, the method basically remains the same. The strain-load relationship is determined by a matrix equation, which includes the influence coefficient matrix. Included as the load quantities have been individual loads as well as load distributions, as summarized by Jenkins and DeAngelis [Jenkins & DeAngelis 1997]. Worth noting here is that, even though the results are not directly applicable in this study, the loads of complex wing structures can be accurately solved with very little error, which demonstrates the potential of the method. Nowadays, aerodynamic influence coefficients are still used as a computational tool to calculate aerodynamic effects acting on a wing.

### **1.3.3 Force identification**

Accordingly, the inverse load sensing method described here could be regarded as force identification. Stevens [Stevens 1987] has presented an extensive overview of the force identification problem of structures. The solution processes have since developed, and there are several applications of the method involving the same main principles. As already mentioned, the book about modern experimental stress analysis of partially specified problems by Doyle [Doyle 2004] focuses mainly on force identification. It discusses the use of strain, as well as acceleration measurements in different inverse force identification problems. These include identification of static forces and tractions, dynamic impact forces and tractions as well as nonlinear forces. The methods represented by Doyle can be utilized on complex structures with relatively low computational costs by using FEM in the process. The same type of treatment with FEM was also proposed for 2-D structures utilizing displacement or strain data [Maniatty et al. 1989], and, in contrast, FEM was directly applied using static condensing to the external load identification problem [Nagakiri & Suzuki 1999]. FEM was also utilized to characterize a discrete truss structure as the applicability of the inverse force identification approach was investigated in the case of static strain measurements [Turco 1998], and in the case of dynamic acceleration measurements [Turco 2005].

Interestingly, Shen [Shen 1986] investigated the identification of distributed static loadings based on displacement and strain measurements on beams making use of Bernoulli-Euler beam theory. The results indicated that the inverse force identification method is feasible in

static cases for elementary beam structures. Particularly, strain data was found to be preferable to displacement data in these kinds of inverse problems.

There have been many different force identification approaches for the determination of time-varying transient forces such as impact forces, for which the response data is collected using acceleration or strain sensors. The outcome of their formulations typically leads to deconvolution, which essentially makes the solution difficult. Therefore, a variety of approaches have been investigated. For example, modal methods for time domain data [Busby & Trujillo 1987; Hollandsworth & Busby 1989] and Fourier methods for frequency domain data [Martin & Doyle 1996a, 1996b] have been used. A modal approach to force identification problems for an exciting beam [Pezerat & Gyuander 1995] and a plate [Pezerat & Gyuander 2000] have also been discussed. The identification of external structural loads from measured harmonic responses, and, particularly, the related sensitivity issues were examined by Karlsson [Karlsson 1996]. For flow-induced vibration applications, modal force identification approach has been discussed [Granger & Perotin 1999a, 1999b]. Liu and Shepard [Liu & Shepard 2006] have proposed an improved modal method for determining a spatial force distribution. Finally, a transient force identification method that utilizes FEM was proposed by Adams and Doyle [Adams & Doyle 2002], and was also utilized by Doyle [Doyle 2004].

There are several publications about moving force identification on a bridge using different measurement signals [Chan et al. 2001a, 2001b; Zhu & Law 2002; Law et al. 2004] and there is a good overview of recent research in that field by Yu and Chan [Yu & Chan 2007].

All of the force identification problems include the problem of ill-posed equations and regularization. Thus, there are many publications that have discussed conditioning of the system equations, and further developed the regularization of the problem [Busby & Trujillo 1987; Thite & Thompson 2003, 2004, 2006; Choi et al. 2007a, 2007b; Jacquelin et al. 2003].

The idea of having the structure itself acting as a sensor is not very rare as was already mentioned by Stevens [Stevens 1987]. For example, in a more recent paper [Gobbi et al. 2005], influence coefficients were utilized to determine the forces and moments acting on a

heavy vehicle tire based on measured deformation data of the special wheel structure. In fact, there are also commercial applications for measuring the forces acting on a wheel of a vehicle that are based on the same principle, for example, from MTS sensors [MTS 2008]. The force identification studies mentioned above show that in static or dynamic cases, single forces, force components, and spatial force distributions as well, can be reconstructed on the basis of structural measurement signals in miscellaneous cases. In our application, the loading distribution is acting on a complicated tubular beam-like shell structure, the measurement data is partially specified, and the measurement environment is dynamic. This really represents a challenge in the determination of what the requirements to effectively apply the inverse load sensing method are.

#### **1.4 Other interesting inverse problems**

Of the many inverse applications outside of structural analysis that are worth mentioning, there is the now popular research area of digital image processing. In tomography and other medical imaging applications, where blurred images have presented problems for example, inverse techniques such as regularization, have led to great benefits [Kaipio & Somersalo 2005; Kolehmainen et al. 2003; Siltanen et al. 2003]. There is a considerable amount of useful knowledge on how to handle the types of inverse equations that occur in these kinds of inverse problems, and the mathematical treatments of the ill-posed problems have been extensively developed. A good overview of them and some interesting research topics are discussed in the book by Kaipio and Somersalo [Kaipio & Somersalo 2005], where, in particular, the concept of error sources in inverse problems and the connection to statistical methods are studied.

#### **1.5 Objective and scope of the study**

The objective of this work is to develop and investigate an inverse load sensing method for solving continuous load distributions of a structure based on strain data. In particular, the feasibility of the method is to be verified. Furthermore, considerable concern is directed towards the different possibilities for utilizing the method and towards the problems emerging from the inverse nature of the problem. The inverse load sensing method is investigated by simulation, as well as tested in practical measurements of two smaller case studies, and, finally, a pilot roll press.



### **1.5.1 Scope of the study**

The main applications of the method are the rolls used in paper machines that are affected by line loading and can be considered beam-like. Furthermore, the results obtained here for roll structures could also be utilized for other complex beam-like structures.

### **1.5.2 Initial assumptions**

These initial assumptions are made before the analyses. The beam-like structure (roll) is regarded as linearly elastic and isotropic. Initially, the effects of temperature changes in the structure itself are considered to be insignificant. In addition, the shear deformations that appear in the nip contact during the run are assumed to be insignificant. Thus, only transverse loading is considered to have an effect in the nip and the rolls.

The problem field is essentially dynamic, since the rolls are rotated in the governing paper machine applications. Nevertheless, this load sensing case can be, and is, regarded as quasi-static. This is justifiable, since the dominant input line load distribution, and therefore the strain response it causes as well, can be regarded as stationary, and the rate at which it changes is slow. As a result, some kind of tracking, as well as adaptations, have to be included in the measurement process in order to take into account all the significant dynamic effects that occur in the measured strain response. Therefore, the examinations and calculations are first done from a static point of view.

### **1.6 Contributions of the thesis**

These original contributions have been developed over the course of this work:

1. An inverse load sensing method for line load determination of beam-like structures is proposed and investigated numerically and experimentally.
2. The feasibility of the inverse load sensing method is evaluated in the case of solving the line load acting on a roll structure.

## **2. Description of the operational environment**

The motivation for this study originates from the unit processes and elements of paper manufacturing machines. In this chapter, the background and the operational environment for the inverse load sensing method are discussed.

### **2.1 The problem environment: rolls and roll pair applications in paper machines**

Rolls and roll pairs are an essential part of the paper manufacturing process. They are used to guide the web through the production line. In some unit processes, such as in pressing, surface sizing, coating, calendering and winding, the paper web is compressed and led through the contact zone between two rolls. The contact zone is typically called a nip. The main interest of this study is in surface sizing and calendering, where the objective is the improvement of the printing properties of the paper. In these unit processes, one of the most important controlling parameters is the line loading distribution in the nip, i.e., the nip load, which originates from the compression.

In the nip, both the paper and the elastic rolls experience deformations caused by the loading. The objective of this study is to utilize the deformations of the roll by calculating the nip load based on the strain measured in the deformed roll. But first, the foregoing unit processes and conventional methods for controlling the nip load are discussed.

#### **2.1.1 Surface sizing using film size press**

Surface sizing is an important paper finishing process. It could also be categorized as a coating process, since a thin film is transferred to the surface of the paper. There are a number of paper coating techniques, of which film size press, i.e., a process for surface sizing, is of particular interest, since it involves a roll nip. In surface sizing, paper properties such as surface strength and inner strength, are significantly improved to achieve better printing quality of the paper [Lehtinen 2000].

The present-day surface sizing unit, typically a film size press, consists of a roll pair and a film metering system. The rolls used in a film size press are either soft, polymer-covered

rolls that have cast iron frames, or plain hard metal rolls. The film substance is first metered onto the surface of the soft roll and then transferred onto the surface of the paper in the compressed nip. The amount of the film substance transferred is dependent of the hardness of the soft roll. The coating is typically applied simultaneously, having two soft rolls in the nip. Thus, both sides of the paper (both rolls) are treated at the same time [Lehtinen 2000]. As an example of a film size press, Optimizer coating unit from Metso Paper is presented in figure 5.

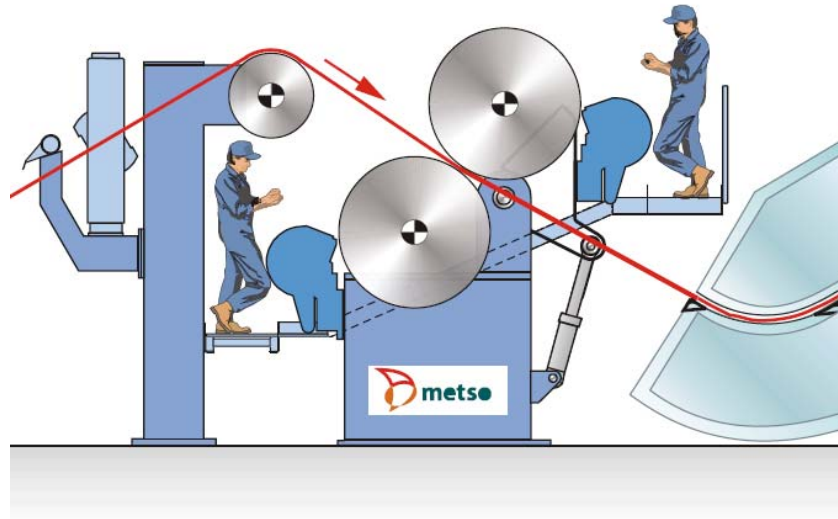


Figure 5. Optimizer coating unit [Metso Paper 2008].

In a film size press, the nip load is one of the main control parameters, and it is conventionally produced by hydraulic actuators at both ends of the roll. Because of the nature of the film and the transferring process, the application in the nip is very sensitive to disturbances. One of the main problems is controlling the loading, as well as keeping the run free of vibrations [Lehtinen 2000]. Here, the interest is obviously focused on the former, more precisely on the cross direction (CD) line loading distribution.

### 2.1.2 Calendering

Calendering is one of the paper finishing processes. Typically in the calendaring process, which can be performed online or offline, roll pairs or roll stacks are pressed together and heated, while the paper is led through the nip or nips. As the result of this thermo-mechanical process, the surface and structural properties of the paper, such as smoothness and gloss, are improved [Jokio 1999].

The loading of the calender is produced by a hydraulic cylinder mechanism at both ends of the rolls, and the heat comes from heated rolls. Nowadays, there are many different calendering applications, such as machine calendering, soft calendering and supercalendering to name but a few. Nevertheless, in all calendering applications, nip load is the most important control parameter. Compared to surface sizing, the loads in the calender nips are notably higher and the loading systems are more sophisticated as well: techniques such as zone-controlled rolls are often used to ensure an even CD line loading distribution. Typical examples of a multi-nip supercalender and a machine calender are presented in figure 6. The nip loading is also dependent on the surface material of the roll. Longer nip times and longer nips are made possible by the use of soft polymer covers on the rolls instead of plain hard metal rolls. In addition, there are many different roll designs, the selection of which depends on the calendering case and the desired line load level [Jokio 1999].

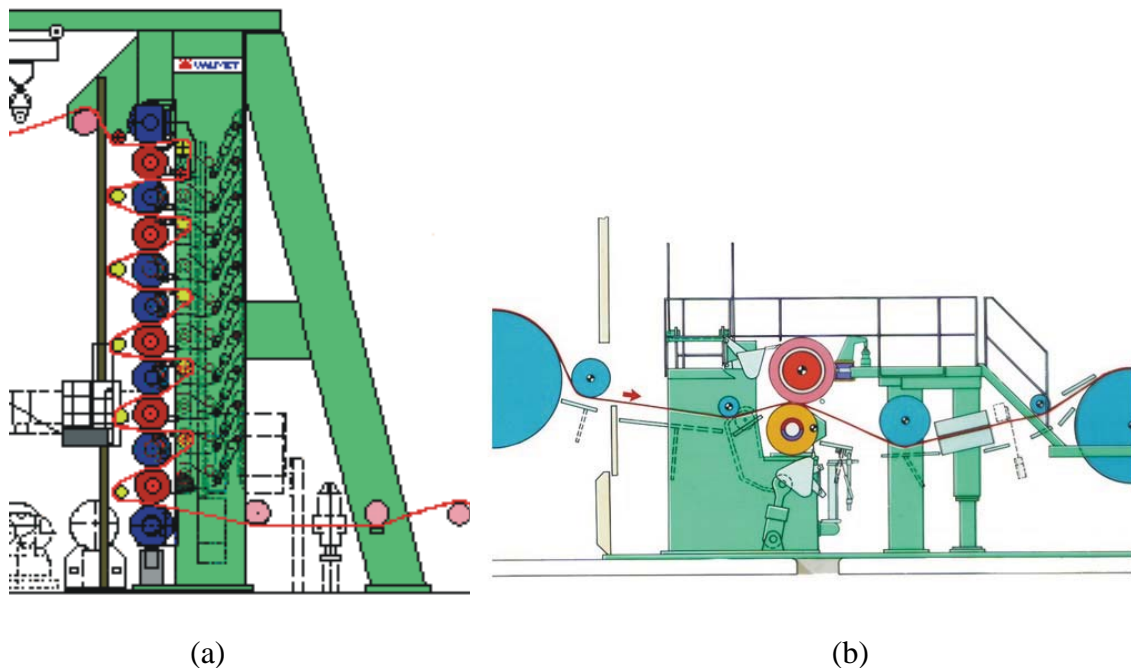


Figure 6. Multi-nip calender Optiload (a) and a machine calender (b) [Knowpapp 2007].

### 2.1.3 Techniques for controlling the CD nip load

The CD loading in the nip is preferably an even line load, as illustrated in figure 7, to ensure even quality of the paper in the CD. Consequently, the nature of the structure and the loading mechanism of the roll pair lead to undesirable uneven profiles, examples of which are also presented in figure 7. An uneven CD loading profile is a typical problem in

both of the handled unit processes and may be worse in the more sensitive coating processes. To overcome this problem, there are a couple of conventional approaches, specifically, the usage of crowned or zone-controlled rolls.

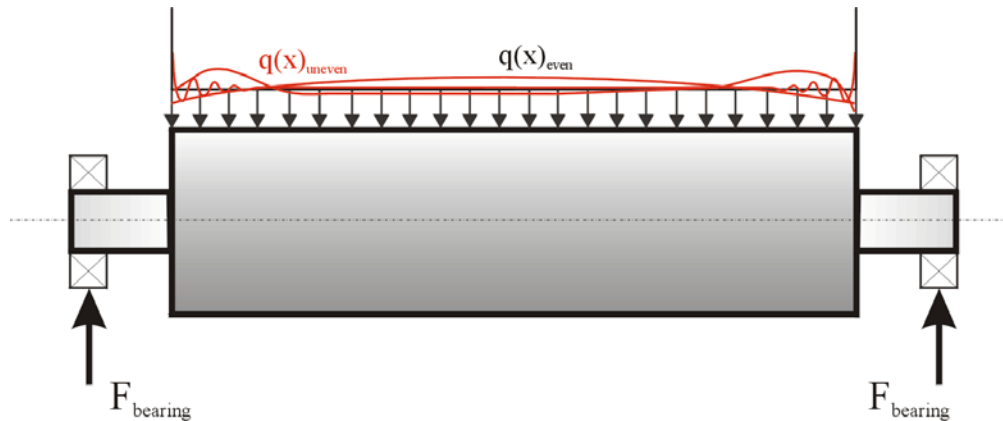


Figure 7. Examples of even (black line) and uneven (orange line) nip profiles.

Crowning is a method whereby the surface of the rolls is ground into a slightly barrel-shaped form, because this kind of shape evens the loading profile across the roll contact. This grinding treatment can be made for both solid hard rolls and for covered soft rolls. Crowning of the surface of the roll takes into account the deflection of the roll under the line load. Thus, the real deflection mode of the roll under a nominal load is the ideal ground profile. Clearly, the weakness of crowning is its ideal suitability for the nominal load only [Paulapuro 2000]. An example of a crowning shape is illustrated in figure 8.

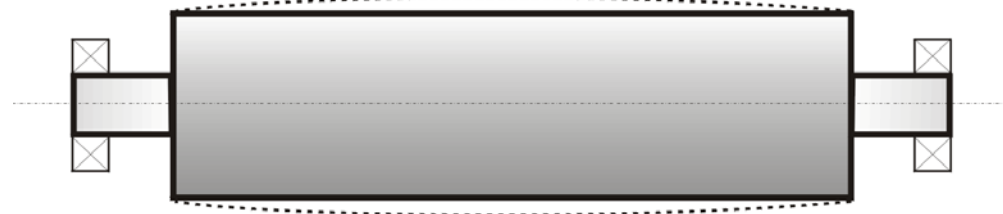


Figure 8. Crowning shape of a roll (dashed line).

Zone-controlled rolls or “adjustable crown rolls” refer to rolls, in which the deflection compensation can be adjusted locally in the CD by specific actuators. Typically, the design of such rolls consists of a stationary shaft, around which the shell rotates. The deflection compensation is created by an internal force between the shaft and the shell which corresponds to the external loads, the nip load and also the deflection of the counter roll. The rolls are divided into 5-60 loading zones, depending on the intention, and the actual internal force is created by hydraulic loading shoes or loading elements as shown in

figure 9. The actuators operate the ring sectors of the shell independently, thereby enabling local corrections to the line loading profile in the nip. These types of rolls are self-loading, which means that the shell moves relative to the shaft and, during operation, the roll shaft is fixed to the frame. The principle of self-loading is demonstrated in figure 10. Thus, the nip can be closed and opened by the internal forces alone. The self-loading zone-controlled rolls are not susceptible to vibrations. If necessary, the profiling of the nip load can be controlled by not only the loading zones at the nip, but also by counter zones at the opposite side of the nip, or in other angular positions of the roll, as also illustrated in figure 9 [Paulapuro 2000; Venemies 1999].

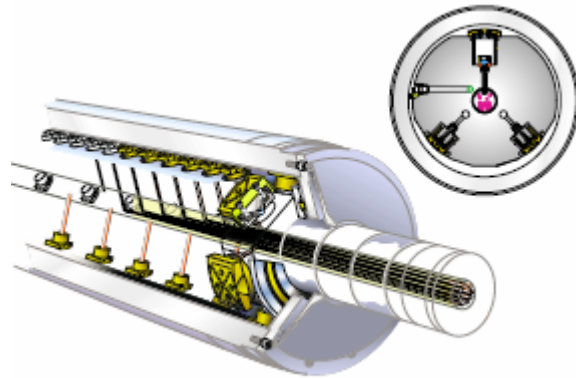


Figure 9. Zone controlled SymCD/HP roll and its loading elements [Metso Paper 2008].

The space between the shaft and the shell is filled with oil. The loading elements, together with the oil, create a combined hydrostatic and hydrodynamic bearing, as the ends of the shell have roller or, for more precise roll end-control, sliding bearings. For better edge load control of the nip, adjustable bearing loading is used [Venemies 1999]. The effect of bearing loading is presented in figure 10.

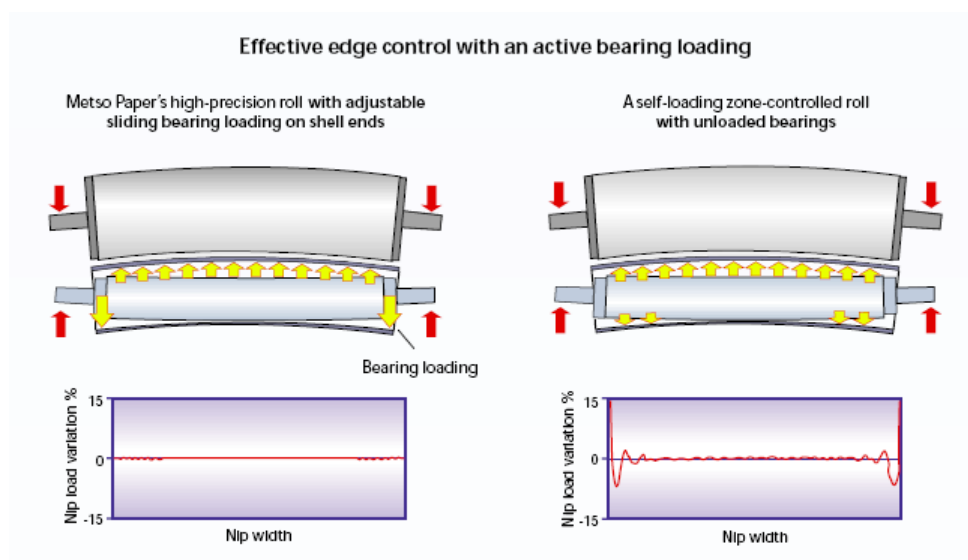


Figure 10. The effect of self-loading and bearing loading of Symroll [Metso Paper 2008].

Evidently, the input for the zone controls is obtained from the end of the production line from the CD scanner quality measurements of the paper just before winding. Nevertheless, the measurement data is not received right at the spot (in the nip), where the proposed method would work, and thus improve the process.

Nowadays, Metso has a new innovation for measuring the nip load profile called iRoll. It is used in winding nips to measure the nip load distribution, as well as line tension. The measurement is based on an electromechanical film sensor, which is integrated in a spiral shape into the roll structure, typically between the polymer cover and the roll shell. During a run, only a narrow section of the sensor strip is in the nip at a time, and the data transmission from the roll is wireless, and thus operates in real-time. This enables one to obtain a signal about the complete CD line loading profile of the nip using mapping during one revolution [Ainasoja 2008, Metso Paper 2008]. The iRoll is presented in figure 11.

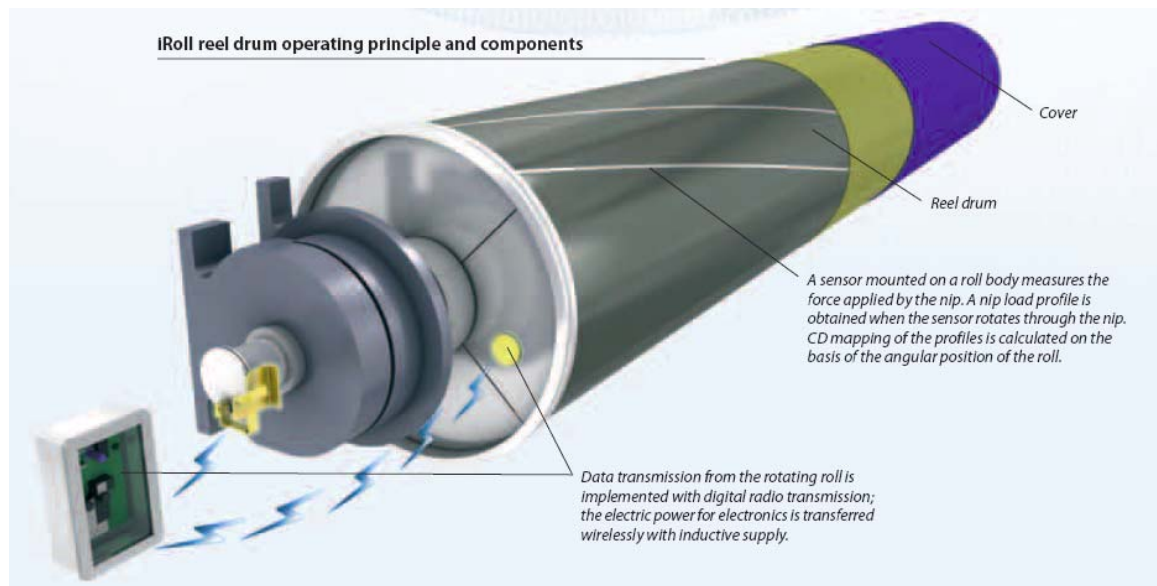


Figure 11. The iRoll innovation [Metso Paper 2008].

With iRoll, the online measurement of line loading profile of a nip is done right at the spot. Nevertheless, the measurement system is not used in applications with heavy loading, such as film size presses and calendars, because of high pressure and high deformation of the sensor. Also, the measurement system is not absolute, in the sense that it only measures the profile, while the magnitude of the loading is still based on traditional force sensors measurements at the ends of the rolls. With the proposed method of inverse line load sensing, application to heavy processes, and magnitude, as well as the profile measurements of the line load, would both be attainable. Thus, it would represent an improvement to the nip load measurements.

## 2.2 The pilot roll press

The experimental work of this study is mainly carried out with the pilot roll press unit built in the Laboratory of Machine Dynamics. The pilot roll press provides a valid measurement environment, and is used to verify and test the inverse load sensing method in practice. In this chapter, the construction of the pilot roll press is described.

The pilot roll press is illustrated in figure 12. It is built in a scale of 1:2 with respect to a real-size production machine roll nip unit used in paper mills. It is designed and verified to be used as an experimental set-up for dynamic testing corresponding to a real-size machine. Moreover, various kinds of offline, as well as online, measurements can be conducted with the pilot roll press [Kivinen 2001].

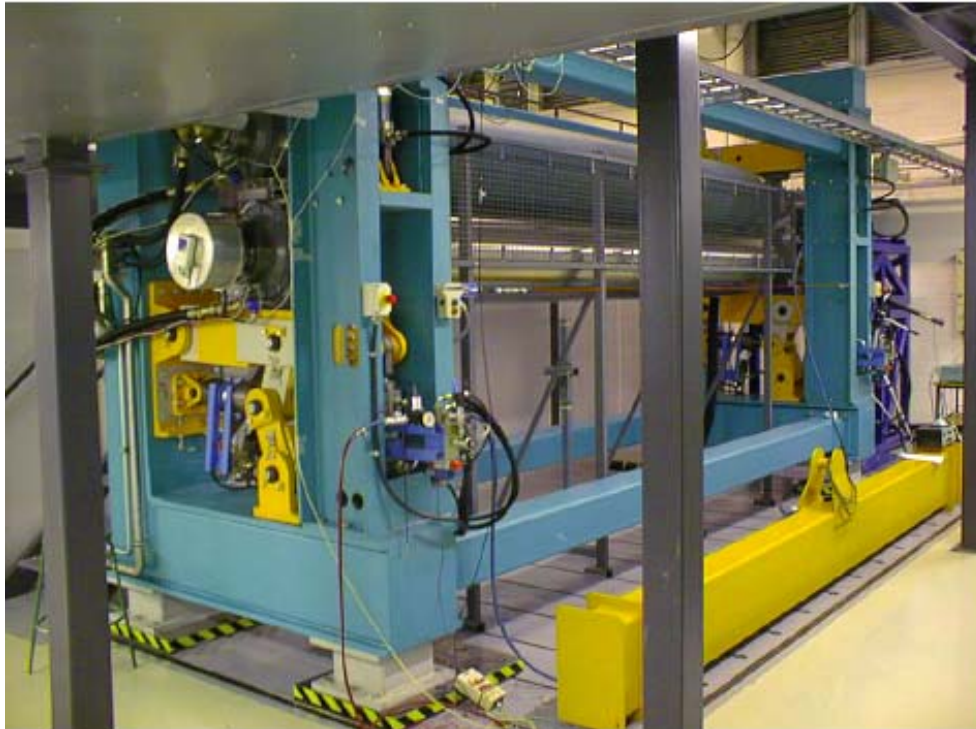


Figure 12. The pilot roll press.

The construction of the installation consists of a steel frame, a hydraulic mechanism to open and close the roll contact, the rolls and their drives, and a 100-ton concrete plate, on which the structure stands. The lower roll has an integrated wireless measurement system, which enables on-line strain gage and accelerometer measurements. The upper roll has an integrated inner water-cooling system, as in production machines, as well as sensors and a wireless radio link. There is no paper web led through the roll nip.



The aim of this work is to investigate and develop an inverse method for measuring the line loading in the nip. The inverse method is based on strain measurement data from the roll contact. Therefore, the details of the rolls, the measurement system and the loading system are briefly presented in the chapters to follow.

### 2.2.1 The rolls and the loading mechanism

The rolls are manufactured of cast iron, and the ends of the rolls are machined and attached to the shells by multi-bolt joints. The roll pair consists of a hard lower roll and a soft upper roll. The design of the rolls is identical, except that, in order to obtain a soft surface for the upper roll, its metallic shell is covered with a special soft polyurethane cover. The surfaces of the rolls are appropriately ground to reach the optimum line load response in the nip. They are treated with the previously introduced technique of crowning. In this case, crowning is applied to the metal surface of the lower roll, and to the polymer covered surface of the upper roll. The design line load (nominal load) of the crowning is 15 kN/m, at which, in theory, the roll bending and flattening effects are compensated and the line loading is uniform across the whole nip.

The installation is equipped with a wireless measuring system as presented in figure 13, with which online measurement data from inside the lower roll can be collected. The sensors of the lower roll are connected to a measurement PC, with which the information is transferred to the monitoring and analysis computers via WLAN. The wireless measurement network and operation of the installation is presented in detail by Salmenperä et al. [Salmenperä et al. 2002].

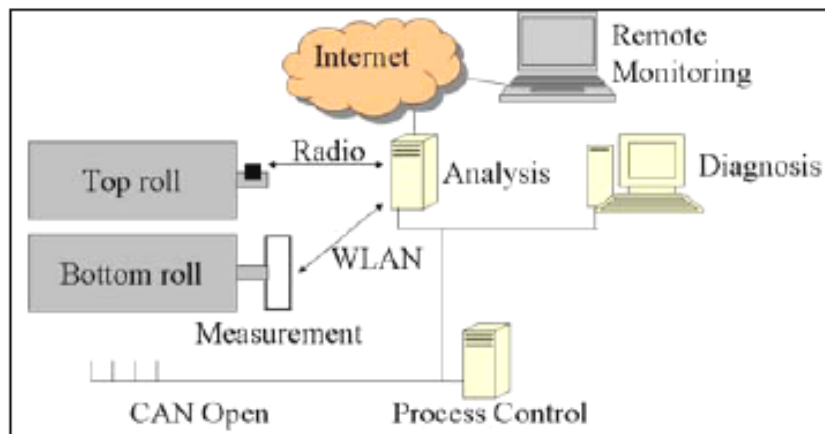


Figure 13. The measurement system of the pilot roll press.

The inner wall of the lower roll is equipped with strain gages, accelerometers and acoustic emission sensors, as illustrated in figure 15. The strain gages are connected into Wheatstone bridge circuits. The thermal effects of their leadwires are compensated with a three-wire arrangement, and their coefficient of thermal expansion is chosen to be similar to that of the shell material, which eliminates errors caused by temperature changes. The sensors of the lower roll have been utilized in a number of studies, such as in the case of verifying the strain measurements [Keskinen et al. 2002], in the case of analysis of the whirling response [Järvinen 2003], and in the case of verifying the numerical modelling of the roll nip unit [Järvenpää 2005].

The loading mechanism of the pilot roll press is illustrated in figure 14. It is a patented construction [Pat. FI 110712 B 2003]. The contact opening and closing mechanisms are operated by hydraulic actuators on the lower roll side (6). The loading solution is non-traditional, in the sense that the actuators are horizontally pushing a four-bar linkage which transmits the power to the roll nip (9). In contrast, the traditional approach is that the hydraulic force is applied vertically. When applying the line load, the upper roll arms are pushed against the supporting frame with a locking cylinder (8), from which the force-feedback can be measured using force sensors in between. When closed, the nip is at an angle of 10 degrees from the vertical direction [Kivinen 2001].

Typically, control and application of the line load is based on the signals from the two force sensors at both ends of the roll. But, if one could measure the line loading straight from the source, from the roll passing through the nip, control based on that would be more accurate. In the case of the zone-controlled roll, the control would be even more accurate. Given that the measured axial deviations in the line load could also be fixed locally.

### **2.2.2 The roll drives**

While this research was in progress, the roll drive system has undergone some development, so that one must speak of three different configurations. In the first stage, the electric drives were attached to the rolls using gearboxes and a universal shaft. In the second stage, the gearboxes were removed and the drive mechanism became direct-drive without any gearboxes, while still using the original electric motors. In the present, third, stage, the special direct roll drives were fitted straight to the ends of the rolls. These drive

changes were made in order to decrease vibration sources and to simplify the design by using direct drives. They do not have a notable effect on the load sensing method based on strain measurements because the support of the rolls is basically the same in all of them.

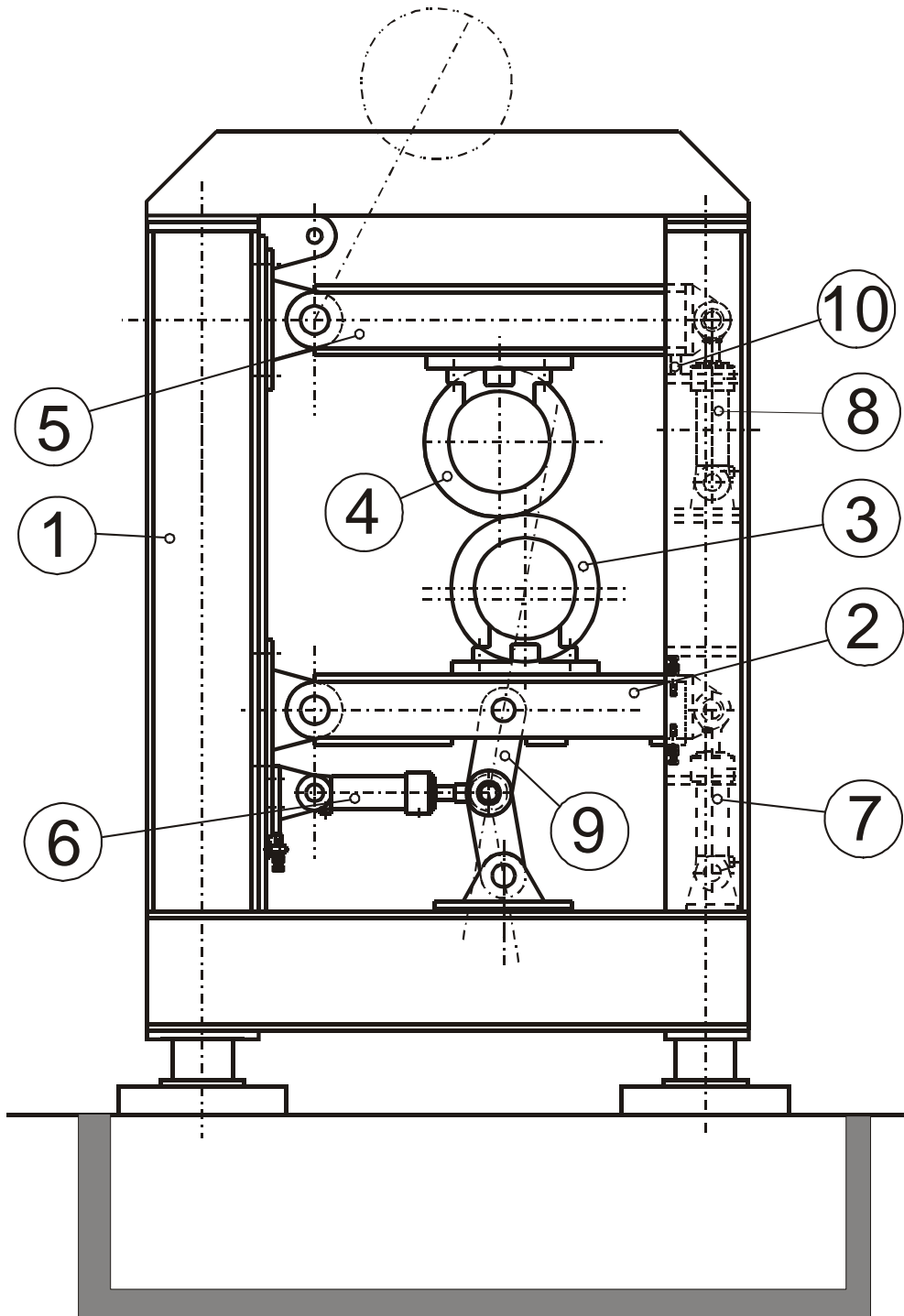


Figure 14. The loading mechanism of the pilot roll press: Frame (1), Lower arm (2), Lower roll (3), Upper roll (4), Upper arm (5), Loading cylinder (6), Excitation/damping cylinder (7), Locking cylinder (8), Loading-toggle-four-bar-linkage (9), Force sensor (10) [Kivinen 2001; Pat. FI 110712 B 2003].

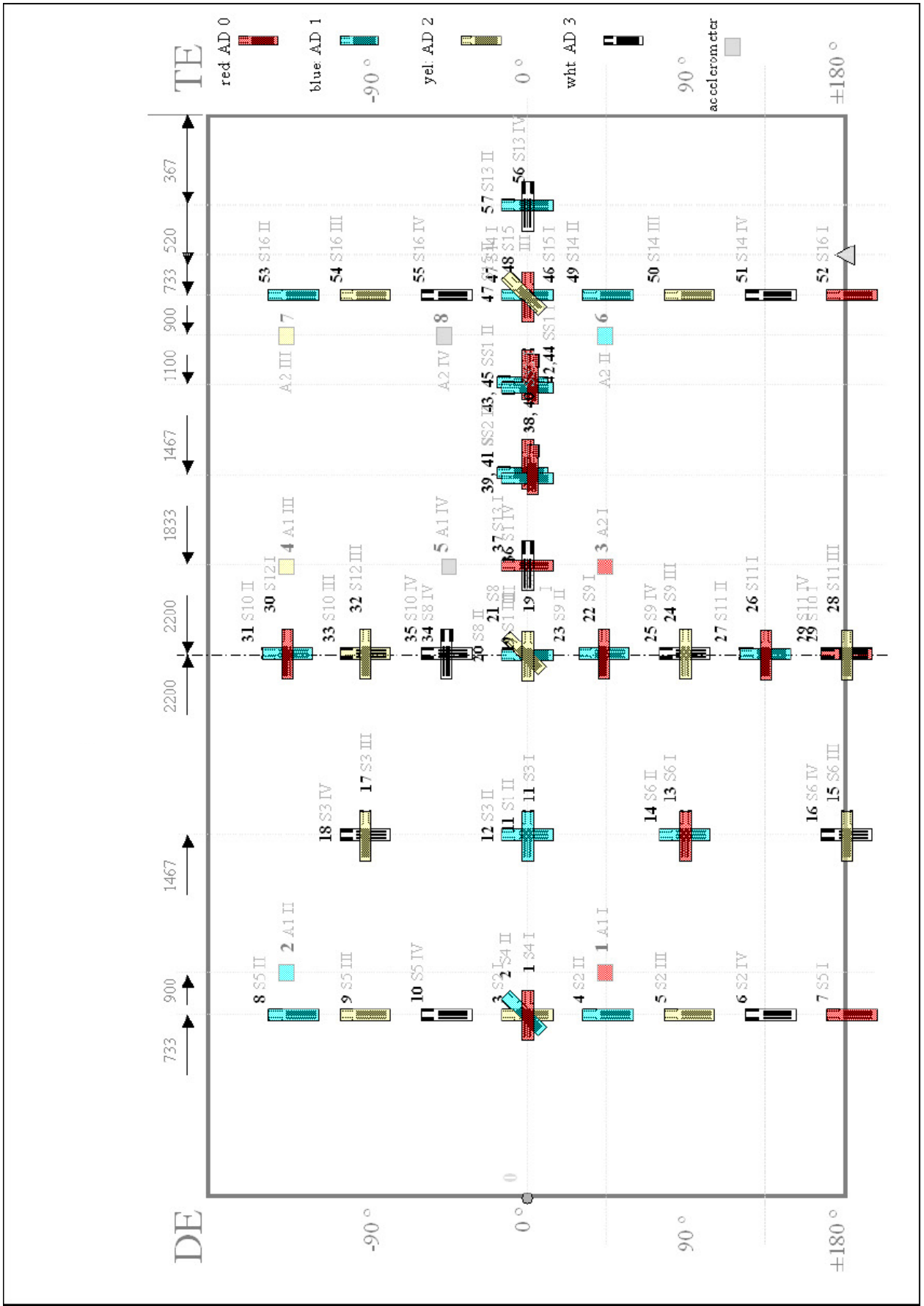


Figure 15. The sensors of the lower roll.

### **3. Inverse load sensing method and formulation**

In this chapter, the basic concept of the inverse load sensing method and the utilization of the influence coefficient method (ICM) are presented. The ICM also has some similarities to the FEM and the relationship between the two is discussed. In addition, the nature and the influence of different kinds of errors in the process are considered.

By their nature, inverse problems are often ill-posed. Nevertheless, this weakness can be effectively handled by introducing regularization to the equations. Thus, the different regularization techniques are discussed and utilized.

Finally, the use of ICM in the case of load sensing of an elastic roll structure is discussed. Two different approaches to the method are proposed.

#### **3.1 The Formulation of ICM**

The influence coefficient method (ICM) is a straightforward approach for solving unknown quantities of a system. Generally speaking, it is possible to depict any kind of problem with this method by mathematically linking together the unknowns to some known quantities, thereby formulating them in terms of influence coefficients. The influence coefficients are determined so as to characterize the relationship between the input and the response of a system, of which the one is initially known and the other unknown, that depending on the application.

In the formulating process, one needs to assess the given problem by the means of idealized equations. These equations can be linear or nonlinear, exact or non-exact, discrete or continuous, time-varying or stationary, and so forth. The main idea is to find a good and simple solution, which is applicable to the given problem. When the problem field is restricted to linear systems, the theory of superposition can be utilized.

In this study, the subject is an elastic beam-like structure, a roll, which is assumed to behave linearly. Thus, a linear structural analysis, which has to follow the elementary laws and rules of mechanics, is performed. Thus, the influence coefficients are determined by

means of tools used in the field of structural analysis. In this study, the aim is to solve the line loading distribution of the roll by utilizing strain gage measurements. Strain gages are an accurate means of making strain measurements at different points of the structure and give reliable information about even relatively small deformations [Dally & Riley 1991]. Shen [Shen 1986] has also shown that using the strain data in this kind of structural inverse load distribution problems is useful.

Accordingly, the unknown input loading causes a measurable strain response. Thus, the force-strain relationship can be described mathematically in the same fashion as the force-displacement relationship in the theory of matrix structural analysis [Przemieniecki 1968]. The mathematical form of the influence coefficient method is

$$\boldsymbol{\varepsilon} = \mathbf{Z}\mathbf{f} \quad (1)$$

where  $\boldsymbol{\varepsilon}$  is the strain vector,  $\mathbf{Z}$  the coefficient matrix and  $\mathbf{f}$  the loading vector.

The elements of the strain vector  $\boldsymbol{\varepsilon}$  represent the strain at the known measurement points, the elements of load vector  $\mathbf{f}$  characterize the load conditions of the structure, and the influence coefficient matrix  $\mathbf{Z}$  describes the interdependency of the two serving as the system matrix. The problem is inverse in the sense that loading is determined indirectly by measuring strain.

Solution of the input loading  $\mathbf{f}$  using Eq. (1) leads to an inverse linear matrix equation, which might cause problems for the solution accuracy. However, this choice of approach is justified, because the determination of the influence coefficient matrix  $\mathbf{Z}$  can be made neatly as follows. The problems arising from the inverse equation are discussed later in this chapter. Suppose the force vector is combined from a complete set of linearly independent unit load case vectors

$$\mathbf{f} = \mathbf{\Lambda}\tilde{\mathbf{f}} \quad (2)$$

where the  $\tilde{\mathbf{f}}$  vector contains the loading case factors, and the column vectors of load case matrix  $\mathbf{\Lambda}$  are the unit load case vectors given by

$$\mathbf{\Lambda} = [\mathbf{\Lambda}_1 \quad \mathbf{\Lambda}_2 \quad \dots \quad \mathbf{\Lambda}_n] \quad (3)$$

The relationship between load case factors and strains is now

$$\boldsymbol{\varepsilon} = \mathbf{Z}(\boldsymbol{\Lambda}\tilde{\mathbf{f}}) \quad (4)$$

The problem now reduces to the solution of the unknown loading components  $\mathbf{f}$  and loading case factors  $\tilde{\mathbf{f}}$  using the measured information coming from the strain gages. In order to use the model, one has to first determine the coefficients in matrices  $\mathbf{Z}$  and  $\boldsymbol{\Lambda}$ . By definition,  $\boldsymbol{\Lambda}$  is known, because it is given by the user of the model. The influence matrix  $\mathbf{Z}$  has to be more carefully analyzed.

In order to apply the method to a certain structure, one has to first determine the influence coefficient matrix  $\mathbf{Z}$ . This is done by applying unit loads at desired loading points. These unit loads can be discrete point forces or continuous loading functions. The influences of the unit loads, the unit strain responses at the specified measurement points, are thereafter stored as the columns of the influence coefficient matrix.

If one has  $m$  measurement points,  $\mathbf{Z}$  can be formed column-by-column. The column vectors  $\mathbf{z}_i$  are determined by loading the structure with each of the loading cases individually, for which the magnitudes in each case are characterized by loading factors  $f_i$  to assure unit loadings. The strain response  $\boldsymbol{\varepsilon}_i$  of each unit loading case is thereby solved. These loading cases form a set, the overall contribution of which is determined by Eq. (2). For each loading case,

$$\mathbf{z}_i = f_i^{-1} \boldsymbol{\varepsilon}_i \quad (5)$$

During each cycle of defining the column vectors  $\mathbf{z}_i$ , each loading case is set to a certain (unit) value while the rest of the force components are set zero. By repeating this kind of point load procedure  $n$  times, one can form  $\mathbf{Z}$  from the column vectors  $\mathbf{z}_i$ ,

$$\mathbf{Z} = [\mathbf{z}_1 \quad \mathbf{z}_2 \quad \cdots \quad \mathbf{z}_n] = \begin{bmatrix} Z_{11} & Z_{12} & Z_{13} & \cdots & Z_{1n} \\ Z_{21} & Z_{22} & Z_{23} & \cdots & Z_{2n} \\ \vdots & \vdots & \vdots & \ddots & \vdots \\ Z_{m1} & Z_{m2} & Z_{m3} & \cdots & Z_{mn} \end{bmatrix} \quad (6)$$

The determination process can be implemented on the basis of experimental measurements using unit loadings or a computational method, an analytical or a FE model, with which one can determine the strain-force relationship. Eventually, the determination of the unknown load distribution leads to the following cases, in which  $m$  is the number of independent measurement points and  $n$  the number of independent loading cases:

- a) There are more strain points than loading cases,  $n < m$ .
- b) There are as many strain points as loading cases,  $n = m$ .
- c) There are fewer strain points than loading cases,  $n > m$ .

The number of equations in case (a) is larger than the number of unknown loading cases. Thus, the information available for solving the factors is larger than is needed. The solution can, however, be evaluated numerically by means of a least squares (pseudo-inverse) solution in the form

$$\mathbf{f} = (\mathbf{Z}^T \mathbf{Z})^{-1} \mathbf{Z}^T \boldsymbol{\varepsilon} \quad (7)$$

Situation (b) is solved by taking an inverse of the symmetric matrix  $\mathbf{Z}$ , using the equation

$$\mathbf{f} = \mathbf{Z}^{-1} \boldsymbol{\varepsilon} \quad (8)$$

In case (c), the number of equations is less than the number of unknowns. Thus, there is not enough information available for the solution.

For cases (a) and (b), the decomposition of load components for different load cases is obtained by

$$\tilde{\mathbf{f}} = \boldsymbol{\Lambda}^{-1} \mathbf{f} \quad (9)$$

Accordingly, the problem is now stated as an inverse problem. The inverse of influence coefficient matrix  $\mathbf{Z}$  has to be used in order to solve for the loading, originally the input of the system. Typically, the inverse matrix equations can cause problems and are difficult to solve, especially if the linear matrix equation concerned is ill-posed, i.e., if it does not fulfil



the conditions of a well-posed equation as defined by Hadamard (see for example [Engl et al. 1996, p. 31]). This means that small errors in the known response, which is the strain data in this particular case, cause large errors in the unknown force input to be solved. Furthermore, the system matrix is then called ill-conditioned. To overcome the ill-posed problem, one has to obtain more information on the system, modify the matrix, or express the system in such a way that no inverse has to be created. In this work, the approach chosen is to obtain more information on the system, and rephrase the problem as a regularized minimization problem, which will be the subject of section 3.4. But first, let us consider the similarities of FEM and the influence coefficient method in the next section, and also discuss the latter choices of conditioning the system matrix and expressing the system as a forward matrix equation.

### 3.2 FEM and ICM

The basic concept of the influence coefficient method (ICM) is similar to the finite element method FEM. The actual continuous system is formulated into a discrete system of a finite number of degrees-of-freedom (dof's), upon which matrix algebra operations can be formed. This kind of force-displacement relationship is the basis of FEM, the force or displacement method, of which the displacement method is clearly the most popular and typical of the two [Przemieniecki 1968].

The advantage of ICM is that it is based on the direct relationship between the known and the unknown quantities, and it is fairly easy to apply to practical measurements. One could limit the computations to only the interesting or measurable degrees-of-freedom, or treat them in a suitably enhancing way. This approach gives the option to choose the input and response quantities more freely, as compared to FEM. In addition, ICM is an efficient approach to the problem, because *a priori* information about the system can be used in the representation of the system. That enables one to get the same information with fewer elements in the system. Basically, one could consider the influence coefficient method as a specialized case of FEM, because ICM is more direct and more practical with actual measurements. Or, it can be thought of as being the other way around, namely that FEM is a special case of ICM, because it is an idealized presentation of the force-displacement relationship of a structure.

### 3.2.1 The Mathematical connection of FEM and ICM

In any case, one can treat the elementary force-displacement equations of FEM in such a way that they reflect the relationship between strain and load directly, because strain is connected to the displacement by the constitutive equations. Following the displacement method of FEM, the elementary equation of the displacement method is

$$\mathbf{F} = \mathbf{K}\mathbf{U} \quad (10)$$

where  $\mathbf{F}$  is the load vector,  $\mathbf{K}$  is the stiffness matrix and  $\mathbf{U}$  is the displacement vector.

By considering the elementary equation at the element level, a definite connection between FEM and ICM can be found. If one introduces a strain-displacement matrix  $\mathbf{B}$ , which is actually a linear operator matrix, of which the form is determined by the type of element used, then the strain of the element is given by

$$\boldsymbol{\varepsilon}_e = \mathbf{B}\mathbf{u} \quad (11)$$

where  $\mathbf{u}$  is the local displacement vector.

Substituting that into Eq. (8), at the element level,

$$\mathbf{f}_e = \mathbf{Z}_e^{-1}\mathbf{B}\mathbf{u} \quad (12)$$

Thus, at the element level, the stiffness matrix is

$$\mathbf{k}_e = \mathbf{Z}_e^{-1}\mathbf{B} \quad (13)$$

If the force method of FEM is considered, the force-displacement relationship is formed with a sensitivity matrix, which is actually the inverse of the stiffness matrix. Thus

$$\mathbf{U} = \mathbf{K}_f\mathbf{F} = \mathbf{K}^{-1}\mathbf{F} \quad (14)$$

where  $\mathbf{K}_f$  is the flexibility matrix.

At the element level, the connection between the flexibility matrix and the influence coefficient matrix could be determined as in (13) with the strain-displacement matrix  $\mathbf{B}_f$ , but with the exception of not having to invert  $\mathbf{Z}_e$  [Przemieniecki 1968] by

$$\mathbf{k}_{fe} = \mathbf{Z}_e \mathbf{B}_f \quad (15)$$

As mentioned earlier, the influence coefficients act as sensitivities between the input and the response, as does the flexibility matrix in (15), thus it is also called a sensitivity matrix.

These two links to the matrices of FEM represent the possibilities for the internal utilization of FEM in this inverse problem. In the approaches presented to make use of FEM internally, the sensitivity was determined between the strain and the force. However, the difference, as compared to ICM, is that in FEM the characteristics of the system are restricted by the elements into which the system is divided into. Thus, with ICM, one is less dependent on the modal mesh and its nodes, quantities and characteristics.

When the objective, here the elastic roll, is already specified with its particular measurement system, the elements used in FEM are not suitable. Specifically, not all of the degrees-of-freedom used in FEM elements can be defined, because of the lack of measurement data. Thus, the problem is partially defined, and, in the present case, the influence coefficients are rather useful, because they can be fairly freely determined for a linear structure. In theory, if all the dof's of an element mesh could be measured, the global stiffness and sensitivity matrices could be directly utilized. This is possible, for example, with truss structures as proposed by Turco [Turco 1998, 2005]. Moreover, there are ways to decrease the number of dof's in FEM. For example, one could apply stiffness condensation by using master dof's [Nagakiri & Suzuki 1999]. But the effort expended to adapt the partially defined measurement system into the 3-D mesh and condense most of the dof's, would most likely lead to complicated and uncertain expressions. On the other hand, when the measurement system could be designed, bearing in mind the utilization of the FE modal mesh, the straightforward internal approach with FEM could be done as described, if one had access to the system matrices. In any case, the suitable approaches to mesh and measurement setup for internal FEM considerations are left out of the scope of this study, since there are better ways to exploit FEM in the study.

### 3.2.2 Using FEM as an external tool

So far, one has handled FEM internally and in close connection with our main problem, in the sense that one would require ready easy access to the formation of the finite element matrices, vectors and so forth. This could become very difficult, or even impossible, when commercial FEM programs are used. Besides, the outcome of our problem has not even been suitable for that. Fortunately, FEM can be more efficiently utilized by using it externally, in parallel with the main problem. FEM could be used solely as a computational tool for calculating the influence coefficients. This approach was also used by Doyle with a method similar to ICM for partially defined structural problems called sensitivity response method [Doyle 2004]. The unit load procedure is carried out with an accurate FE model of the given structure, and the strains are calculated at the desired points (nodes), i.e., the measurement points. This way, the commercial software could be more easily integrated, and complex 3-D structures could thereby be handled as well. The principle of using a computational model, such as FE model, as an external tool in the inverse load sensing problem, is shown in figure 16.

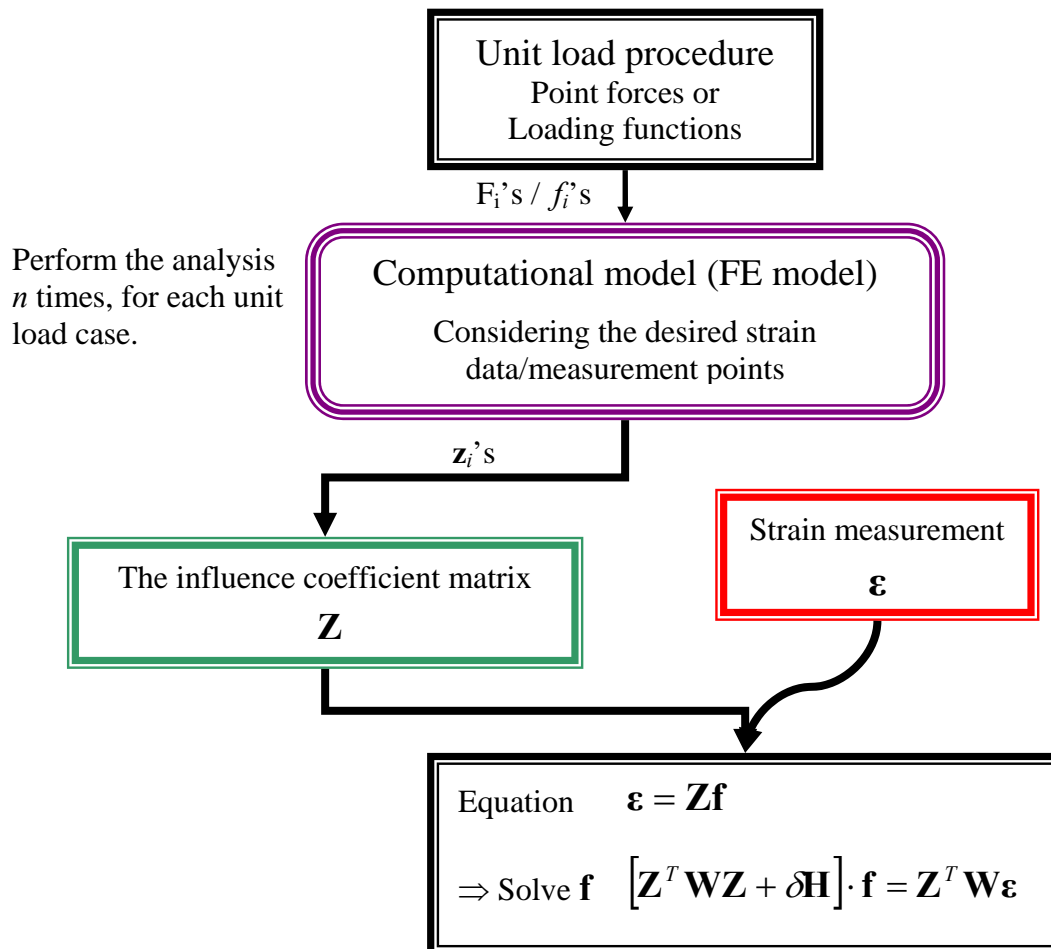


Figure 16. The principle of utilizing a computational model with ICM.

Although FEM has a lot of similarities in ideas and expressions to ICM, the best way to use it in our problem is to use it as described. In addition, other computational methods could be used in the same fashion. Naturally, analytical models such as the Bernoulli-Euler beam theory, or other suitable theories, could be utilized in the same manner. But the weakness of beam theory becomes apparent, when one handles complex structures, such as the tubular shell structure discussed in this work, for example. Overall, the accuracy might not be adequate, and one can only solve for the bending strain with beam theory. Furthermore, the utilization of more accurate analytical models such as ring and shell theories, is inconvenient as compared to FEM

In comparison, using the “complete” stiffness matrices of FEM, the solution error is known to be small, because of the high accuracy of the double precision numbers used in the matrices and vectors, even though it involves some inverse calculations or eliminations. For the partially defined problem that uses the directly determined influence coefficient matrix, on the other hand, solution errors are very likely to appear, mainly because of model compatibility problems, which also include round-off and truncation errors. Typically, large solution errors are caused whenever the elements of the model matrix ( $\mathbf{K}$  or  $\mathbf{Z}$ ) greatly vary due to large stiffness variations ( $\mathbf{K}$ ) or large variations in the influence coefficients ( $\mathbf{Z}$ ), which are ultimately consequences of the incompleteness of the model. The stiffness variations in FEM can be handled by using a more appropriate or accurate model. But in the case of the influence coefficient matrix, the model is already based on partial knowledge of the structural behaviour, and cannot, for the most part, be improved. Hence, large variations in the matrix elements are inevitable, and, more importantly, the matrix  $\mathbf{Z}$  is very likely to be/remain ill-conditioned, and the equation ill-posed, which causes stability problems in the inverse solution. Working with real-life measurements always implies disturbances in the strain data, and, almost certainly, a vague unstable inverse solution [Bathe 1982; Zienkiewicz et al. 2005].

### **3.2.3 Discussion about forward solution**

One way to avoid the inverse solution and eliminate the difficulties associated with ill-posed equations would be to use unit strains instead of loadings, thereby creating a forward solution to the problem of solving unknown loadings, as the response. However, it would be impossible to do the unit strain procedure in practice, although feasible computationally.

As Eq. (10) shows, the displacement method of FEM determines exactly the connection of force and deformation needed for the forward solution. Thus, in theory, FEM could be used to avoid inverse problems. However, in the present study, the inverse approach to the partially defined problem is preferred. The ill-conditioning of the inverse matrices can be reduced or eliminated by slightly modifying the equations using regularization. Next section 3.3 discusses the errors in the solution and section 3.4 proposes suitable regularization techniques to overcome the problems of errors and ill-conditioning.

### **3.3 Errors in the solution**

The errors in the inverse load sensing solution, i.e., the solution errors, are composed of many parts, of which the most relevant are discussed in this chapter. The main factors causing solution errors are the modelling error and the measurement error.

#### **3.3.1 Modelling and measurement error**

Modelling error is simply the error which arises between the computational model from which the system matrix  $\mathbf{Z}$  is determined, i.e., the FE model and the actual structure which is measured. Thus, one has to have a very accurate model of the measured structure, whether it is analytical or computational, from which the strain data is accurately obtained, as compared to the actual strain measurements of the structure. Thus, the modelling error includes the round-off errors, the truncation errors and the discretional errors of the computational model, which are common when FEM is used.

When working with FEM, it is worth noting that the primary variable in FEM is displacement and not strain, which is the measured variable in this work. That being so, the strain at the desired points has to be carefully calculated in order to achieve the best results. For the 3-D FE model of the roll in this study, quadratic shape functions are used, and the strain is therefore linearly distributed along the element surfaces and edges.

A very considerable factor influencing the solution error is the measurement error. When practical measurements are made, there is always some amount of measurement error in the shape of noise, other physical disturbances, errors in the measurement equipment and sensors, or just operational errors. The level of the measurement error might be relatively

small, but its influence on the solution error is always significant, when dealing with ill-posed inverse equations.

### **3.3.2 Errors in the inverse procedure**

Other elements that contribute to the inverse solution error are the condition of the system matrix, which is dependent of the variations of the elements of the matrix, and truncation and round-off errors arising during the inverse calculation process itself. In small systems the determination of the system matrix could lead to a better conditioned system matrix, but still regularization would more likely still be needed. In larger systems that consist of a lot of measurement data, the condition of the system matrix can not be significantly improved, since the equation is notoriously ill-posed. Round-off and truncation errors can be reduced by using double precision numbers.

### **3.3.3 Handling of the error**

Overall, the errors in the inverse load sensing procedure are very harmful for the outcome of the ill-posed equation. In any case, the influence of the previously mentioned errors on the actual solution, especially modelling error and measurement error, can be reduced by using suitable regularization parameters. Nevertheless, regularization does not change the fact that the outcome of bad modelling or insufficient measurements can not be improved by regularization or other mathematical stunts. In other words, regularization is effective up to a certain point only, and its feasibility strongly depends on the measurement data and modelling of the application. Thus, the feasibility of the inverse load sensing method has to be studied, taking into account the presence of errors, and trying to reduce their influence. The solution error can be decreased by optimal regularization.

## **3.4 Inverse problems: ill-conditioning and regularization**

The inverse problem solving approach nearly always leads to an ill-posed equation. The equation does not fulfil the conditions that Hadamard defined for a well-posed equation. In practice, the ill-conditioning means that minor inaccuracies or deviations in the measured data cause large errors in the loading solution. Thus, the results obtained with the particular equations and calculations are not reliable.

Typically, one can evaluate the condition of the particular inverse equation by defining a condition number for the system matrix  $\mathbf{Z}$  using singular value decomposition. Therefore, the condition of the equation depends solely on the system matrix and its properties. The condition number  $\chi$  is the division of the largest singular value  $\sigma_{max}$  by the smallest  $\sigma_{min}$

$$\chi(\mathbf{Z}) = \frac{\sigma_{max}}{\sigma_{min}} \quad (16)$$

Or, by using norms of the matrices,

$$\chi(\mathbf{Z}) = \|\mathbf{Z}\| \|\mathbf{Z}^{-1}\| \quad (17)$$

If the difference between the largest and the smallest singular value is large, or if the smallest singular value is very small, then the condition number becomes large. If the condition number is greater than 1, the matrix is considered ill-conditioned and the entire equation is therefore ill-posed. In that case, the response obtained from the equation is not going to be stable. This is very likely to happen in the case of the partially defined influence coefficient method.

These difficulties can, however, be overcome by modifying Eq. (1) in such a way that the inverse least squares problem becomes a minimization problem. The procedure is called regularization, in which a certain regularization term or terms are added to eliminate the ill-conditioned behaviour. The procedure actually tunes the lowest singular value so that the condition number is not as high. This leads to an “almost correct” response instead of an exact one. This approach is logical, since the measurement data is always somewhat disturbed or inaccurate and also because the model does not completely describe the measured structure. The amount of “the slight incorrectness” is proportional to the added regularization term [Kaipio & Somersalo 2005].

### 3.4.1 Regularization

Nowadays there are a number of regularization techniques available, because of the increasing interest in inverse problems. The book [Engl et al. 1996] of Engl et al. covers



the basic mathematics of regularization and describes the different regularization techniques. In addition to those techniques, Kaipio and Somersalo present some interesting applications of regularization [Kaipio & Somersalo 2005], and a good tutorial of regularization is presented by Neumaier [Neumaier 1998].

Regularization has previously been used in applications that are close to the subject of the current study as well. The given problem could be categorized as a force identification problem, studies of which were discussed in chapter 1. These studies offer various regularization results, which can be exploited here. For example, a number of cases, in which Tikhonov regularization is used effectively with whole-field measurements, and, also with other structural measurements are presented by Doyle [Doyle 2004]. In force identification applications, iterative regularization techniques have been tried, such as [Thite & Thompson 2003b] for example.

Based on applicability, and positive results from the previously-mentioned studies, the regularization technique chosen for use here is Tikhonov regularization. It is a classical regularization method, which was also used by Adams and Doyle [Adams & Doyle 2002] for instance. In Tikhonov regularization, the forward problem, Eq. (1), is solved for  $\mathbf{f}$  by solving the set of simultaneous equations

$$[\mathbf{Z}^T \mathbf{W} \mathbf{Z} + \delta \mathbf{H}] \cdot \mathbf{f} = \mathbf{Z}^T \mathbf{W} \boldsymbol{\varepsilon} \quad (18)$$

where  $\delta$  is the regularization parameter,  $\mathbf{H}$  is a positive definite matrix and  $\mathbf{W}$  describes relative weights on the data. The degree of regularization is controlled with the regularization parameter  $\delta$  and the matrix  $\mathbf{H}$ , and the response can be weighted in accordance with the weighing matrix  $\mathbf{W}$ . The first two both have important and influential functions in the inverse solution, and will be briefly discussed later in this chapter.

Equation (18) can actually be regarded as a minimization of a functional,

$$\arg \min_{\mathbf{f}} \left\{ \|\mathbf{Z} \mathbf{f} - \boldsymbol{\varepsilon}\|^2 + \delta \|\mathbf{D} \mathbf{f}\|^2 \right\} \quad (19)$$

in which  $\mathbf{D}$  describes the smoothness of the solution. It will be discussed later in this chapter together with the matrix  $\mathbf{H}$ .

In order for the Tikhonov regularization to work effectively, one must have some *a priori* information about the solution of the inverse problem. For example, if the value of  $\mathbf{f}$  is known to be close to vector  $\mathbf{f}^*$ , one can use a minimization of a functional

$$\arg \min_{\mathbf{f}} \left\{ \|\mathbf{Z}\mathbf{f} - \boldsymbol{\varepsilon}\|^2 + \delta \|\mathbf{D}(\mathbf{f} - \mathbf{f}^*)\|^2 \right\} \quad (20)$$

A numerically effective way to solve  $\mathbf{f}$  is to use the stacked form of the Tikhonov regularization for Eq. (19). It simply reduces to an over-determined system of normal equations, which have a unique solution given as

$$\mathbf{f} = \tilde{\mathbf{Z}}^{-1} \tilde{\boldsymbol{\varepsilon}} \quad (21)$$

where

$$\tilde{\mathbf{Z}} = \begin{bmatrix} \mathbf{Z} \\ \sqrt{\delta} \mathbf{D} \end{bmatrix} \text{ and } \tilde{\boldsymbol{\varepsilon}} = \begin{bmatrix} \boldsymbol{\varepsilon} \\ 0 \end{bmatrix} \quad (22a, b)$$

For the utilization of Eq. (20) one has to apply

$$\tilde{\mathbf{Z}} = \begin{bmatrix} \mathbf{Z} \\ \sqrt{\delta} \mathbf{D} \end{bmatrix} \text{ and } \tilde{\boldsymbol{\varepsilon}} = \begin{bmatrix} \boldsymbol{\varepsilon} \\ \sqrt{\delta} \mathbf{D} \mathbf{f}^* \end{bmatrix} \quad (23a, b)$$

This formulation of the stacked form is adequate for the scope of this work, but in large-scale inverse problems, the utilization of iterational solution methods, such as the conjugate gradient method for example, can be advantageous [Kaipio & Somersalo 2005].

### 3.4.2 The regularization parameter $\delta$

The degree of regularization is characterized by the regularization parameter  $\delta$ . There are a number of ways to determine the regularization parameter  $\delta$ , an appropriate method can be found by considering the nature of the inverse system. One has to have some kind of *a priori* information about the system, and, furthermore, the quality of the input has an influence on the suitability of a certain method. A good basis for selecting appropriate

methods to determine the regularization parameter  $\delta$  is obtained by investigating different force identification approaches, and, also, other inverse problems. In two references [Doyle 2004; Press et al. 1992], it is suggested that a good starting point for the suitable regularization parameter could be obtained from

$$\delta = \text{Tr}(\mathbf{Z}^T \cdot \mathbf{Z}) / \text{Tr}(\mathbf{H}) \quad (24)$$

This equation actually balances the weights of the two parts in Eq. (18) [Press et al. 1992]. Moreover, *a priori* information is taken in to account, as matrix  $\mathbf{H}$  appears in the expression.

Morozov's discrepancy principle could be considered for choosing the regularization parameter  $\delta$  as well [Engl et al. 1996; Kaipio & Somersalo 2005]. It is a suitable method for problems in which the data is known to be noisy. Here, this technique is attractive, since strain gage measurements are applied, and one has a good estimate of the magnitude of the error. Thus, the regularization parameter  $\delta$  can be defined by using Morozov's discrepancy principle and with the aid of knowledge of the magnitude of the error  $\kappa$  in the input data. Then

$$\|\mathbf{Z}\mathbf{f}_\delta - \boldsymbol{\varepsilon}\|^2 \leq \kappa \quad (25)$$

is acceptable. According to Morozov's discrepancy principle,

$$\|\mathbf{Z}\mathbf{f}_\delta - \boldsymbol{\varepsilon}\|^2 = \kappa \quad (26)$$

Thus, the regularized solution satisfies the data just as much as error level is, if possible, or up to the error level. Therefore, the regularization parameter  $\delta$  should be chosen according to (26). In addition, the measurement  $\boldsymbol{\varepsilon}$  should fulfil condition (27) in order for Morozov's principle to be valid, i.e.,

$$\|\mathbf{P}\boldsymbol{\varepsilon}\| \leq \kappa \leq \|\boldsymbol{\varepsilon}\| \quad (27)$$

where  $\mathbf{P}$  is the orthogonal projection to the current subspace [Kaipio & Somersalo 2005].

Furthermore, another effective and established method for defining the appropriate regularization parameter is the L-curve method, which was proposed by Hansen [Hansen 1992]. In this method, a logarithmic L-shaped curve is constructed to illustrate the relationship of the residual norm (data misfit) and the solution (semi)norm. A typical L-curve, with its logarithmic axes, is presented in figure 17. The ideal value of the regularization parameter is obtained in the slope point of the graph, where the relationship of the two is mostly “in balance”, and can be defined from it. Thus, the L-curve method is actually *a posteriori* method [Hansen 1991].

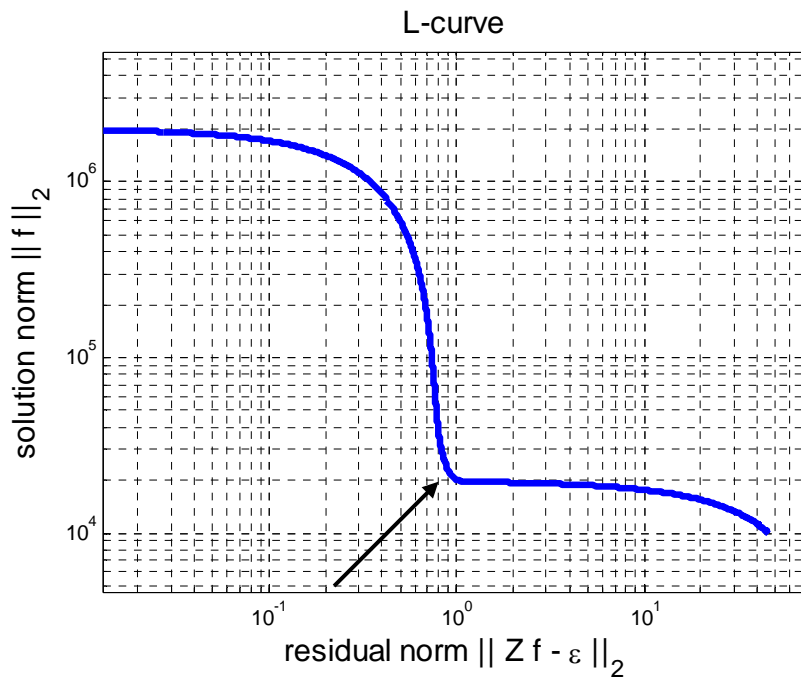


Figure 17. The L-curve and the ideal position of the regularization parameter pointed out with an arrow.

For the Tikhonov regularization method, a comparison of different parameter selection procedures in inverse force identification problems has been studied [Busby & Trujillo 1997; Jacquelin et al. 2003; Choi et al. 2007b]. In conclusion, the L-curve method was found to perform best. In comparison, the discrepancy principle tends to give slightly smaller parameter estimates as compared to the L-curve [Engl et al. 1996].

### 3.4.3 The effect of matrices $\mathbf{D}$ and $\mathbf{H}$

The solution of the regularization also depends on the choice of matrix  $\mathbf{H}$  in (18). It is a positive definite matrix, and constructed from a matrix  $\mathbf{D}$ , which describes the dependency

of the elements between each other, i.e. the smoothness, in the solution vector  $\mathbf{f}$ . The  $m \times m$  matrix  $\mathbf{H}$  is obtained from  $\mathbf{D}$  by

$$\mathbf{H} = \mathbf{D}^T \mathbf{D} \quad (28)$$

If there is no connection between the elements of  $\mathbf{f}$  or, more commonly, if a good starting point is needed, then one could use  $m \times m$  unit matrix as  $\mathbf{H}_0$  ( $\mathbf{D}_0$ ). Given simply by

$$\mathbf{H}_0 = \mathbf{D}_0 = \begin{bmatrix} 1 & 0 & \dots & 0 \\ 0 & 1 & \dots & 0 \\ \vdots & \vdots & \ddots & \\ 0 & 0 & & 1 \end{bmatrix} \quad (29)$$

This is called zeroth-order regularization. If the elements of  $\mathbf{f}$  are known to have some kind of connection *a priori*, for example, if the solution is known to be smooth or continuous, one could use first order linearization  $(m-1) \times m$  matrix  $\mathbf{D}_1$  [Doyle 2004]

$$\mathbf{D}_1 = \begin{bmatrix} -1 & 1 & 0 & \dots \\ 0 & -1 & 1 & \dots \\ 0 & 0 & -1 & \dots \end{bmatrix} \quad (30)$$

Other functionals that describe the dependency of elements of  $\mathbf{f}$  can be used as well. Depending on the case, the suitable matrix  $\mathbf{D}$  (thus matrix  $\mathbf{H}$ ) is chosen.

#### 3.4.4 Inverse crime

When testing the inverse system by simulated calculations, where one artificially generates the measurement data by computations, it is important to keep in mind the concept of inverse crime. Inverse crime occurs, when one simulates the model in an incorrect way, using the same system for the simulation, as was used for the determination of the system matrix. This leads to over-optimistic results, because one can not assume the system model to be the exact description of the behaviour of the real system. Then, the modelling error is ignored [Kaipio & Somersalo 2005, 2006; Wirgin 2004].

The inverse crime should always be avoided, if possible. Typically, one has to use a different and more accurate computational model for the numerical simulation of the measurement data. Therefore, the strain data should be calculated with a non-congruent and more accurate FE model to simulate the measurement data than the FE model of the actual system matrix. Another way to avoid the modelling error is to test the system with random error added to the strain data.

### 3.5 Determination of influence coefficients of a roll structure

Now, let's return to the application of the inverse load sensing method of the line loading distribution of a roll structure. Consider a roll which is affected by a unique line loading, shown in the figure 18. The strains of the inner wall of the roll can be measured, and the axial loading profile of the line load is to be solved on the basis of the strain data with the influence coefficient method.

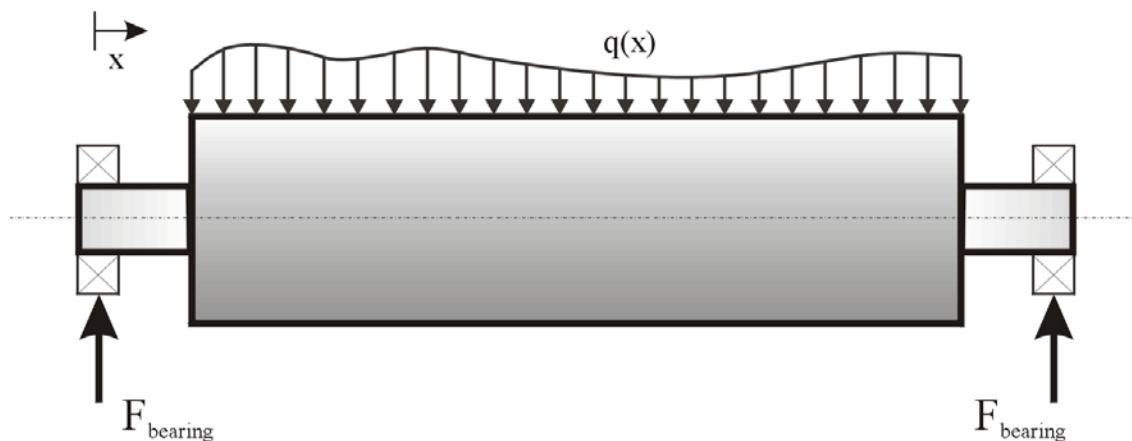


Figure 18. A roll structure under line loading.

First, one has to decide how to describe the axial line loading case properly; accordingly, one has to decide how to determine the influence coefficients. Here, two different approaches to the problem are considered the principle of which is demonstrated in figure 19. As illustrated in figure 19a, a set of discrete unit point forces is used to describe the line loading distribution, and as illustrated in figure 19b, a set of continuous unit loading functions is used to describe the line loading distribution. Using these two unit load approaches, one is able to carry out the determination of the influence coefficients, i.e., the unit load procedure.

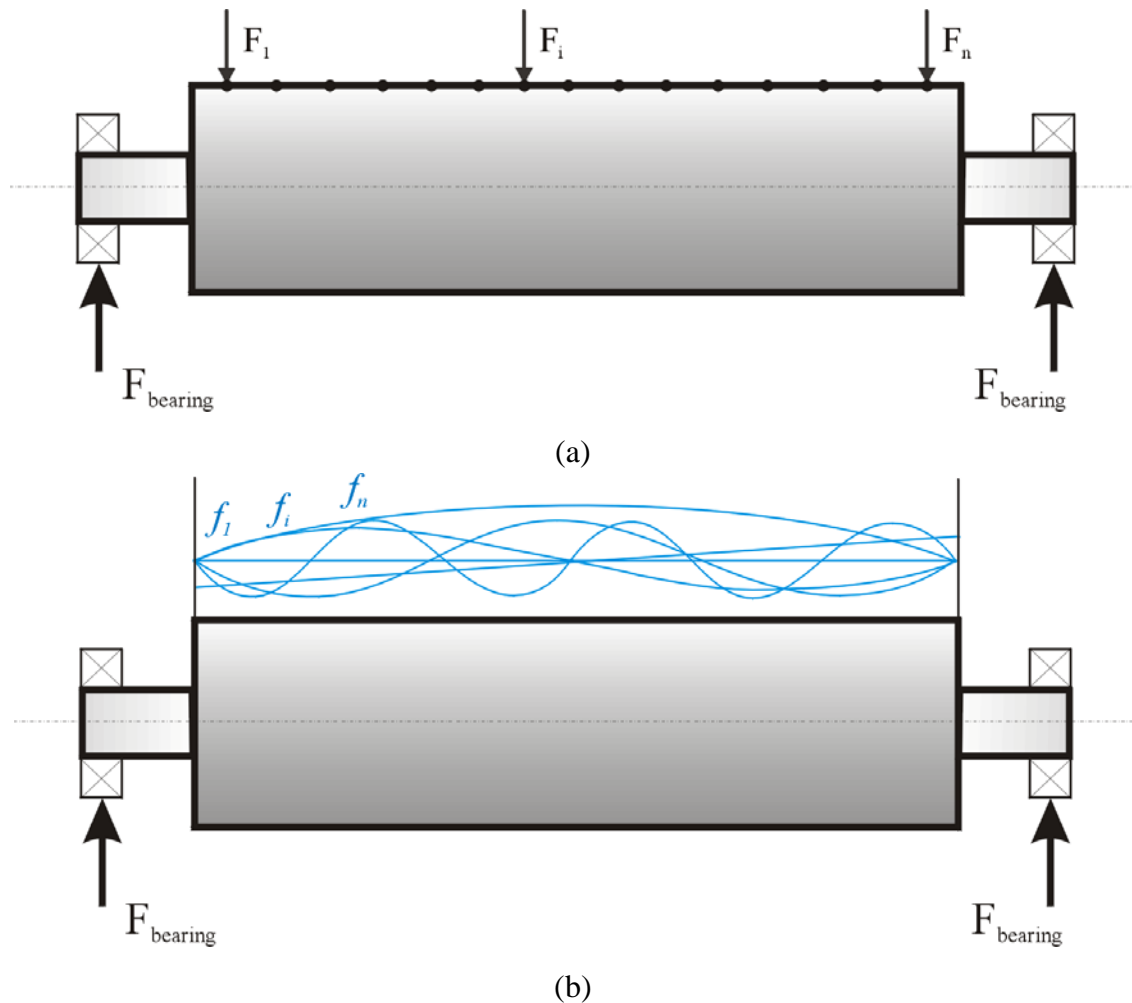


Figure 19. Examples of unit point force (a) and unit loading function (b) approaches of ICM acting on a roll structure.

### 3.5.1 Unit point force approach

The first approach of using unit point forces is convenient, because it is simple to imply computationally, as well as experimentally. In the computational approach, it is possible to use an analytical solution such as, in this case, the Bernoulli-Euler beam theory, or a purely numerical method like FEM. In both cases, point loadings are easy to apply as nodal forces. In the experimental case, point forces are easy to produce fairly accurately too. In describing the actual continuous line loading by discrete forces, the accuracy is improved, naturally, by increasing the number of discrete forces. Also, every type of continuous loading is describable with point forces.

### 3.5.2 Unit loading function approach

The latter approach of using continuous unit loadings is obvious, because the actual loading case, the line loading, is continuous as well. On the downside, it is very difficult to do the experimental arrangement for it. Thus, the computational treatment remains as the only realistic way of doing this. In this approach, the continuous loadings present a basis for the line loading; they act as basis functions of the line loading. Thus, for describing every type of load distribution with this continuous basis, the basis functions need to be carefully defined. Evidently, complete functional bases are the most suitable. The same type of approach using influence coefficients as functions was proposed for a simple Bernoulli-Euler beam [Hurty & Rubinstein 1964]. Furthermore, the same type of method of modal functions has been used in force identification studies [Perezat & Gyuander 1995; Liu & Shepard 2006]. Moreover, this type of functional approach that uses complete functional bases has been investigated for paper machine applications by Shakespeare [Shakespeare 2001].

In the present case, two complete well-behaving functional bases are considered, namely, two beam eigenmode function bases. Because the line loading varies axially, and the roll structure can be regarded as a beam, both eigenfunction bases are justified. When the number of basis functions is sufficient enough, the basis is theoretically complete. However, in practice, the number of strain gages is limited which thereby also limits the number of basis functions used. Therefore, the basis can not really be complete, although with these functional bases the presentation is very accurate with only a relatively small number of functions.

For the unit load function approach, eigenmode functions from the Bernoulli-Euler beam theory are used. More precisely, the eigenmodes are taken from the length of the shell of the roll  $L$ , for which end conditions are found to be simply supported (SS) or free-free (FF). In addition, the rigid body modes are included as unit functions as well. The rigid body modes for the length  $L$  are simply

$$\phi(z)_{r1} = 1 \quad , \quad \phi(z)_{r2} = \left( z - \frac{L}{2} \right) \quad (31)$$



The simply supported eigenmode basis for  $k$ th eigenfrequency is obtained from

$$\phi(z)_{SS} = \sin(\beta z) \quad (32)$$

where the variable  $\beta$  is obtained from the frequency equation

$$\sin(\beta L) = 0 \quad (33)$$

$$\Rightarrow \quad \beta = \frac{k\pi}{L} \quad (34)$$

The free-free eigenmode basis for  $k$ th eigenfrequency is obtained from

$$\phi(z)_{FF} = \psi(\cos \beta z + \cosh \beta z) + (\sin \beta z + \sinh \beta z) \quad (35)$$

where the coefficient  $\psi$  is

$$\psi = -\frac{\sin(\beta L) - \sinh(\beta L)}{\cos(\beta L) - \cosh(\beta L)} \quad (36)$$

and the variable  $\beta$  is obtained from the frequency equation

$$\cos(\beta L) \cosh(\beta L) = 1 \quad (37)$$

In this case the root  $\beta$  has to be numerically calculated, but for large values of  $k$

$$\beta \approx (2k + 1) \frac{\pi}{2L} \quad (38)$$

In addition, the existence of hyperbolic functions in Eqs. (35) and (36) leads to problems in computational precision with large values of  $k$ . To avoid those problems approximations

$$\psi \approx -1 \quad \text{and} \quad \phi(z)_{FF} = -\cos(\beta z) + \sin(\beta z) \quad (39a, 39b)$$

are used for values  $k > 11$ .

These two represented eigenmode functional bases are used as the functional influence coefficients. Finally, the influence coefficients of the roll structure can be determined for a unique continuous line loading acting on the roll according to the different ways presented in section 3.5. This enables one to obtain the required system matrix for the inverse load sensing method. However, this approach ignores all of the other forces acting on the roll, such as body forces as well as other external point forces and tractions. In a rotating roll of a nip unit, a number of dynamic forces act on the roll among the to-be-measured continuous line load. For consistency, one has to take all the dynamic forces into account. In the next chapter, the dynamics of the rotating rotor (roll) are discussed more carefully.

## 4. Dynamics of a flexible rotor

In this chapter, the dynamics of a flexible rotor are considered. This is done keeping in mind that the main application of the method presented is to a roll, which is regarded as a continuous rotor. The important equations relating to the rotor dynamics of a roll structure are derived, and solved for the relevant loading cases. In addition, the influence coefficient balancing procedure of a flexible roll is presented as well.

### 4.1 Equations of motion for a flexible continuous rotor

The vector representation of a flexible rotating rotor can be presented in fixed and rotating coordinate systems as shown in figure 20.

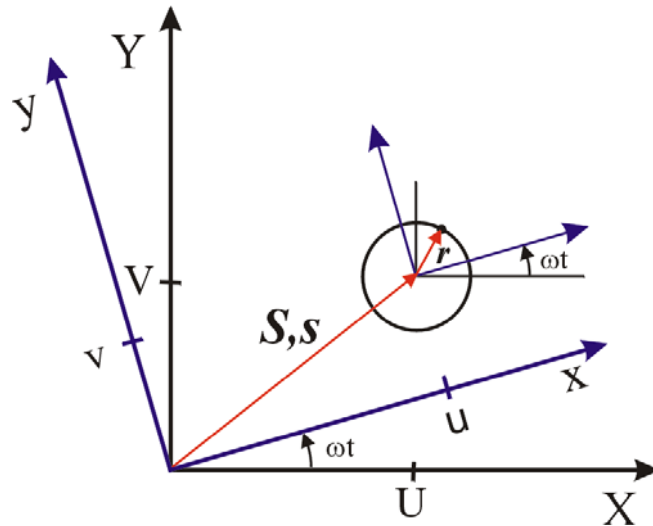


Figure 20. The vector representation of a rotor in two coordinate systems.

$\mathbf{S}$  is the elastic displacement vector in a fixed coordinate system,  $\mathbf{s}$  is the elastic displacement in the rotating coordinate system,  $\mathbf{r}$  is the local position vector and  $\omega$  is the rotational speed. The rotating roll is considered a continuous beam structure. Thus, the significant displacement is in bending in the lateral  $z$ -direction and the displacements  $\mathbf{S}$  and  $\mathbf{s}$  are

$$\mathbf{S} = \begin{Bmatrix} U(z) \\ V(z) \end{Bmatrix} \quad (40)$$

and

$$\mathbf{s} = \begin{Bmatrix} u(z) \\ v(z) \end{Bmatrix} \quad (41)$$

The two coordinate systems have the relation

$$\mathbf{S} = \mathbf{A}\mathbf{s} \quad (42)$$

where the transformation matrix

$$\mathbf{A} = \mathbf{A}(t) = \begin{bmatrix} \cos \omega t & -\sin \omega t \\ \sin \omega t & \cos \omega t \end{bmatrix} \quad (43)$$

is therefore time-dependent.

One could also take into account the rotational degrees-of-freedom shown in figure 24 by introducing the vector form

$$\mathbf{\Theta} = \begin{Bmatrix} \theta_X(z) \\ \theta_Y(z) \end{Bmatrix} \quad (44)$$

The derivation of the equations of motion follows [Chen & Gunter 2005] for rotating Bernoulli-Euler beams. In general form, the Lagrange energy equations are given by

$$\frac{d}{dt} \left( \frac{\partial T}{\partial \dot{q}_i} \right) - \frac{\partial T}{\partial q_i} + \frac{\partial U_{pot}}{\partial q_i} = \Sigma F_i \quad (45)$$

where  $T$  is the kinetic energy,  $U_{pot}$  potential energy,  $q_i$  the general coordinate, and  $\Sigma F_i$  global non-conservative loading components.

The translational kinetic energy of a material point of a rotor (shaft segment) in the fixed coordinate system is

$$T_{tr} = \frac{1}{2} \int_0^L (\rho A (\dot{U}^2 + \dot{V}^2)) dz \quad (46)$$

where  $\rho$  is the density and  $A$  the cross-sectional area of the rotor. And using the vector notations (40), it reduces to

$$T_{tr} = \frac{1}{2} \int_0^L (\rho A \dot{\mathbf{S}}^T \dot{\mathbf{S}}) dz \quad (47)$$

The angular moments of a material point of the rotor (shaft segment), assuming small angular displacements, are

$$\begin{aligned} L_X &= I_d \dot{\theta}_X + I_p \omega \dot{\theta}_Y \\ L_Y &= I_d \dot{\theta}_Y - I_p \omega \dot{\theta}_X \\ L_Z &= I_p \omega \end{aligned} \quad (48)$$

where  $I_d$  and  $I_p$  are the diametrical and polar moments of the beam cross-section, and terms  $I_p \omega \dot{\theta}_Y$  and  $-I_p \omega \dot{\theta}_X$  the gyroscopic moments. Thus, the rotational kinetic energy is

$$T_{rot} = \frac{1}{2} \int_0^L (I_d (\dot{\theta}_X^2 + \dot{\theta}_Y^2) + I_p \omega (\theta_Y \dot{\theta}_X - \theta_X \dot{\theta}_Y) + I_p \omega^2) dz \quad (49)$$

The last term of (49) is caused by spinning energy and can be ignored from the elastic displacement investigation. Using the vector notions from (44), and the relation  $I_p = 2I_d$  for a circular cross section, rotational kinetic energy reduces to

$$T_{rot} = \frac{1}{2} \int_0^L I_d \dot{\Theta}^T \dot{\Theta} dz + \int_0^L I_d \omega \Theta^T \begin{bmatrix} 0 & -1 \\ 1 & 0 \end{bmatrix} \dot{\Theta} dz \quad (50)$$

in vector notation. The bending strain of a rotor shaft segment at a local material point  $\mathbf{r}$  in the rotating reference is

$$\boldsymbol{\varepsilon} = -\mathbf{s}''\mathbf{r} \quad (51)$$

which produces the potential energy

$$U_{pot} = \frac{1}{2} \int_0^L E \mathbf{s}''^T I_d \mathbf{s}'' dz \quad (52)$$

where  $E$  is Young's modulus and  $I_d$  the diametrical moment.

This can be transformed back into the fixed reference frame using (42). For a symmetrical rotor ( $\mathbf{A}\mathbf{A}^T = \mathbf{I}$ ),

$$U_{pot} = \frac{1}{2} \int_0^L EI_d \mathbf{S}''^T \mathbf{S}'' dz \quad (53)$$

Using Lagrange equations, the equations of motion of a rotor (shaft segment) in the fixed coordinate reference can be simplified for a differential slice of the rotor by recalling the relations  $\theta_x = \frac{\partial U}{\partial z}$ ,  $\theta_y = \frac{\partial V}{\partial z}$  and the dynamic moment equation for a Bernoulli-Euler beam, given by

$$V_{X,Y} - \frac{\partial M_{X,Y}}{\partial z} = M_{RI} + M_{GYRO} \quad (54)$$

On the left side of Eq. (54),  $V_{X,Y}$  represents the shear force and  $M_{X,Y}$  represents the bending moment in the X- and Y-directions, respectively. The right side of Eq. (54) consists of rotary inertia  $M_{RI}$  and gyroscopic moment  $M_{GYRO}$ , which originate from the rotational displacements. Thus, for a differential slice of the rotor, the equations of motions for a rotating Bernoulli-Euler beam in the fixed coordinate reference are obtained as

$$\begin{aligned} EI_d U'''' + \rho A \ddot{U} - \frac{\rho A R^2}{4} (\ddot{U}'' + 2\omega \dot{V}''') + c \dot{U} &= F_X(t) \\ EI_d V'''' + \rho A \ddot{V} - \frac{\rho A R^2}{4} (\ddot{V}'' + 2\omega \dot{U}''') + c \dot{V} &= F_Y(t) \end{aligned} \quad (55)$$

These equations include the rotary inertia and gyroscopic moment as 3<sup>rd</sup> and 4<sup>th</sup> terms, and the effects of damping  $c$  originating from the velocity dependent dissipation of energy. They can also be found from the rotor dynamics literature [Ehrich 1992; Yamamoto & Ishida 2001]. Moreover, with a Bernoulli-Euler beam, one ignores the effects of shearing and shear coupled with rotary inertia, each of which can be modelled with Timoshenko beam theory.

#### 4.2 Solving the equations of motion for typical loading cases

The equations of motion for a flexible rotor were derived in the last section. In this chapter, Eq. (55) is solved for typical loading cases of the governing roll structure.

The integrations of the Lagrange energy equation can be performed by transforming from the fixed global coordinate system of the rotor into the principal coordinate system. It can be done by using the transformation

$$\mathbf{S} = \mathbf{N}^T \mathbf{X} \quad (56)$$

where

$$\mathbf{N} = \begin{bmatrix} \mathbf{n} & 0 \\ 0 & \mathbf{n} \end{bmatrix} \quad (57)$$

and

$$\mathbf{n} = \begin{bmatrix} n_1(\xi) \\ n_2(\xi) \\ \vdots \\ n_k(\xi) \end{bmatrix} \quad (58)$$

The vector  $\mathbf{n}$  consists of suitable basis functions  $n_i(\xi)$  's. In the case of a finite element treatment, the basis functions (shape functions) would be chosen to fit the conditions at the nodes of the (beam) element concerned and the local coordinate system. In our case, it is sufficient to use only the stationary eigenfunctions, i.e., the natural modes of the beam, as a

basis in the principal coordinate system, which includes the translational displacements. Thus, the displacements of the rotor are expressed in terms of the natural modes.

The rotor is assumed to be simply supported with stiff supports. Thus, the natural modes are the sine wave functions previously presented in section 3.5 by Eq. (32). Finally, by using modal coordinates, the equations for a rotor having a constant rotational speed, which is a typical situation for paper machine rolls, are obtained. The equations of motion for the two degrees-of-freedom in the generalized matrix form are given by

$$\mathbf{M}\ddot{\mathbf{X}} + (\mathbf{C} + \omega\mathbf{G})\dot{\mathbf{X}} + \mathbf{K}\mathbf{X} = \mathbf{Q} \quad (59)$$

where the matrices are

$$\mathbf{M} = \mathbf{M}_{tr} + \mathbf{M}_{rot} = \rho A \int_0^L \mathbf{N}\mathbf{N}^T dz - I_d \int_0^L \mathbf{N}'\mathbf{N}'^T dz \quad (60)$$

$$\mathbf{G} = -(-2\mathbf{g}) = -I_p \int_0^L \mathbf{N}' \begin{bmatrix} 0 & 1 \\ -1 & 0 \end{bmatrix} \mathbf{N}'^T dz \quad (61)$$

$$\mathbf{K} = EI_d \int_0^L \mathbf{N}''\mathbf{N}''^T dz \quad (62)$$

$$\mathbf{Q} = \int_0^L \mathbf{F}\mathbf{N} dz \quad (63)$$

Matrix  $\mathbf{C}$  corresponds to damping, which is initially assumed to be zero ( $c = 0$ ).

#### 4.2.1 Response to gravity

Gravity acts on a flexible roll structure as a constant body force in the negative Y-direction, and it can be regarded as a conservative force associated with a potential energy. Treating the gravitational potential according to Lagrange's equations, and using a fixed global coordinate system, the right side of (55) reduces to

$$\mathbf{F}_g = \begin{bmatrix} 0 \\ -\rho A g \end{bmatrix} \quad (64)$$



Because gravity is independent of time, for the stationary situation of the roll, all the time-dependent terms can be neglected in (59). Thus, for the case of gravity, one is left with the equation for the static case, in which the modal coordinates could be utilized, using (62) and (63), given by

$$\mathbf{K}\mathbf{X}_g = \mathbf{Q}_g \quad (65)$$

The response to gravity in the fixed coordinate reference is calculated from the equation

$$\mathbf{S}_g = \mathbf{N}^T \mathbf{X}_g = \mathbf{N}^T \mathbf{K}^{-1} \mathbf{Q}_g \quad (66)$$

#### 4.2.2 Response to unbalance force

The unbalance force is related to the rotational speed. Since the rotational speed is assumed to be constant, the non-conservative force caused by unbalance in the equations of motion of a rotor (55) is

$$\mathbf{F}_{ub} = \omega^2 \mathbf{A} \boldsymbol{\mu}(z) = \omega^2 \mathbf{A} \begin{bmatrix} \mu_X \\ \mu_Y \end{bmatrix} \quad (67)$$

where the first mass moment with respect to neutral axis ( $z$ ) is

$$\boldsymbol{\mu}(z) = \int_A \boldsymbol{\rho} \mathbf{r} dA \quad (68)$$

The unbalance forces cause whirling of the rotor. If one changes to the rotating coordinate reference of (41) by using the transformation matrix  $\mathbf{A}$ , the higher order and time-dependent terms can be neglected. Hence, the dominating equations of motion, which consider static, as well as dynamic unbalance, are reduced to

$$EI_d \mathbf{s}'''' - \omega^2 \rho A \mathbf{s} = \omega^2 \boldsymbol{\mu}(z) \quad (69)$$

where the second term on the left is caused by the centrifugal force and is a function of the rotational speed. The solution of (69) can be obtained using the modal coordinates, given as

$$\mathbf{s} = \mathbf{s}_{ub} = \omega^2 (\mathbf{K} - \omega^2 \mathbf{M})^{-1} \mathbf{Q}_{ub} \quad (70)$$

where

$$\mathbf{Q}_{ub} = \int_0^L \boldsymbol{\mu}(z) \mathbf{N} dz \quad (71)$$

### 4.2.3 Response to lateral line loading

In a paper machine nip contact, the lateral (CD) line loading acts against the rolls as the dominating load. When studying the deformations of one of the rolls, it can be regarded as a continuous traction load acting on the roll surface. Thus, the right side of the Eq. (55) is given in the vector component form as

$$\mathbf{F}_q = \begin{bmatrix} q_X(z) \\ q_Y(z) \end{bmatrix} \quad (72)$$

Furthermore, the treatment of the equations of motion follows the same path as with the gravitational force. The equations of motion reduce to the static form, similar to (65) in the stationary case, since the loading is independent of time. The magnitude of the line loading across the rotor in the z-direction and the angular position  $\alpha$  of the line loading with respect to the fixed X-axis, can be taken account with

$$\begin{aligned} q_X(z) &= q(z) \cos \alpha \\ q_Y(z) &= q(z) \sin \alpha \end{aligned} \quad (73)$$

where  $q(z)$  is the line load profile in the radial direction at the nip. Thus, the solution for the line loading case is obtained by using the principal coordinates given as

$$\mathbf{S}_q = \mathbf{N}^T \mathbf{K}^{-1} \mathbf{Q}_q \quad (74)$$

In conclusion, the quasi-static treatment of the line load, and thus the influence coefficient method as well, is justifiable when the rotational speed is kept constant.

Interestingly, when the rotor is unbalanced and the line loading is acts on it, the deformation (strain) response is difficult to handle. The influences of the two are very hard to distinguish from measurement data since the frequencies of each of them are controlled by the rotational speed. Considering the strain measurements of the inverse load sensing method, this kind of situation should be avoided.

#### **4.2.4 Other components affecting the deformations in rotation**

The rotary inertia and the gyroscopic moments in the equations of motion do not actually have any influence on the responses of the governing undamped loading cases. In fact, these dynamic terms have a noticeable effect on the response at higher speeds. In addition, the effect of shear deformations was assumed to be insignificant since the displacements are small.

Moreover, these rotor investigations did not consider the effects of shell displacements or modes. For a constant rotational speed, the significant shell displacements can be assumed to behave in the same manner as the bending displacements. Thus, their quasi-static treatment in the case of gravity and a lateral line loading is justified, and the dynamical components in them can be regarded as insignificant.

It can also be mentioned that the elastic natural modes of a tubular shell structure, such as the lower roll of the pilot roll press, occurs at higher frequencies than the rotational frequencies of a normal run [Järvinen 2003]. Nevertheless, considering the strain measurements of the inverse load sensing method, all resonance situations should be avoided. Moreover, the rotational speed related vibration caused by the roll unbalance is harmful, since it would confuse the strain measurement data and could not be filtered properly.

### 4.3 Balancing of flexible rotors

The balancing procedure of flexible rotors can be done on the basis of either of two different techniques: modal balancing [Bishop & Gladwell 1959; Kellenberger 1972] or influence coefficient balancing [Goodman 1964; Lund & Tonnesen 1972; Tessarzik et al. 1972]. In the modal balancing procedure, the modal unbalance components are determined experimentally, and eliminated from the rotor step-by-step. In influence coefficient balancing, the influences of trial weights on the measured vibration at multiple points are determined experimentally. And formulating those influences in mathematical form, the correction masses of the rotor can be evaluated. In addition, unified methods, which combine the advantages of both of the methods, have been proposed [Tan & Wang 1993; Kang et al. 1996]. In this study, the obvious interest is in influence coefficient balancing, since it relies on the same procedure as the inverse method for load sensing does here.

Influence coefficient balancing for the continuous rotor was introduced by Goodman [Goodman 1964]. Since then, the progress of the method has been steady, and there have been many impressive scientific publications that have considered, for example, the basics of the method, the feasibility of the method, and the development of the algorithm of the method.

We will first consider the original algorithm for the influence coefficient balancing of a continuous rotor. The procedure depends on the number of measurement planes, i.e., measurement points  $m$ , and the number of correction planes  $n$  that one uses for the balancing. The balancing procedure can be carried out for one or more different rotational speeds. In the former case,  $m$  is equal to  $n$  [Tessarzik et al. 1972], and in the latter  $m$  is greater than  $n$  [Goodman 1964].

The basis of the balancing procedure is the assumption of linear dynamical characteristics of the flexible rotor which, in principle, include all of the vibrational modes. The vibrational response of the rotor can be given as a superpositional sum of the selected balancing planes. Thus, the response of the rotor at each balancing plane is determined by placing one or more trial masses at the planes, and measuring the deflection response of each trial mass at each measurement point in both the X- and Y-directions. Performing the

measurement in two directions ensures that the magnitude, as well as the phase (angular position) of the unbalance in each plane can be detected. This procedure can be given as

$$\begin{aligned}\Delta\mathbf{U} &= \mathbf{Z}_x \mathbf{F} \\ \Delta\mathbf{V} &= \mathbf{Z}_y \mathbf{F}\end{aligned}\quad (75)$$

where the influence coefficient matrix  $\mathbf{Z}$  is constructed by placing trial weights  $\hat{m}$  in the balancing planes into a known angular position, in the x-direction for instance. Thus,

$$\begin{aligned}\mathbf{z}_x^i &= \frac{1}{\omega^2 \hat{m}} \Delta\mathbf{U} \\ \mathbf{z}_y^i &= \frac{1}{\omega^2 \hat{m}} \Delta\mathbf{V}\end{aligned}\quad (76)$$

and based on the measurements in both the X- and Y-directions and the magnitude of the trial weights, the elements of the influence coefficient matrix  $\mathbf{Z}$  are determined. This procedure can also be expanded to  $k_\omega$  rotational speeds, in which case the trial weight measurements are repeated  $k_\omega$  times at each different rotational speed. Thus, there are more equations than unknowns, and the optimal answer is calculated by the sum of least squares as proposed by Goodman [Goodman 1964]. Then, the general correction weights are

$$\boldsymbol{\mu} = \omega^2 (\mathbf{Z}^T \mathbf{Z})^{-1} \mathbf{Z}^T \mathbf{S}_{ub} \quad (77)$$

where  $\mathbf{S}_{ub}$  includes the measured displacements originating from the initial unbalance of the rotor. If the number of trial weights equals the number of measurement points as proposed by Tessarzik et al. [Tessarzik et al. 1972], the correction weights are

$$\boldsymbol{\mu} = \omega^2 \mathbf{Z}^{-1} \mathbf{S}_{ub} \quad (78)$$

Matrix  $\mathbf{Z}$  represents the measured dynamical response of the rotor at the measurement points and rotational speeds. In the case of a simple rotor, such as a single disk on a shaft, this dynamical relation can be determined theoretically, but for continuous flexible rotors, the experimental approach is more popular, since it is fairly practical and easy to apply in

different rotor systems, and the theoretical relation is often troublesome to obtain. In the case of a flexible continuous rotor, the modal coordinates can also be utilized as

$$\boldsymbol{\mu} = \omega^2 \mathbf{N}^T (\mathbf{Z}^T \mathbf{Z})^{-1} \mathbf{Z}^T \mathbf{X}_{ub} \quad (79)$$

Moreover, FEM has also been utilized in balancing flexible rotors. For instance, Kang has investigated the utilization of the method in the case of unsymmetrical applications, such as for crankshafts, and proposed a modified influence coefficient method, which utilizes the FEM models in the determination of the influence coefficients [Kang et al. 1996, 1997, 2000].

Because of the mathematical basis this procedure shares with the inverse line load sensing, the same conclusions apply: this is also an ill-posed inverse problem and therefore sensitive to the condition of the matrix  $\mathbf{Z}$ . Even so, the tolerance for measurement errors in the influence coefficient balancing is relatively acceptable, 3-4 % [Lund & Tonnesen 1972; Kang et al. 2003], and the balancing procedure itself has been efficient, since performing appropriate repetitions. the balancing result could be improved up to some point. Nevertheless, for instance, a method is discussed, with which the condition number of the influence coefficient matrix is minimized by choosing the most suitable measurement points [Kang et al. 2006].

As presented, influence coefficient balancing has been acknowledged as a feasible inverse method for rotor balancing. The major difference with respect to the inverse line loading case is that the phase, or the rotational dimension of the quantity measured (unbalance/distributed loading), is fixed in the line loading case. The correction weights of the rotor balancing can be placed in different angular positions freely and effectively, whereas the line loading case can be corrected only in one angular position, namely, the nip. This proves the line loading case to be more sensitive and difficult. Moreover, enhancements have to be sought from regularization and the use of functional coefficients. Finally, the optimization of the condition number of the system matrix could be considered.

## 5. Analysis of the accuracy and sensitivity issues of the inverse load sensing method

The accuracy and sensitivity of the inverse load sensing method are mainly dependent on the measurement points, as well as the model and the approach to modelling itself. In this chapter, a closer look to the matters mentioned above is taken by examining the selection of optimal measurement points and the description of line loading by the two unit loading cases.

### 5.1 Preliminary analysis of the strain set-up and the unit point force cases

Initially, the measurement points should be located in the roll structure in such a manner that sufficient strain information about the deformation caused by the current line load would be available. A good starting point would be to examine the actual strain plots of the roll installation under nominal loading and run. The respective axial and the tangential strains measured from the centre of the roll inner wall are presented in figure 21. These strain plots show unfiltered raw signals that include the effects of gravity and centrifugal forces.

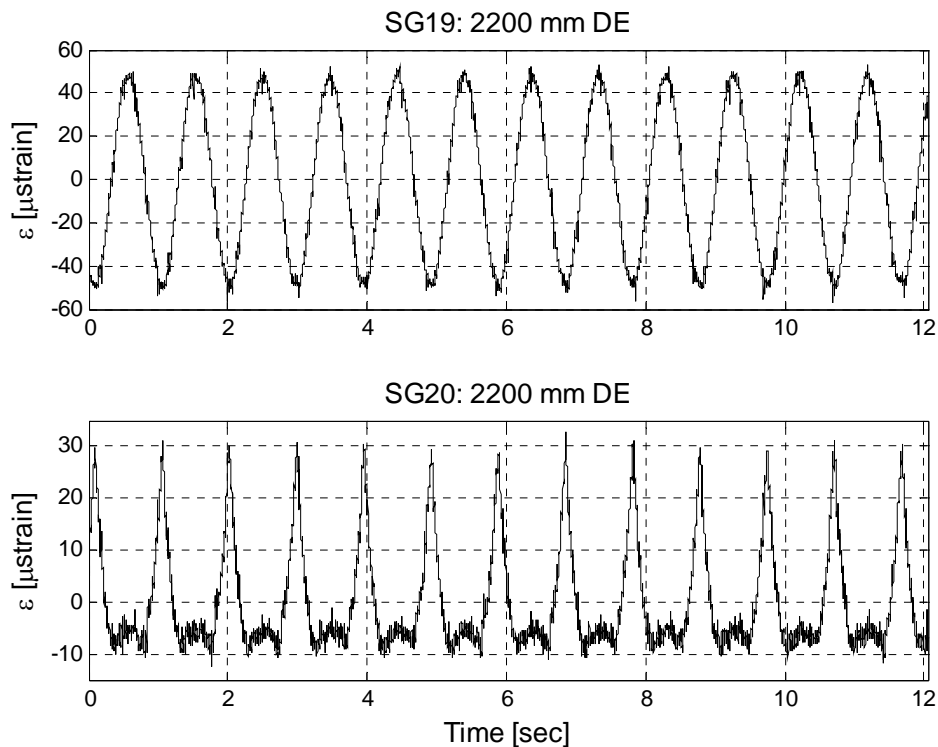


Figure 21. Measured axial (upper) and tangential (lower) strains under nominal loading of lower roll.

During each revolution, the most sensitive (most detectible) measurement instants or positions can be clearly distinguished. They are clearly located near the local extreme values. These peak values occur, when the measurement point is in the nip and when it is opposite the nip. The same conclusion is made for both axial and tangential strains. Accordingly, the best angular measurement positions for both measurement directions are the line load angular position and the angular position opposite to it. These positions are chosen for closer examination, as the preliminary analysis, in the case of unit point force cases. From now on, they are referred as the “top” and “bottom” positions, respectively.

For the preliminary analysis, four different point force distributions were selected, which respectively consist of 5, 10, 22 and 44 point forces naturally corresponding to the number of unit loads. In every case, the point forces are positioned such that each one individually acts on a small segment of the line of contact between the rolls, i.e.; the point forces are equally spaced and they each describe the corresponding line load acting on these incremental areas (line load segments) equivalently. These four point force cases are compared to a constant line loading case. Each case is analyzed with the beam theory, as well as an FE model. The bending strains are calculated in both the top and the bottom surfaces of the inner wall, using both computational models, while the tangential strains are obtained with the FE model only. The dimensions of the roll structure are collected in table 1 and the load cases investigated are illustrated in table 2. These presented dimensions correspond to the dimensions of the roll structure of the nip unit, and will be used in the calculations of that particular structure.

Table 1. The dimensions and material constants of the roll structure.

The length of the roll shell	$L$	4.4 m
Dimension a	$a$	0.475 m
Outer roll diameter	$R$	0.525 m
Inner roll diameter	$r$	0.475 m
Young's modulus of shell (GRS300)		140 GPa
Poisson number of shell		0.27
Young's modulus of ends (GRP400)		180 GPa
Poisson number of ends		0.27



Table 2. The four different unit point force cases.

Unit point force cases	
case I	
$d5 = 880 \text{ mm}$	
case II	
$d10 = 440 \text{ mm}$	
case III	
$d22 = 200 \text{ mm}$	
case IV	
$d44 = 100 \text{ mm}$	

The application of beam theory to the roll structure is straightforward. One can solve the axial strains of the roll by calculating the strain at the desired measurement points from the bending moment  $M_t$ . When the boundary conditions are known,  $M_t$  can be solved from the beam equations

$$EI_z \frac{\partial^4 w}{\partial x^4} = -q(x) \quad (80)$$

$$M_t(x) = -EI_z \frac{\partial^2 w}{\partial x^2} \quad (81)$$

where  $E$  is the elastic modulus of the beam,  $I_z$  the moment of the cross section,  $q(x)$  the loading and  $w$  the vertical displacement. The properties of the shell material GRP300 were used in the beam theory calculations. The bending strain of the inner roll surface is then calculated with a straightforward application of Hooke's law

$$\varepsilon(x) = \frac{M_t(x)}{EI_z} r \quad (82)$$

where  $r$  is the inner radius of the roll.

The FE model used here is constructed of the ends and the shell. It has 179194 10-node tetrahedral elements and 292761 nodes with quadratic shape functions. There are three element layers on the shell, and both ends are simply-supported from the rotational centres of the bearings. This FE model is also used for the determination of the influence coefficient matrix of the roll structure, and is illustrated in figure 22.

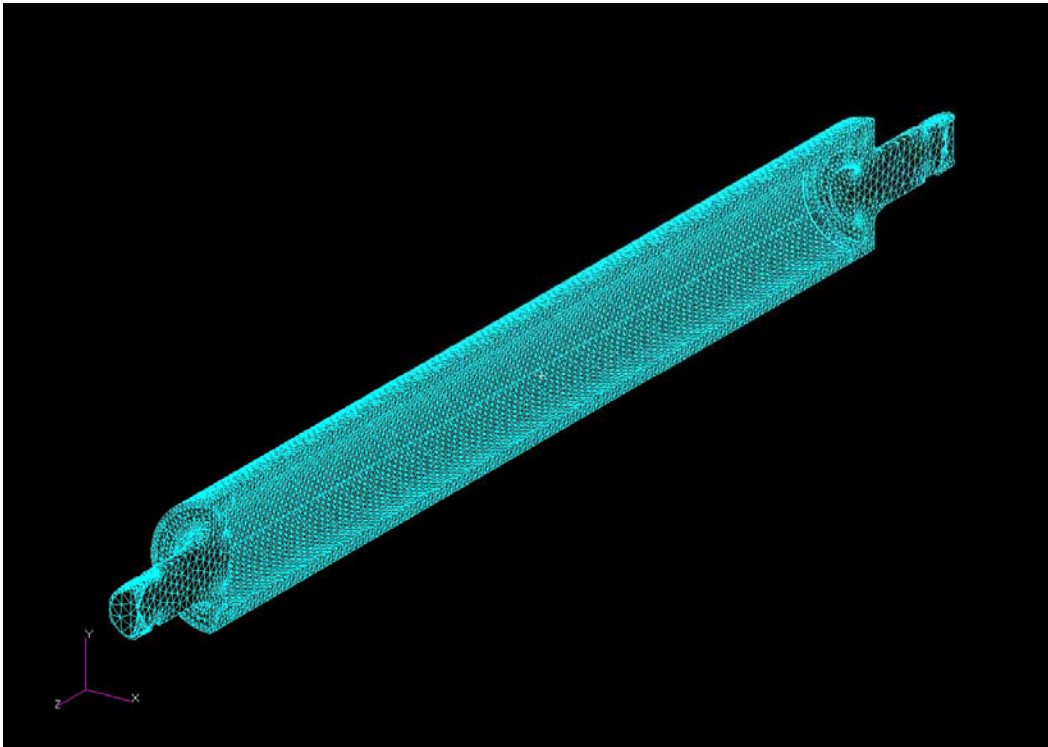


Figure 22. The FE model used for the unit loads.

The results of the point force analyses are shown in figures 23-28 respectively.

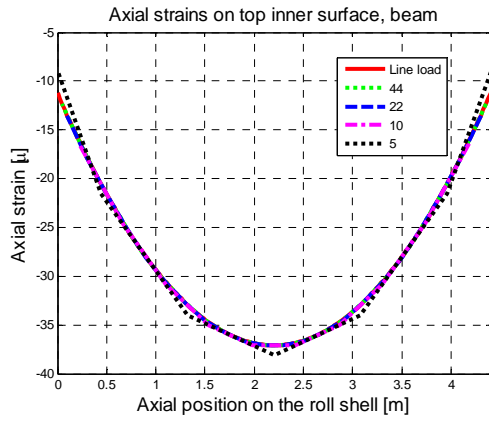


Figure 23. Top axial strain, beam theory.

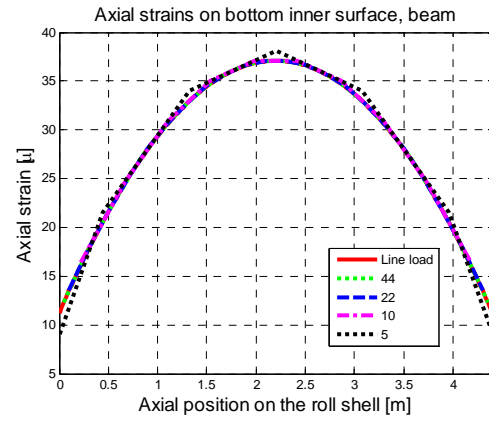


Figure 24. Bottom axial strain, beam theory.

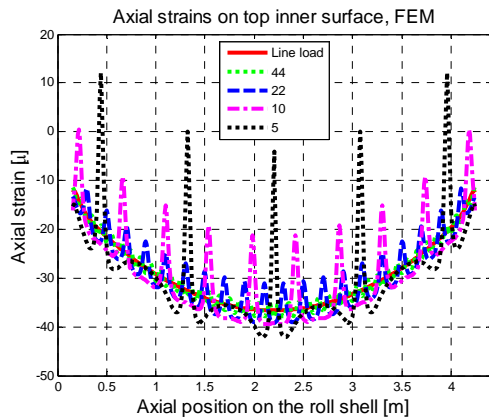


Figure 25. Top axial strain, FE model.

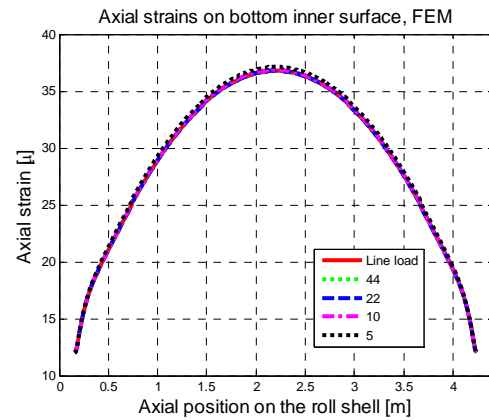


Figure 26. Bottom axial strain, FE model.

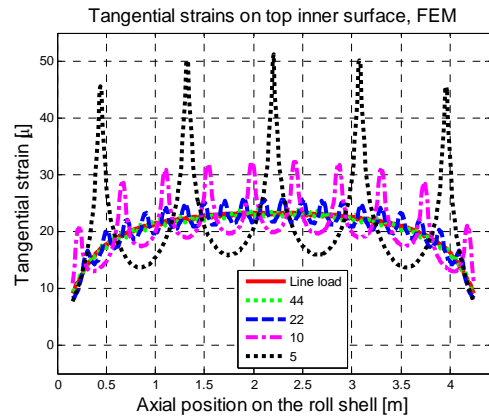


Figure 27. Top tang. strain, FE model.

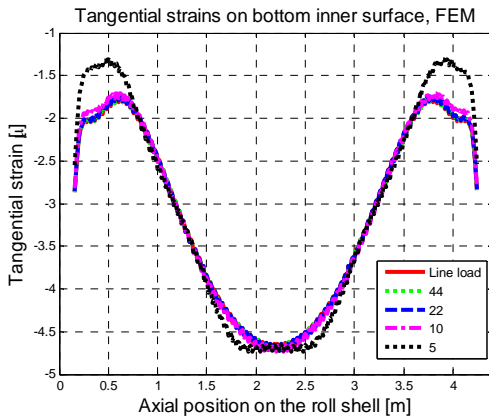


Figure 28. Bottom tang. strain, FE model.

Replacing a continuous line load with a discrete load distribution has a noticeable effect on the behaviour of the roll structure. On a local scale, the deformations increase near the point forces. If one takes a closer look at the bending strain in the roll structure based on the beam theory, as in figures 23 and 24, it is evident that there are differences between the strains in the continuous line load case and the those in the case of coarsest point force distribution; these differences are found near the application points of the point forces in the latter case. But at one point between each point force location, the bending strain is the

same for both loading cases. These points are located exactly at the boundaries between the smaller incremental segments of the line load. Thus, if one would like to measure line load using this kind of point force distribution, these points between the point forces would be the best choices, according to the beam theory. When looking at the strains computed with the FE model, especially in the axial direction, it shows that the two coarser load cases (I and II) tend to give a bit lower strains than the actual line load case. Cases III and IV are almost identical to the actual line load, thus, at least 22 point forces on a structure like this seem to be enough for describing the line load and adequate for line load sensing.

Beam theory does not take account of the shell deformations, and does not therefore distinguish the top and bottom loading cases. From the strain plots of the FE model, in figures 25-28, it is clearly evident that the shell deformation has a significant influence on the strains at the “top” position. The local strains near the point forces are significantly large and, the coarser the distribution, the bigger the effect of local strains, as the strain plots of cases I and II seem to considerably deviate from those of the line loading case. Accordingly, in the “top” position, the strain distribution from the point force cases does not represent the strain distribution of the line loading well, even though it is statically equivalent to it. This corresponds to Saint Venant’s principle, which states that in the immediate vicinity of the points of application of the loads, the stress (strain) distribution can not be assumed to be independent of the actual mode of application of the loading (see for example [Outinen & Salmi 2004, p. 133]). Furthermore, the computation in the immediate vicinity of the points of loading is often unreliable, even when FEM is used.

On the basis of Saint Venant’s principle and figures 25 and 27, one can draw the conclusion that if one is trying to measure line loading on this kind of a roll structure with a discrete measurement system, the measurement points have to be located a bit away from the loading points, but still located where they remain sensitive to the loading. As shown in figures 26 and 28, measurement points located at the “bottom” position are suitable for line load sensing since the local strains of the discrete loadings are not harmful. Considering real measurements, the use of strain gage rosettes would be convenient since they measure the strain at a point in two or more directions.

Now, considering the axial position of the measurement points, it can be said that one would naturally tend to measure as extensively as possible along the length of the roll. The

choice is obvious, since the line loading to be measured affects on the entire length of the roll. Another concern is the location of various measurement points with respect to one another. Ultimately, the axial strain set-up has an influence on the system matrix, and more importantly, on the condition of the matrix. In conclusion, different load set-ups that cover the inner width of the roll efficiently at the “bottom” position are proposed and tried. In the case of real measurements, where the strain set-up is already fixed, the maximum number of strain points is utilized.

## 5.2 Preliminary analysis of the unit loading function cases

The selection of loading points with the continuous unit loading functions is not as tedious as with the unit point forces since the continuous basis generates the same strain response as the actual function it describes, according to linearity and the theory of superposition. In comparison, one has to choose the appropriate number of functions in order to describe different loading profiles accurately. To get an idea of the accuracy of different function sets, their error norm percentages for two typical loading profiles, a linear “hat” type (HAT) and a sine type (SINE) as illustrated in figure 29, are calculated.

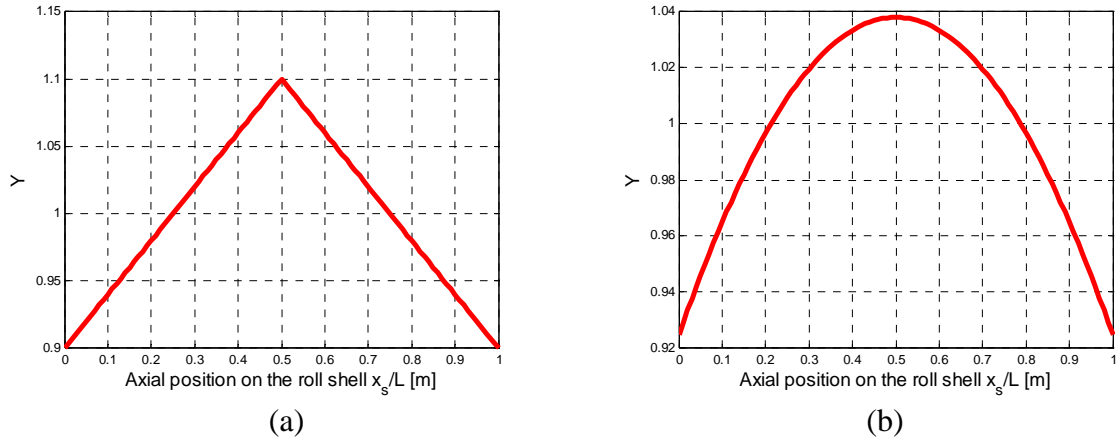


Figure 29. Linear HAT (a), and SINE (b) loading profiles.

The total error norm percentage is calculated by

$$error_p = \frac{\|\mathbf{f}_{orig} - \mathbf{f}_{calc}\|}{\|\mathbf{f}_{orig}\|} \quad (83)$$

where  $\mathbf{f}_{orig}$  describes the original known load and  $\mathbf{f}_{calc}$  the calculated load.

The curve fitting is carried out using the Matlab® function “lsqcurvefit”, which is a nonlinear curve fitting algorithm in the least-squares sense, it is applied to each function set and the fits are then compared to the original loading function (profile). The errors for these two function sets are shown in table 3. For the SINE profile, the error is relatively small, and this conclusion can also be drawn in the case of the profile having the same mathematical basis as the function set itself (constant, line, sine etc.) On the other hand, when the profile is different from the shape of the functional basis, as the linear HAT function is, the accuracy is somewhat lower.

Table 3. Magnitude of error while using FF and SS functional bases.

Number of functions / Function basis used	Loading profile	5	10	22	44
SS, error norm (%)	HAT	0.52	0.20	5.65e-2	2.24e-2
FF, error norm (%)	HAT	0.47	0.19	5.49e-2	2.22e-2
SS, error norm (%)	SINE	4.45e-2	9.29e-3	1.11e-3	1.85e-4
FF, error norm (%)	SINE	7.61e-2	1.71e-2	2.54e-3	7.12e-4

In addition, the influence of random error in the coefficients of each function set is tested by adding 1 % of normally distributed random error to each of the coefficients and making the comparison. The cases are plotted in figures 30 and 31, and the error percentage presented in table 4. Here, the effect of error is clearly evident, the estimations oscillating vigorously, although the profiles are still somewhat recognizable. The problem with the error is that it mostly effects the smallest coefficients of estimates that are supposed to be zero or close to zero. The errors in these coefficients are the main source for the unwanted deviations, as demonstrated. Nevertheless, the two handled function sets are considered and used for describing typical line loading profiles.

Table 4. Magnitude of error while fitting FF and SS functional bases with random error percentage of 1 %.

Number of functions / Function basis used	Loading profile	5	10	22	44
SS, error norm (%)	HAT	1.48	1.54	3.36	4.26
FF, error norm (%)	HAT	2.88	3.09	4.85	7.29
SS, error norm (%)	SINE	1.41	2.17	2.76	3.84
FF, error norm (%)	SINE	1.74	3.32	3.62	6.34

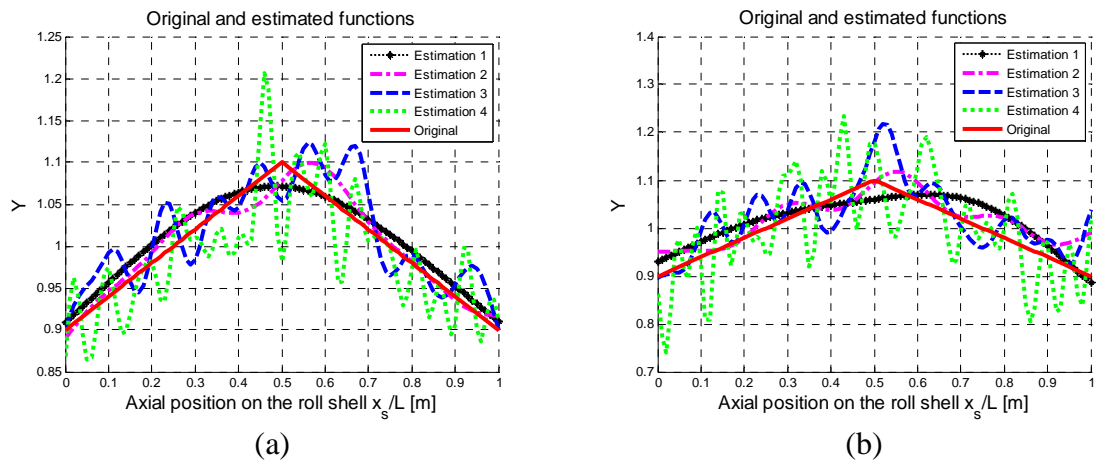


Figure 30. Curve fitting to linear HAT function with added error of 1 %, SS (a), FF (b).

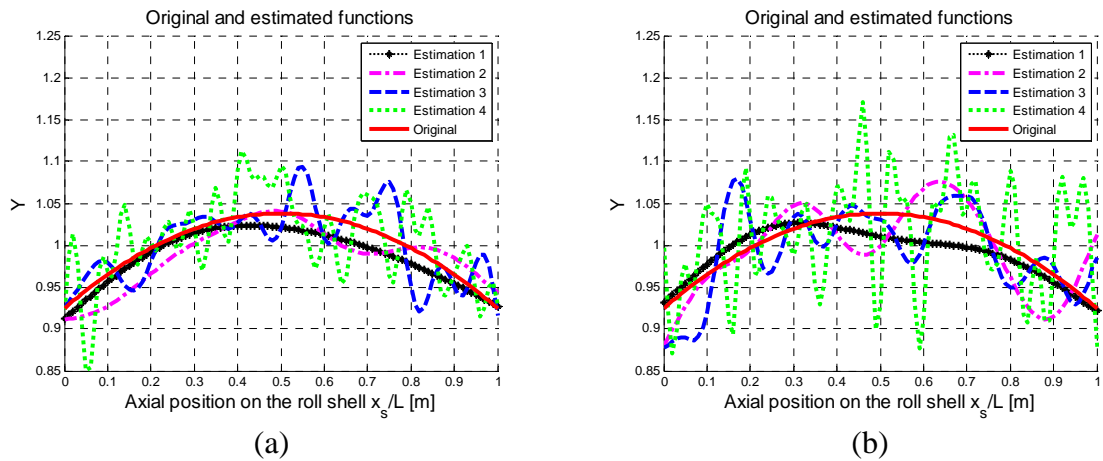


Figure 31. Curve fitting to SINE function with added error of 1 %, SS (a), FF (b).

### 5.3 Considerations on strain

#### 5.3.1 Strain calculation of FEM

Regarding the method that makes use of FEM, it turns out that the FEM mesh has a strong influence on solution accuracy. As mentioned earlier, strain is not the primary variable of FEM, but rather displacement is. Strain is the derivative of displacement, and, thus the strains at individual nodes are calculated by integrating the strain over the whole element over the shape functions. Then, the estimation of the strain at different nodes is usually done by averaging. A more accurate way of calculating strain at nodes of the element mesh is to use “super-congruent” points, which can be determined by patch tests [Zienkiewicz et al. 2005].

In this study, the magnitudes of the strains at measurement points are relatively small, only about 10 – 70 microstrain ( $10^{-6}$  m/m). If one were to use the patch test for instance, then in comparison to typical averaging, there would be noticeable “errors” in the strain values that would be included in the modelling error. The errors that originate from the actual modal mesh and elements, moreover, are included in the modelling error strain values. Another source of errors is the actual measurement data (the response data), which includes measurement error. If one considers the influence of the differences of patch test and averaging on the other presented error sources, their influence is smaller and therefore insignificant. Thus, the strain values of the different nodes can be adequately calculated simply by averaging.

Ultimately, this assumption is valid for the strain points of the roll structure, and for different kinds of structures, especially the more complicated ones, the strain determination by averaging versus by the patch test have to be carefully considered and, if necessary, the influences of the strain determination have to be confirmed by tests. Furthermore, the inverse calculation model has to describe the behaviour of the measured structure well, and the inverse calculation process has to have enough tolerance for errors to get reliable results. This has to be confirmed by testing the measurement systems and structures. These tests for the roll structure will be done in the following chapters, first evaluating different strain and load set-ups using simulations in chapter 6 and then evaluating the feasibility and suitability for the real-life measurements in chapter 7, in which the strain points are already fixed.

### **5.3.2 Mapping of strain**

Mapping could be utilized for obtaining more strain information about the structure in the cases, for which there is a limited amount of strain data. This has clearly been demonstrated to be feasible for beam structures by Shen [Shen 1986], and for whole-field strain measurements with different structures by Doyle [Doyle 2004]. Hence, the use of mapping considering this problem is justified.

When considering the strain plots of figures 23-28, where the roll was under constant line load, one could infer that mapping might be a good tool, since the strain distributions in both the axial and tangential direction are nicely continuous at the chosen “bottom” position. But on the other hand, the mapping of strains merely adds to the degradation of



accuracy and reliability. In fact, the usage of loading functions, or even the description of loading distributions with a couple of point forces, also adds to the inaccuracies from all the other error sources. Thus, for now, the concept of mapping strain is left out of the scope of this study. In sections 6.2.1 and 6.2.2 the proposed method is verified and evaluated for cases with varying amounts of data, by using various simulated sets of strain data.

## **6. Analysis of the inverse load sensing method in different static loading cases**

In this chapter, the feasibility of the method is tested by applying it in different applications. As well as doing measurements, the structures investigated are modelled with appropriate computational models. Firstly, two static structures are studied in the case of point forces acting on them. Then, a roll structure is modelled using the inverse load sensing method, and different strain gage set-ups, and loading approaches are evaluated by using artificially calculated strain data from different load distributions.

### **6.1 Using inverse load sensing method for solving point forces on beam-like structures**

When concentrating on resolving a single point force acting on a structure using strain measurements, the force identification can be done relatively accurately. Doyle [Doyle 2004] demonstrates this for both static and dynamic cases. The capability of the inverse method is also demonstrated in several force identification studies [Busby & Trujillo 1997; Adams & Doyle 2002; Thite & Thompson 2003b] for static and dynamic cases. Here, the method is tested with two different case studies, one of which is a simply supported prismatic beam, and the other a tubular roll-like structure. The two structures are investigated in the case of static point forces acting on them, as was also discussed by the author [Romppanen et al. 2005]. The following section 6.1 merely assures and demonstrates the feasibility of the method in the case of real measurements and point forces.

#### **6.1.1 Case study 1, a simply supported prismatic beam**

Case study 1 is a simply supported prismatic beam made of structural steel that has an overall length of 1000 mm, a supported length of 900 mm and a cross-section of  $15 \times 15$  mm. The beam has, altogether, nine strain gages installed on the bottom of the beam to measure the bending strain. The structure is illustrated in figure 32. The system matrix  $\mathbf{Z}$  was determined experimentally, applying point forces individually, as well as making computational use of the Bernoulli-Euler beam theory, the significant equations of which were presented in section 5.1. All of the nine strain gages were utilized, and together with

nine unit loadings, they produce a square influence coefficient matrix. Thus, Eq. (8) can be used. In the case of the experimental determination, the unit loads are averaged over five measurements. The locations of the strain gages, as well as the unit force set-up, are shown in figure 33.

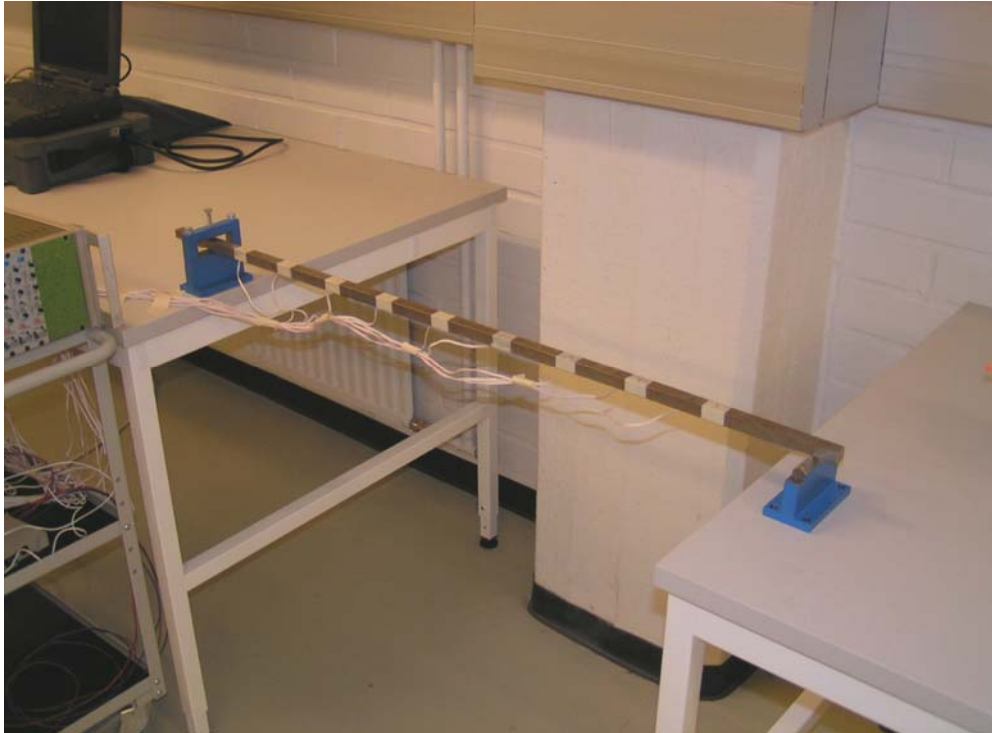


Figure 32. Case study 1.

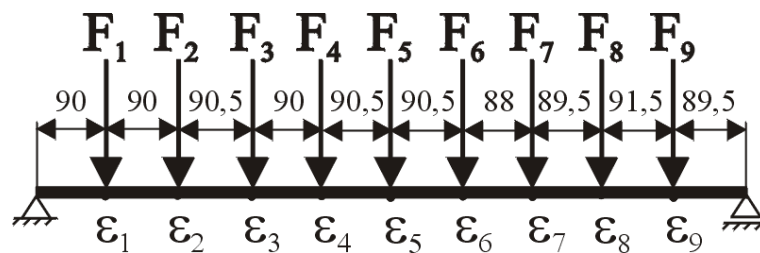
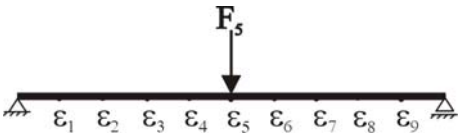
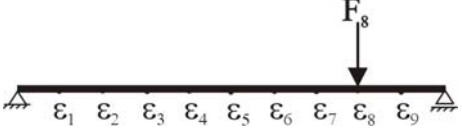
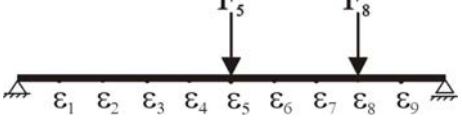
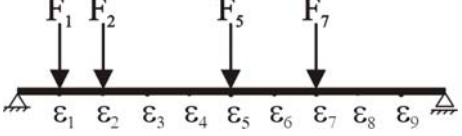


Figure 33. Unit force and strain set-ups of case study 1.

The point forces were applied to the structure by hanging weights at the loading points, and, thereby, the magnitudes of point forces were known. Different point force loadings are applied to the structure, and the calculated inverse solutions based on the measured strain data are compared to the actual magnitudes of the point forces. The inverse solutions are calculated with direct (8) and regularized (19) equations, the condition numbers of the matrices are determined according to Eq. (17), and the error norm percentage based on Eq. (83) was calculated. The results are collected in table 5.

Table 5. Results from the prismatic beam case study,  $\delta = 10^{-2}$ .

Loading case	Inverse solution using the experim. IC matrix	Inverse solution using the experim. IC matrix regularized	Inverse solution from the beam theory	Inverse solution from the beam theory regularized
Condition number of the matrix	38.98		39.93	
 <p>Magnitude of the point force <math>F_5 = 19.72</math></p>	$f = \begin{bmatrix} 2.35 \\ 0.31 \\ -0.84 \\ 0.58 \\ \mathbf{19.92} \\ 0.27 \\ -0.45 \\ -0.02 \\ -0.00 \end{bmatrix}$	$f = \begin{bmatrix} 2.24 \\ 0.31 \\ -0.91 \\ 1.41 \\ \mathbf{18.52} \\ 1.13 \\ -0.56 \\ -0.08 \\ 0.01 \end{bmatrix}$	$f = \begin{bmatrix} -0.07 \\ -0.04 \\ 0.06 \\ 0.50 \\ \mathbf{17.18} \\ 1.59 \\ -1.31 \\ 1.09 \\ -0.86 \end{bmatrix}$	$f = \begin{bmatrix} -0.07 \\ -0.06 \\ -0.07 \\ 1.19 \\ \mathbf{16.16} \\ 2.15 \\ -1.25 \\ 0.90 \\ -0.76 \end{bmatrix}$
Error norm (%)	13.41	16.82	18.20	23.62
 <p>Magnitude of the point force <math>F_8 = 49.20</math></p>	$f = \begin{bmatrix} -1.35 \\ 0.43 \\ -0.53 \\ 0.33 \\ 0.00 \\ -0.01 \\ -0.12 \\ \mathbf{49.40} \\ -0.24 \end{bmatrix}$	$f = \begin{bmatrix} -1.20 \\ 0.30 \\ -0.42 \\ 0.27 \\ -0.08 \\ -0.54 \\ 2.36 \\ \mathbf{45.65} \\ 2.25 \end{bmatrix}$	$f = \begin{bmatrix} -2.02 \\ 0.02 \\ -0.16 \\ 0.45 \\ -1.52 \\ 2.38 \\ -2.59 \\ \mathbf{49.48} \\ -2.66 \end{bmatrix}$	$f = \begin{bmatrix} -1.90 \\ -0.08 \\ -0.10 \\ 0.33 \\ -1.32 \\ 1.58 \\ -0.13 \\ \mathbf{45.99} \\ -0.36 \end{bmatrix}$
Error norm (%)	3.22	10.23	10.39	8.73
 <p>Magnitude of the point forces <math>F_5 = 9.91</math> <math>F_8 = 19.72</math></p>	$f = \begin{bmatrix} 1.15 \\ 0.36 \\ -0.56 \\ 0.38 \\ \mathbf{9.98} \\ 0.04 \\ -0.18 \\ \mathbf{19.74} \\ -0.17 \end{bmatrix}$	$f = \begin{bmatrix} 1.13 \\ 0.34 \\ -0.56 \\ 0.79 \\ \mathbf{9.24} \\ 0.29 \\ 0.74 \\ \mathbf{18.21} \\ 0.83 \end{bmatrix}$	$f = \begin{bmatrix} -0.34 \\ 0.03 \\ 0.04 \\ 0.39 \\ \mathbf{7.99} \\ 1.69 \\ -1.62 \\ \mathbf{20.34} \\ -1.57 \end{bmatrix}$	$f = \begin{bmatrix} -0.31 \\ 0.01 \\ -0.02 \\ 0.70 \\ \mathbf{7.56} \\ 1.65 \\ -0.61 \\ \mathbf{18.84} \\ -0.59 \end{bmatrix}$
Error norm (%)	6.41	11.44	15.87	14.59
 <p>Magnitude of the point forces <math>F_1 = F_7 = 19.72</math> and <math>F_2 = F_5 = 9.91</math></p>	$f = \begin{bmatrix} \mathbf{17.82} \\ \mathbf{10.55} \\ -0.54 \\ 0.42 \\ \mathbf{9.47} \\ 0.87 \\ \mathbf{19.08} \\ 0.24 \\ -0.17 \end{bmatrix}$	$f = \begin{bmatrix} \mathbf{17.34} \\ \mathbf{10.53} \\ -0.17 \\ 0.60 \\ \mathbf{8.68} \\ 2.18 \\ \mathbf{17.56} \\ 1.15 \\ -0.35 \end{bmatrix}$	$f = \begin{bmatrix} \mathbf{15.01} \\ \mathbf{9.45} \\ 0.45 \\ 0.50 \\ \mathbf{7.14} \\ 3.24 \\ \mathbf{15.42} \\ 2.91 \\ -2.13 \end{bmatrix}$	$f = \begin{bmatrix} \mathbf{14.56} \\ \mathbf{9.49} \\ 0.65 \\ 0.65 \\ \mathbf{6.67} \\ 3.99 \\ \mathbf{14.60} \\ 3.26 \\ -2.03 \end{bmatrix}$
Error norm (%)	7.78	13.89	27.28	31.22

The inverse solutions appear to be quite good, when the magnitudes of the point forces are compared to the actual values. The error norm, which is calculated for the solution vector  $\mathbf{f}$  is actually relatively high, but that can be explained by the strong contribution of the force vector elements that should have been zero. All in all, the results are as accurate as anticipated and therefore satisfactory.

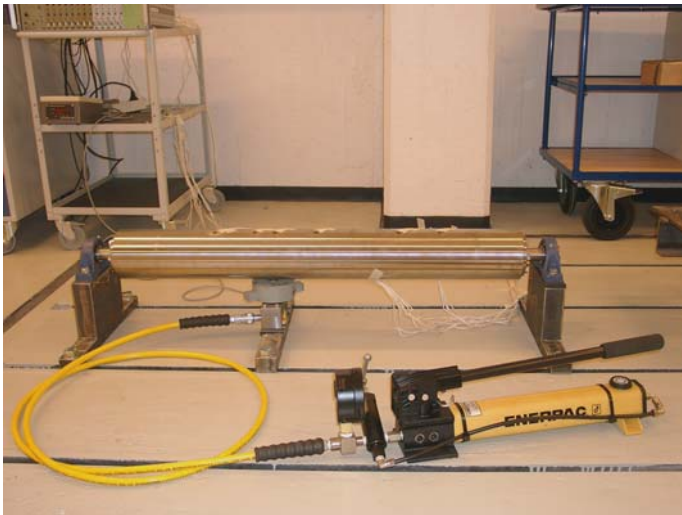
It seems that regularization does not improve the results, but actually produces a greater error than for the direct calculation. The condition numbers, for both experimental and computational influence coefficient matrices, are relatively small. Nevertheless, the matrices are still noticeably ill-conditioned, since the condition numbers are clearly greater than 1. A suitable value of the regularization parameter  $\delta$  is chosen, based on Morozov's discrepancy principle, since the L-curve method does not work properly. A value just smaller than the Morozov one is chosen by trying out different values. The noise level for Morozov's principle is obtained as 1 % of the largest strain value. Moreover, zeroth-order regularization based on (29) is applied, since there is no obvious connection between the elements of the solution vector. As the value of the regularization parameter is increased, a tendency of mitigation in the overall values of the solution vector is obtained.

As the number of point forces acting on the structure at the same time increases, the solution accuracy decreases. This is due to the fact that the unit influences are no longer as readily distinguishable as the strain measurements "scatter" slightly.

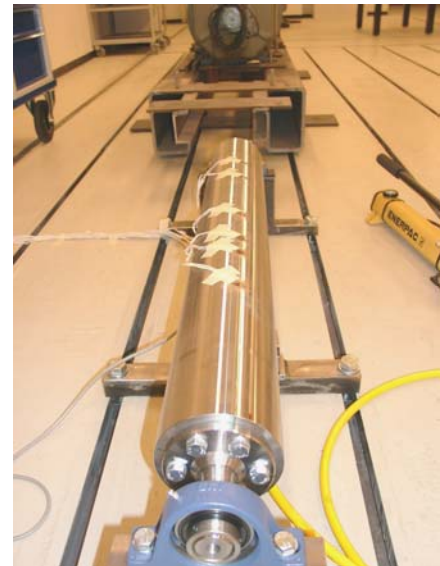
The experimental influence coefficient matrix works out better than the one determined computationally using beam theory. The problem with the beam theory was to choose the right value for Young's modulus. Here, the value of 180 GPa was based on matching the measured strain values to the computed ones. It was observed that the structure did not behave linearly with smaller loadings; in fact, there were small, but noticeable geometric nonlinearities in the structure, since it was not completely straight and uniform. In addition, it was observed that if one knows the loading level to be measured, the influence coefficients should be experimentally determined close to that level, if possible. This assures that the system matrix works optimally.

### 6.1.2 Case study 2, a tubular roll structure

Case study 2 is a tubular beam-like roll structure made of structural steel, which can be rotated. The hollow shell has a length of 1000 mm, and inner and outer diameters of 120 mm and 128 mm, respectively. Both of the ends are mounted on bearings, and the support length of the structure between the bearing centres was 1151 mm. There are altogether 13 strain gages in six strain gage rosettes on the outer wall of the shell, which can be utilized. Thus, the strain is measured in both the axial and tangential directions, and in addition, the center measurement point is also measured in the direction 45 degrees from the principal axes, since there is a tri-axial strain gage rosette. The loading is performed from under the tube structure by using a hydraulic jack. The tube, with its measurement set-up and loading system, is presented in figure 34.



(a)



(b)

Figure 34. Case study 2.

This case study is investigated to obtain more information about the suitability of tangential strain measurements, and also to see, how a more complicated hollow roll-like structure would behave under point loading. The system matrix is composed on the basis of an experimental unit load procedure with five point forces and averaging over five times for each unit load. Only one angular position, where the loading is on one side and the measurement on the opposite side, is used, in accordance with the decision of chapter 5. Thus, the measurement points are located at the “bottom” position (actually on top here, because the loading is from underneath), i.e., on the opposite outer wall with respect to the loading. The strain point locations and the unit load set-up are presented in figure 35.

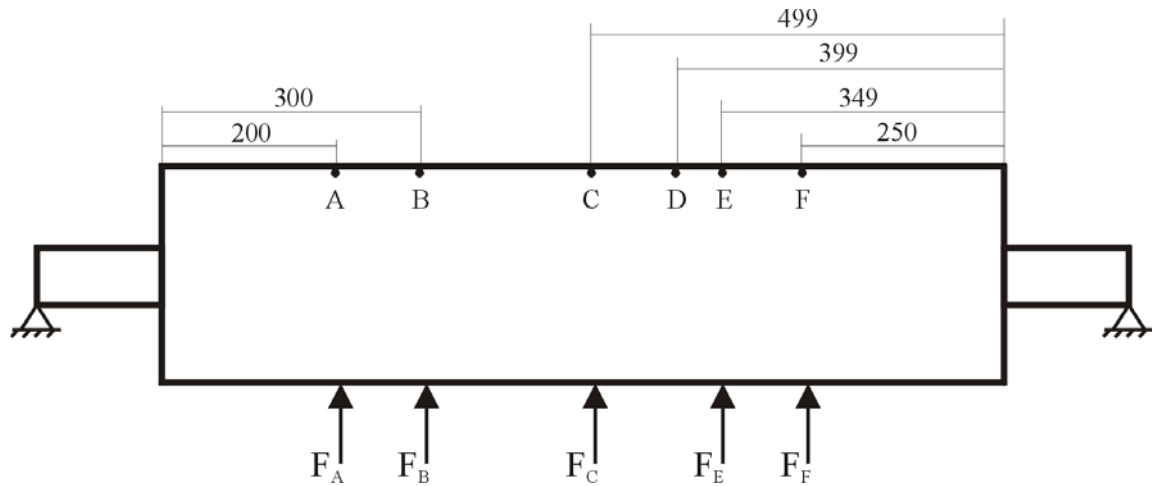


Figure 35. The strain and load set-up of case study 2.

Here, the procedures follow the same approach as in case study 1. Different point loadings are applied to the structure individually, and based on the strain data, inverse solutions are calculated with and without regularization. The actual magnitude of the point forces is known through force cell measurement. Two different variations of strain data are used, in one of which only the axial strains are utilized, and in the other of which all the 13 available strain signals are utilized. These approaches produce non-square matrices, which signifies the use of a pseudo-inverse (7). The results for the 2 different strain set-ups are collected in table 6.

Clearly, similar conclusions can be drawn from this case study to those drawn from the preceding. There are no significant improvements achieved with regularization. The error norms are now considerably lower than in the previous case, and that derives from the larger values of the force vector elements as compared to the case with zero-valued elements. The regularization parameter is chosen in the same manner as for case study 1; utilizing Morozov's principle, since the L-curve method does not work here either. The value of the regularization parameter is much smaller compared to the preceding case, which is a result of the smaller elements of the influence coefficient matrix, because the unit loads caused smaller strains in the structure.

Utilizing all the available measurement data is more efficient than using only the axial strain signals; even the condition number of the system matrix of all strains is smaller. Thus, the use of both axial and tangential measurements is preferable. In conclusion, the inverse load sensing method also works with a more complicated hollow roll-like structure. Accordingly, the results are relatively accurate in the case of sensing point forces. The

suitability of the method, in the case of a continuous loading acting on the roll structure, will be evaluated in the next sections that follow.

Table 6. Results from the tubular roll case study,  $\delta = 10^{-7}$ .

	Inverse solution using the axial strains	Inverse solution using the axial strains regularized	Inverse solution using axial and tang. strains	Inverse solution using axial and tang. strains regularized
Cond. number of the matrix	82.58		35.81	
Loading case 1  Magnitude of the point force  $F_A = 6958.27$				
	$\mathbf{f} = \begin{bmatrix} \mathbf{6822.20} \\ 78.02 \\ 77.44 \\ -42.44 \\ -15.15 \end{bmatrix}$	$\mathbf{f} = \begin{bmatrix} \mathbf{6236.63} \\ 404.79 \\ 381.30 \\ 76.80 \\ -416.20 \end{bmatrix}$	$\mathbf{f} = \begin{bmatrix} \mathbf{6917.42} \\ 36.37 \\ 21.99 \\ -52.22 \\ 36.51 \end{bmatrix}$	$\mathbf{f} = \begin{bmatrix} \mathbf{6820.85} \\ 135.32 \\ -1.87 \\ -44.21 \\ 32.06 \end{bmatrix}$
Error norm (%)	2.60	9.02	1.25	1.99
Loading case 2  Magnitude of the point force  $F_C = 6914.21$				
	$\mathbf{f} = \begin{bmatrix} 8.40 \\ 28.31 \\ \mathbf{6755.37} \\ 124.16 \\ 18.37 \end{bmatrix}$	$\mathbf{f} = \begin{bmatrix} 315.65 \\ -77.13 \\ \mathbf{6481.08} \\ 80.16 \\ 285.16 \end{bmatrix}$	$\mathbf{f} = \begin{bmatrix} -63.39 \\ 55.93 \\ \mathbf{6830.20} \\ 133.95 \\ -60.23 \end{bmatrix}$	$\mathbf{f} = \begin{bmatrix} -84.72 \\ 89.30 \\ \mathbf{6794.94} \\ 174.38 \\ -80.58 \end{bmatrix}$
Error norm (%)	2.96	5.85	2.74	3.24
Loading case 3  Magnitude of the point force  $F_E = 6914.21$				
	$\mathbf{f} = \begin{bmatrix} -26.65 \\ 135.65 \\ -150.45 \\ \mathbf{6919.75} \\ 104.48 \end{bmatrix}$	$\mathbf{f} = \begin{bmatrix} 90.36 \\ 95.72 \\ -185.62 \\ \mathbf{6726.39} \\ 319.93 \end{bmatrix}$	$\mathbf{f} = \begin{bmatrix} -72.17 \\ 87.67 \\ -62.49 \\ \mathbf{6997.66} \\ -11.02 \end{bmatrix}$	$\mathbf{f} = \begin{bmatrix} -62.68 \\ 66.57 \\ -17.34 \\ \mathbf{6902.98} \\ 56.94 \end{bmatrix}$
Error norm (%)	3.33	4.75	2.01	1.61



## 6.2 Using inverse load sensing method for solving distributed loading profile on a roll structure

In this chapter, the roll structure is modelled and the inverse load sensing method is tested for different strain set-ups, as well as different loading approaches. The strain data under the governing load distribution is calculated with an FE model, i.e., the strain measurements are artificially simulated. A different FE model is used for the strain data simulations than was used for to determine the inverse model itself, in order to avoid inverse crime.

### 6.2.1 Analysis of the method when unit point force approach is used

The feasibility of the method is first simulated in the case of different loading distributions which are shown in figure 36.

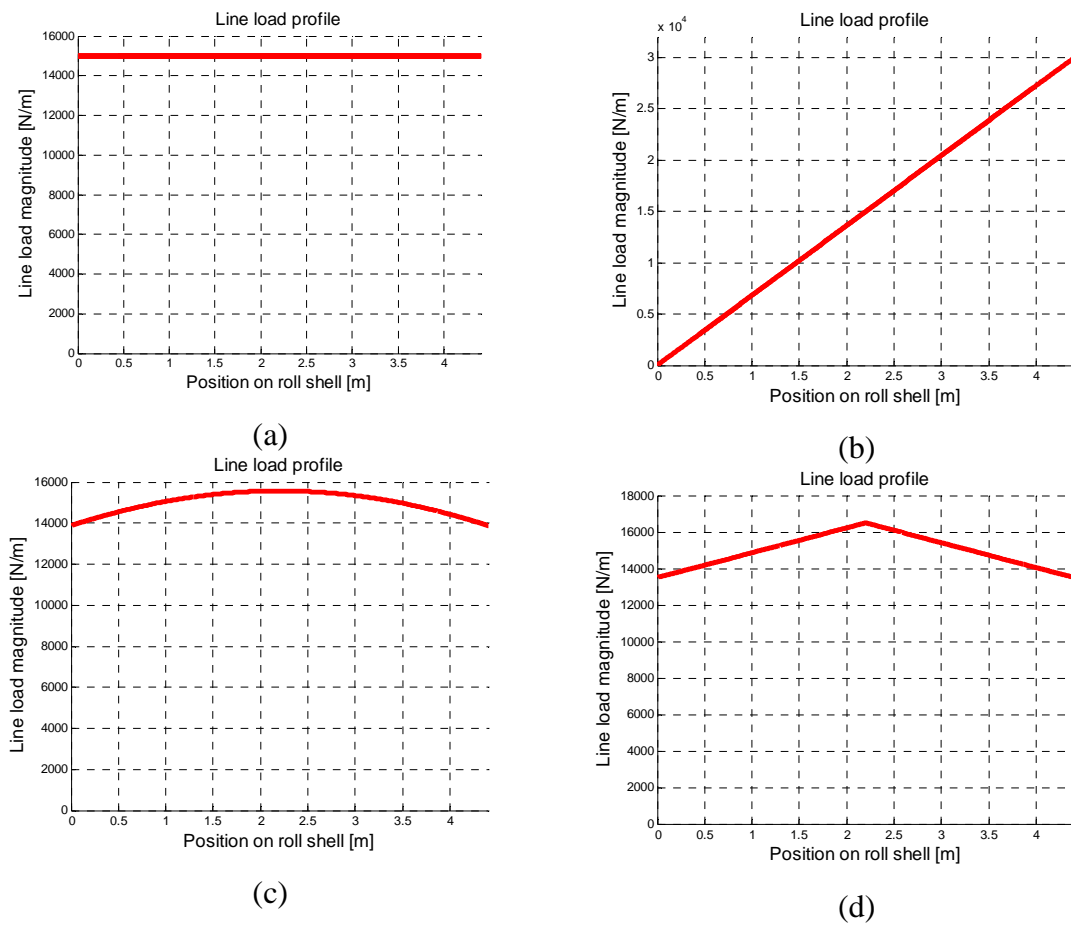


Figure 36. The four different line loading distributions used in the simulations: CONSTANT (a), TRIANGLE (b), SINE (c) and HAT (d).

The FE model used to simulate the strain data artificially is illustrated in figure 37. It has 280073 tetrahedral 10-node elements with quadratic shape functions and 455715 nodes, and the ends are simply supported at the rotational centres of the bearings. It has a finer element mesh than the model used for the influence coefficient matrix, and the node locations of the two meshes are therefore different. Accordingly, the inverse crime is avoided. The determination of strain at the measurement points, which, in this simulation model, are located at the element edges between the nodes in most parts, is accomplished by linear interpolation at the element edges.

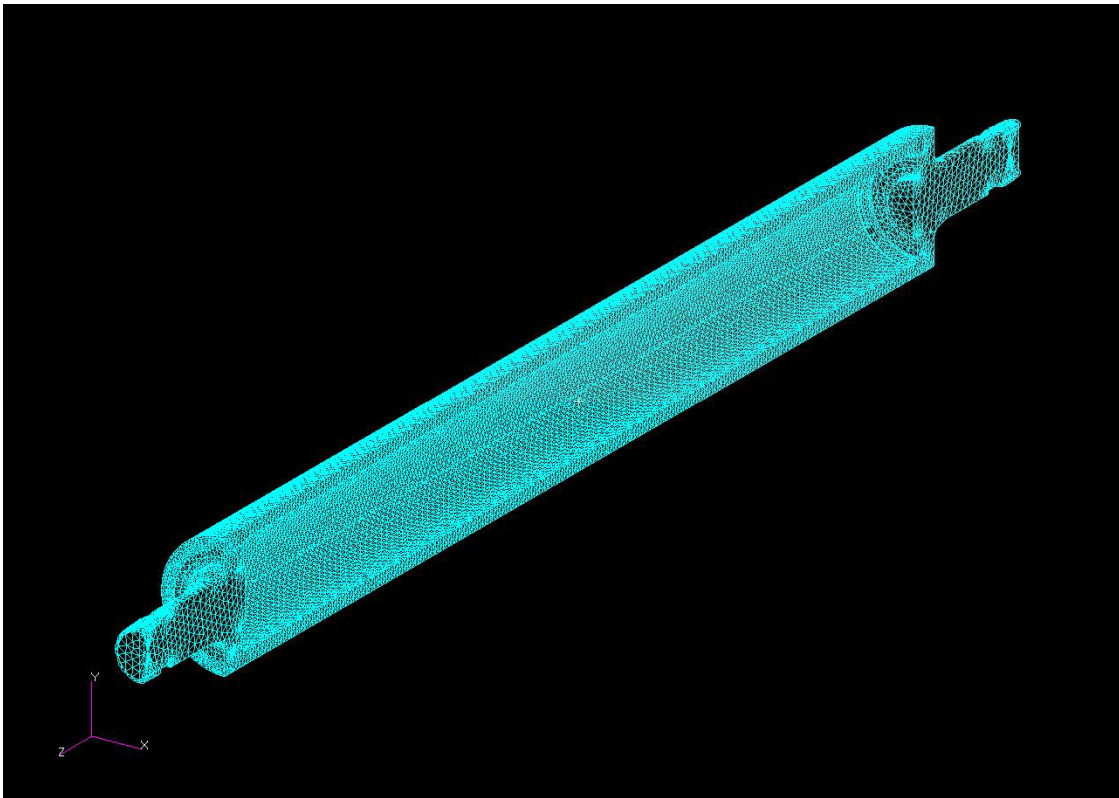


Figure 37. The FE model for the strain data.

The influence coefficient matrices are determined for four different load cases I-IV, using 5, 10, 22 and 44 unit point forces, respectively, as shown in table 7, and the calculations are carried out with the FE model which was already been introduced and used in chapter 5 (figure 22).

The measurement points are chosen to be located at “bottom” position on the inner wall, at the same axial positions as the unit point forces, except for some of the outer most points, which are not on the tubular part of the structure (cases III and IV). Suitable points on the tubular part near the ends are chosen instead. Two different matrices for each unit load case are determined: one that utilizes only axial strains at measurement points, referred as

case A, and the other that utilizes both axial and tangential strain at measurement points, referred as case B. The axial locations of the chosen measurement points are collected in table 8. For each simulated loading case, normally distributed random error of 1 % of the maximum strain value of the measurement points was added.

Table 7. The four different unit point force cases.

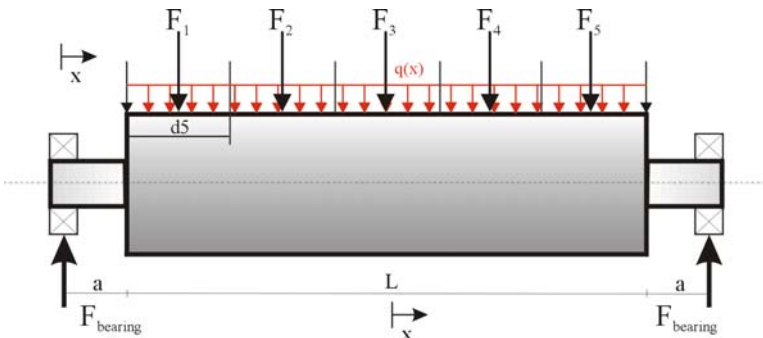
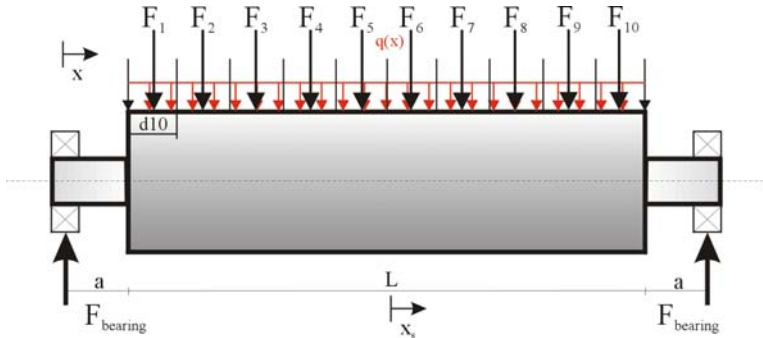
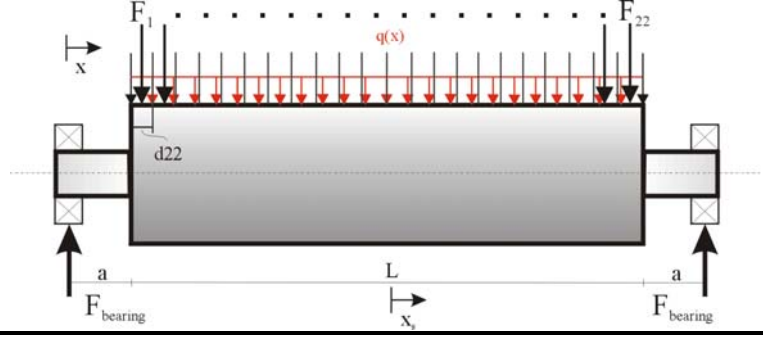
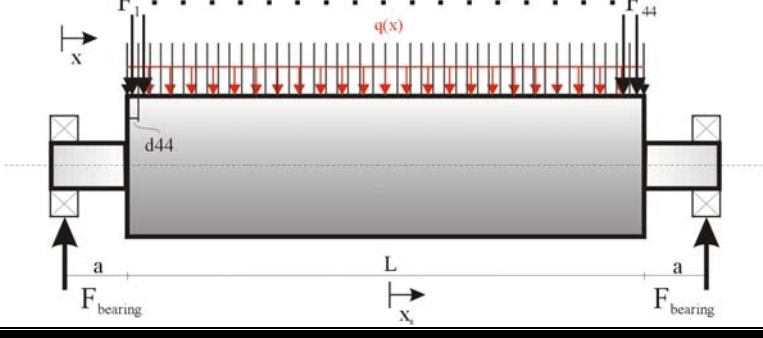
Unit point force cases	
case I	
$d5 = 880 \text{ mm}$	
case II	
$d10 = 440 \text{ mm}$	
case III	
$d22 = 200 \text{ mm}$	
case IV	
$d44 = 100 \text{ mm}$	

Table 8. The measurement/strain points.

Influence coefficient matrix $\mathbf{Z}$	The measurement point locations (in $x_s$ coord.)
$\mathbf{Z}_{5A}$ and $\mathbf{Z}_{5B}$	$[-1.76 \quad -0.88 \quad 0 \quad 0.88 \quad 1.76]^T$
$\mathbf{Z}_{10A}$ and $\mathbf{Z}_{10B}$	$[-1.98 \quad -1.54 \quad \dots \quad 1.54 \quad 1.98]^T$
$\mathbf{Z}_{22A}$ and $\mathbf{Z}_{22B}$	$[-1.98 \quad -1.90 \quad -1.70 \quad \dots \quad 1.70 \quad 1.90 \quad 1.98]^T$
$\mathbf{Z}_{44A}$ and $\mathbf{Z}_{44B}$	$[-2.00 \quad -1.98 \quad -1.90 \quad -1.80 \quad \dots \quad 1.80 \quad 1.90 \quad 1.98 \quad 2.00]^T$

The inverse solutions are calculated with two different Tikhonov regularization approaches presented in section 3.4, namely those using Eqs. (20) and (19). For both methods, the system matrices are the same.

Firstly, the inverse solutions for all of the four different line load distributions are calculated by using the Tikhonov regularization according to the Eq. (20). Significantly, our *a priori* knowledge for this case is that the values of the force vector are similar to each other, and a first order regularization matrix  $\mathbf{D}_1$  Eq. (30) can therefore be used.

Secondly, the inverse solutions for three different line load distributions are calculated by using the Tikhonov regularization according to the Eq. (19), where the values of constant line load distribution of 15 kN/m are used as  $\mathbf{f}^*$ . Naturally, the triangle loading distribution is excluded, since it is not even close to the constant *a priori* knowledge of  $\mathbf{f}^*$  presented above. In this case, the first order regularization does not work, and zeroth-order regularization according to  $\mathbf{D}_0$  Eq. (29) is used instead.

In each case, three different values for  $\delta$  are used. They are chosen on the basis of Eq. (24), and the calculation of the L-curve taking the three values that correspond to the order of magnitude and decade of the two approximations. The approximations according to Morozov's principle are not applicable, since they are clearly too small. The error norm percentage of each case is calculated according to Eq. (83) and the condition number  $\chi$  of the respective system matrices for each  $\mathbf{Z}$  by Eq. (16). The results of the inverse load sensing in the case of a unit point force approach are collected in tables 9 and 10 for Eq. (20), and in table 11 for Eq. (19). In addition, the condition numbers of the system matrices are shown in table 9. The intention is to get an idea about the accuracy of the method, and

also about the implication of different regularization approaches and parameters, respectively.

Table 9. Inverse results using axial and tangential strain data in the case of CONSTANT loading and Eq. (20).

Influence coefficient matrix $\mathbf{Z}$ and cond. number $\chi$	Reg. parameter $\delta$	Error norm of the solution (%)	Influence coefficient matrix $\mathbf{Z}$ and cond. number $\chi$	Reg. parameter $\delta$	Error norm of the solution (%)
$\mathbf{Z}_{5A}$ $\chi_{5A} = 72$	$10^{-7}$	1.78	$\mathbf{Z}_{5B}$ $\chi_{5B} = 8.6$	$10^{-7}$	4.12
	$10^{-6}$	0.87		$10^{-6}$	1.01
	$10^{-5}$	0.30		$10^{-5}$	0.15
$\mathbf{Z}_{10A}$ $\chi_{10A} = 2.4 \times 10^5$	$10^{-7}$	3.16	$\mathbf{Z}_{10B}$ $\chi_{10B} = 170$	$10^{-7}$	3.77
	$10^{-6}$	0.86		$10^{-6}$	1.40
	$10^{-5}$	0.44		$10^{-5}$	0.80
$\mathbf{Z}_{22A}$ $\chi_{22A} = 7.2 \times 10^5$	$10^{-6}$	7.73	$\mathbf{Z}_{22B}$ $\chi_{22B} = 8551$	$10^{-6}$	3.86
	$10^{-5}$	4.09		$10^{-5}$	2.11
	$10^{-4}$	0.81		$10^{-4}$	1.01
$\mathbf{Z}_{44A}$ $\chi_{44A} = 6.5 \times 10^9$	$10^{-6}$	9.18	$\mathbf{Z}_{44B}$ $\chi_{44B} = 3.7 \times 10^7$	$10^{-6}$	6.15
	$10^{-5}$	2.75		$10^{-5}$	3.44
	$10^{-4}$	0.98		$10^{-4}$	2.34

Table 10. Inverse results using axial and tangential strain data in the case of various loadings with Eq. (20).

Influence coefficient matrix $\mathbf{Z}$	Reg. parameter $\delta$	Error norm of the solution (%)	Influence coefficient matrix $\mathbf{Z}$	Reg. parameter $\delta$	Error norm of the solution (%)
TRIANGLE loading					
$\mathbf{Z}_{5A}$	$10^{-8}$	7.45	$\mathbf{Z}_{5B}$	$10^{-8}$	13.83
	$10^{-7}$	11.18		$10^{-7}$	12.24
	$10^{-6}$	30.35		$10^{-6}$	29.21
$\mathbf{Z}_{10A}$	$10^{-8}$	12.66	$\mathbf{Z}_{10B}$	$10^{-8}$	8.40
	$10^{-7}$	4.74		$10^{-7}$	5.39
	$10^{-6}$	8.97		$10^{-6}$	8.28
$\mathbf{Z}_{22A}$	$10^{-7}$	9.75	$\mathbf{Z}_{22B}$	$10^{-7}$	10.48
	$10^{-6}$	6.86		$10^{-6}$	3.42
	$10^{-5}$	7.73		$10^{-5}$	5.87
$\mathbf{Z}_{44A}$	$10^{-7}$	18.98	$\mathbf{Z}_{44B}$	$10^{-7}$	12.55
	$10^{-6}$	9.08		$10^{-6}$	6.91
	$10^{-5}$	7.32		$10^{-5}$	5.52
SINE loading					
$\mathbf{Z}_{5A}$	$10^{-8}$	10.78	$\mathbf{Z}_{5B}$	$10^{-8}$	5.80
	$10^{-7}$	2.36		$10^{-7}$	3.59
	$10^{-6}$	2.72		$10^{-6}$	3.11
$\mathbf{Z}_{10A}$	$10^{-7}$	3.84	$\mathbf{Z}_{10B}$	$10^{-8}$	9.47
	$10^{-6}$	1.89		$10^{-7}$	2.89
	$10^{-5}$	3.11		$10^{-6}$	2.19
$\mathbf{Z}_{22A}$	$10^{-7}$	14.45	$\mathbf{Z}_{22B}$	$10^{-7}$	11.55
	$10^{-6}$	3.39		$10^{-6}$	6.61
	$10^{-5}$	1.14		$10^{-5}$	2.44
$\mathbf{Z}_{44A}$	$10^{-6}$	19.03	$\mathbf{Z}_{44B}$	$10^{-6}$	4.37
	$10^{-5}$	3.84		$10^{-5}$	2.49
	$10^{-4}$	2.39		$10^{-4}$	1.64
HAT loading					
$\mathbf{Z}_{5A}$	$10^{-8}$	2.02	$\mathbf{Z}_{5B}$	$10^{-8}$	7.14
	$10^{-7}$	4.50		$10^{-7}$	3.55
	$10^{-6}$	5.93		$10^{-6}$	5.45
$\mathbf{Z}_{10A}$	$10^{-7}$	5.37	$\mathbf{Z}_{10B}$	$10^{-7}$	4.07
	$10^{-6}$	2.96		$10^{-6}$	3.24
	$10^{-5}$	5.40		$10^{-5}$	5.44
$\mathbf{Z}_{22A}$	$10^{-7}$	10.60	$\mathbf{Z}_{22B}$	$10^{-7}$	16.06
	$10^{-6}$	4.52		$10^{-6}$	7.01
	$10^{-5}$	1.24		$10^{-5}$	3.45
$\mathbf{Z}_{44A}$	$10^{-6}$	1.84	$\mathbf{Z}_{44B}$	$10^{-6}$	6.12
	$10^{-5}$	1.00		$10^{-5}$	2.21
	$2.58 \cdot 10^{-4}$	3.52		$10^{-4}$	1.56

Table 11. Inverse results using axial and tangential strain data in the case of various loadings with Eq. (19).

Influence coefficient matrix $\mathbf{Z}$	Reg. parameter $\delta$	Error norm of the solution (%)	Influence coefficient matrix $\mathbf{Z}$	Reg. parameter $\delta$	Error norm of the solution (%)
CONSTANT loading					
$\mathbf{Z}_{5A}$	$10^{-7}$	3.10	$\mathbf{Z}_{5B}$	$10^{-7}$	3.41
	$10^{-6}$	1.32		$10^{-6}$	0.94
	$10^{-5}$	0.49		$10^{-5}$	0.31
$\mathbf{Z}_{10A}$	$10^{-7}$	5.31	$\mathbf{Z}_{10B}$	$10^{-7}$	8.11
	$10^{-6}$	1.26		$10^{-6}$	1.87
	$10^{-5}$	0.21		$10^{-5}$	0.35
$\mathbf{Z}_{22A}$	$10^{-6}$	1.45	$\mathbf{Z}_{22B}$	$10^{-6}$	2.69
	$10^{-5}$	0.42		$10^{-5}$	0.74
	$10^{-4}$	0.07		$10^{-4}$	0.10
$\mathbf{Z}_{44A}$	$10^{-6}$	2.22	$\mathbf{Z}_{44B}$	$10^{-6}$	5.69
	$10^{-6}$	0.45		$10^{-6}$	1.13
	$10^{-4}$	0.25		$10^{-4}$	0.24
SINE loading					
$\mathbf{Z}_{5A}$	$10^{-8}$	5.61	$\mathbf{Z}_{5B}$	$10^{-8}$	9.56
	$10^{-7}$	4.11		$10^{-7}$	5.53
	$10^{-6}$	3.51		$10^{-6}$	3.22
$\mathbf{Z}_{10A}$	$10^{-7}$	8.43	$\mathbf{Z}_{10B}$	$10^{-8}$	17.28
	$10^{-6}$	4.22		$10^{-7}$	6.96
	$10^{-5}$	3.34		$10^{-6}$	3.07
$\mathbf{Z}_{22A}$	$10^{-7}$	11.11	$\mathbf{Z}_{22B}$	$10^{-7}$	10.20
	$10^{-6}$	3.59		$10^{-6}$	2.56
	$10^{-5}$	3.13		$10^{-5}$	2.89
$\mathbf{Z}_{44A}$	$10^{-6}$	4.18	$\mathbf{Z}_{44B}$	$10^{-6}$	4.91
	$10^{-5}$	2.20		$10^{-5}$	2.72
	$10^{-4}$	3.08		$10^{-4}$	3.15
HAT loading					
$\mathbf{Z}_{5A}$	$10^{-8}$	10.47	$\mathbf{Z}_{5B}$	$10^{-8}$	8.15
	$10^{-7}$	4.04		$10^{-7}$	2.95
	$10^{-6}$	5.39		$10^{-6}$	4.59
$\mathbf{Z}_{10A}$	$10^{-7}$	3.44	$\mathbf{Z}_{10B}$	$10^{-7}$	6.82
	$10^{-6}$	4.85		$10^{-6}$	3.86
	$10^{-5}$	5.42		$10^{-5}$	5.24
$\mathbf{Z}_{22A}$	$10^{-7}$	4.00	$\mathbf{Z}_{22B}$	$10^{-7}$	13.92
	$10^{-6}$	2.57		$10^{-6}$	3.81
	$10^{-5}$	4.98		$10^{-5}$	5.05
$\mathbf{Z}_{44A}$	$10^{-6}$	5.99	$\mathbf{Z}_{44B}$	$10^{-6}$	4.48
	$10^{-5}$	4.47		$10^{-5}$	4.18
	$2.5 \times 10^{-4}$	5.49		$10^{-4}$	5.30

The results of the inverse load sensing can be regarded as relatively accurate. With the most suitable regularization parameter choices, for each specific case, the error norm is only a few percent in the loading cases. In comparison, regularization of Eq. (20) is better, since the results according to Eq. (19) are not as clear in cases of sine and hat loading distributions. In addition, the inverse solutions from Eq. (19) are more susceptible to deviations in the strain data (1 %), which makes it more sensitive.

The condition number of the system matrix is smallest with the smallest matrix and vice versa. It is obvious that one has to use some kind of regularization technique, when the condition number is over 100, which is the case when the number of point forces is greater than 5. Interestingly enough, with 5 point forces, the condition number is quite low, and directly calculated inverse solutions are reasonable with the error level of 1 % used. But nevertheless, as the value of the condition number increases, the value of the suitable regularization parameter increases as well, and it can be concluded that regularization is needed in the case of this inverse load sensing approach.

The selection of the regularization parameter is difficult, since none of the attempted parameter determination methods works consistently. In this case, the selection has to be done based on Eq. (24), an L-curve and a visual examination of the inverse solutions. In many cases, the L-curve gives values that are too large, which makes the inverse solution too insensitive, especially when Eq. (19) is used. In fact, for the “less ill-conditioned” 5 point force case, the L-curve does not work at all. The best choice of  $\delta$  is often a value a little greater than that of Eq. (24), but not as large as approximated by the L-curve. Thus, the “middle value” of each case of tables 9, 10 and 11 is the most suitable, since, in that case, the solution is still sensitive but not unstable. This tendency remains relatively unchanged for parameter values of the same decade. Thus, changing the parameter values approximately with the steps of one decade is sensible, as mentioned by Doyle [Doyle 2004] as well. Furthermore, when the suitable value for  $\delta$  is found for a certain measurement set-up/system matrix, it is applicable from then on.

Most of the solution accuracy can be explained with the favourable *a priori* information, using the first order linearization with Eq. (20), or using zeroth-order regularization with Eq. (19). Without prior knowledge, the solution would not be nearly as good. In conclusion, it can be said that this unit point force approach is effective and feasible. This



is demonstrated in figures 38-49 for Eq. (20) and in figures 50-55 for Eq. (19), which illustrate the inverse solutions of the line load distributions in different cases when suitable regularization parameters  $\delta$  are chosen. The red line represents the known loading distribution, while the bars and blue stems represent the inverse solution.

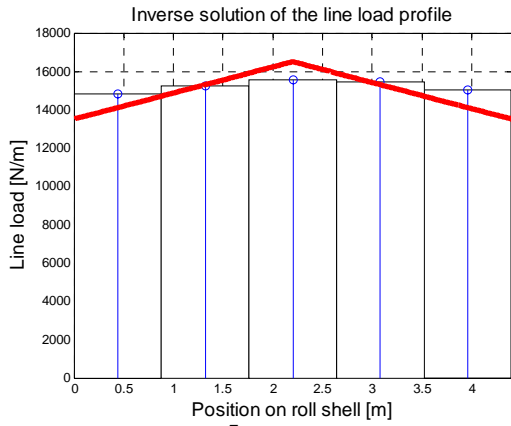


Figure 38.  $\delta = 10^{-7}$ ,  $Z_{5A}$ , Eq. (20).

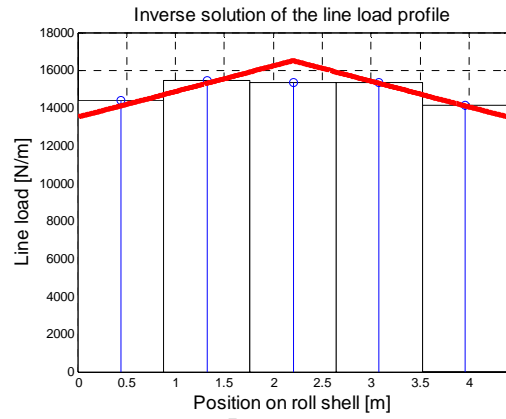


Figure 39.  $\delta = 10^{-7}$ ,  $Z_{5B}$ , Eq. (20).

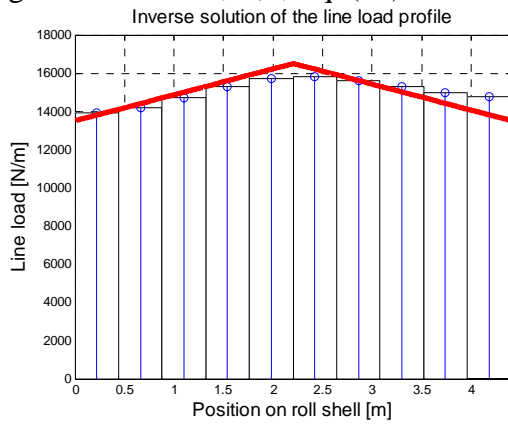


Figure 40.  $\delta = 10^{-6}$ ,  $Z_{10A}$ , Eq. (20).

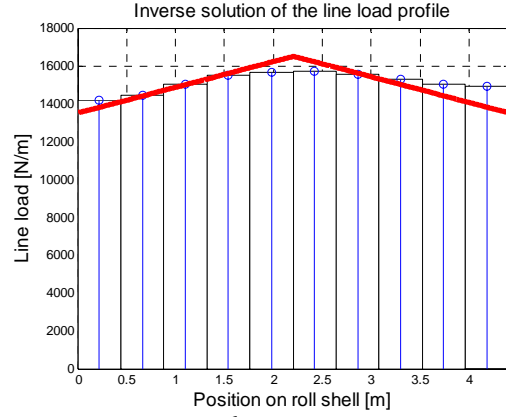


Figure 41.  $\delta = 10^{-6}$ ,  $Z_{10B}$ , Eq. (20).

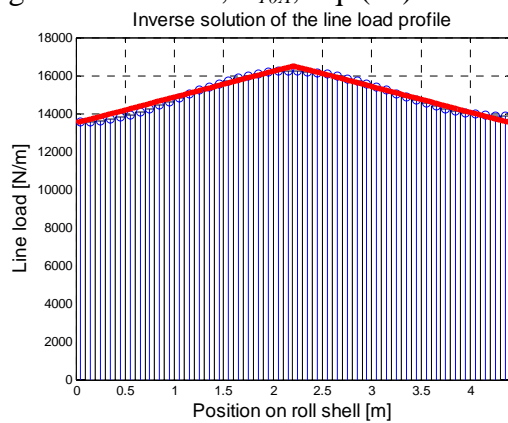


Figure 42.  $\delta = 10^{-5}$ ,  $Z_{44A}$ , Eq. (20).

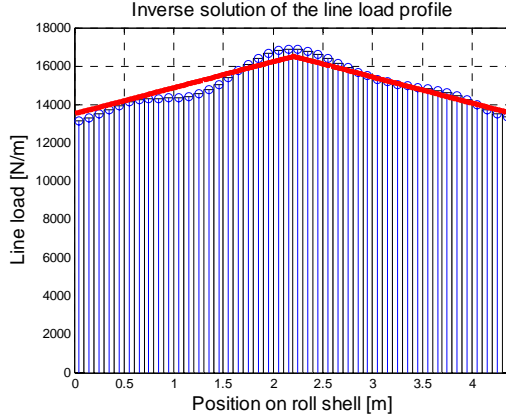


Figure 43.  $\delta = 10^{-5}$ ,  $Z_{44B}$ , Eq. (20).

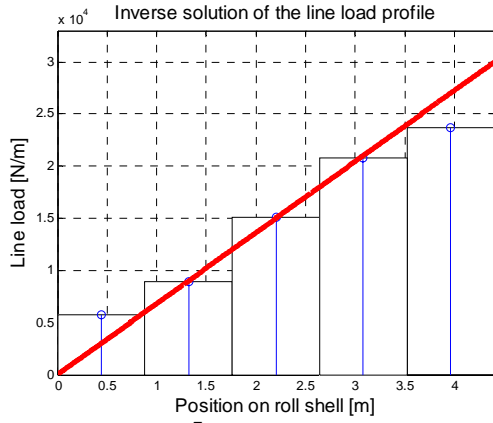


Figure 44.  $\delta = 10^{-7}$ ,  $Z_{5A}$ , Eq. (20).

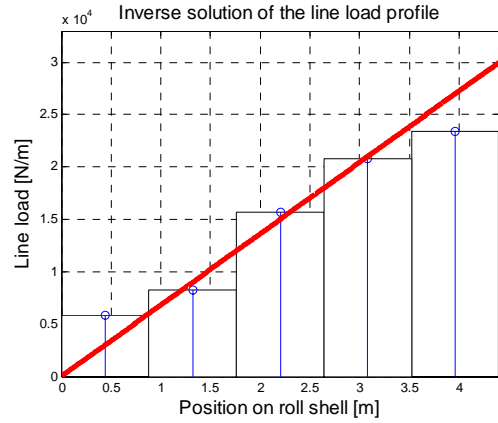


Figure 45.  $\delta = 10^{-7}$ ,  $Z_{5B}$ , Eq. (20).

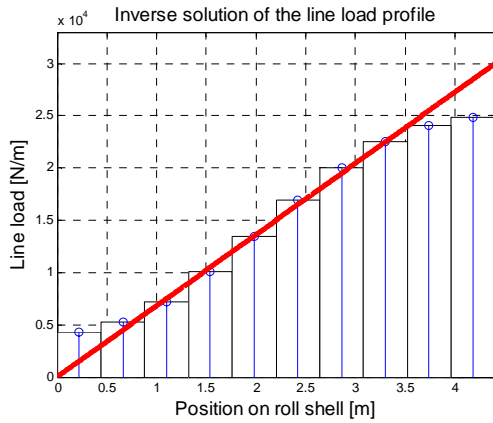


Figure 46.  $\delta = 10^{-6}$ ,  $Z_{10A}$ , Eq. (20).

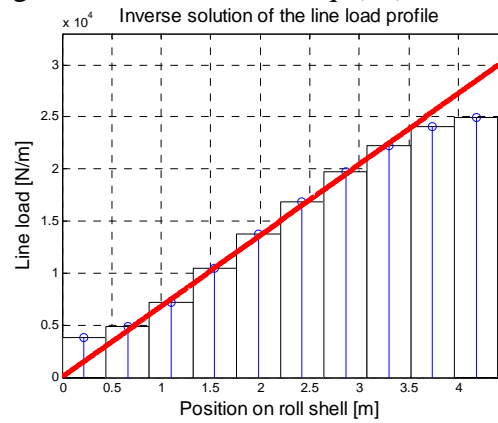


Figure 47.  $\delta = 10^{-6}$ ,  $Z_{10B}$ , Eq. (20).

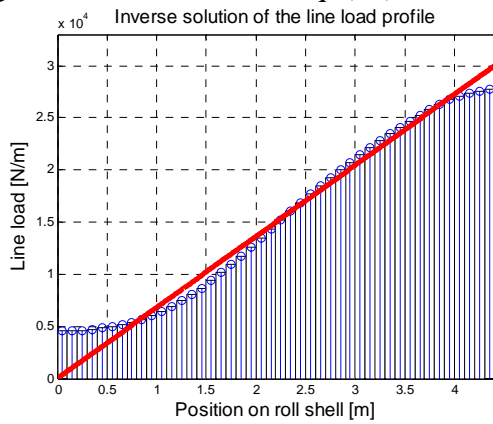


Figure 48.  $\delta = 10^{-5}$ ,  $Z_{44A}$ , Eq. (20).

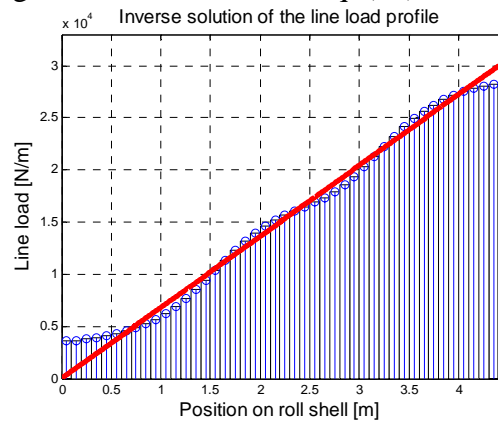


Figure 49.  $\delta = 10^{-5}$ ,  $Z_{44B}$ , Eq. (20).

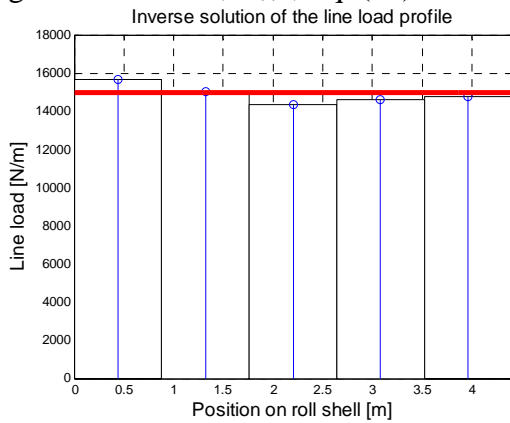


Figure 50.  $\delta = 10^{-7}$ ,  $Z_{5A}$ , Eq. (19).

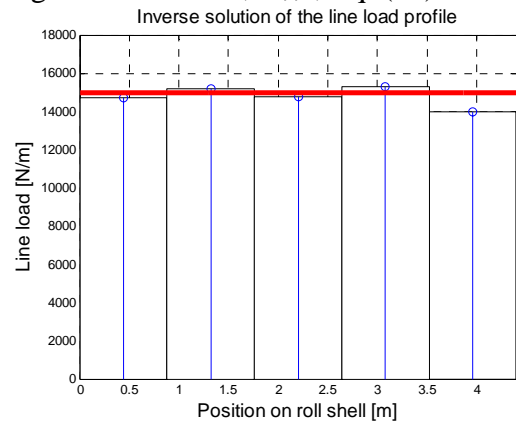
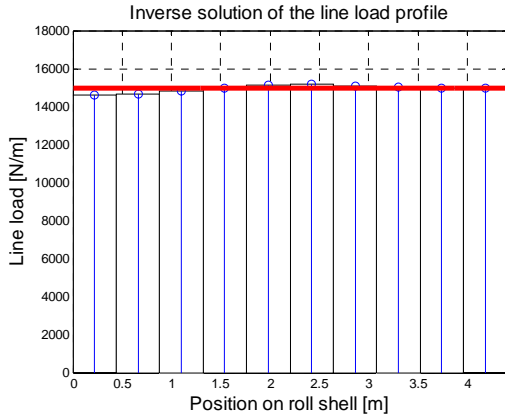
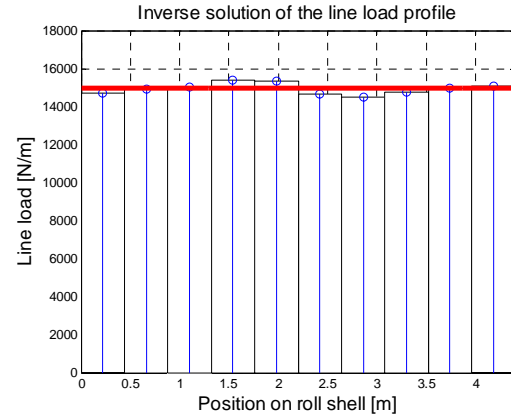
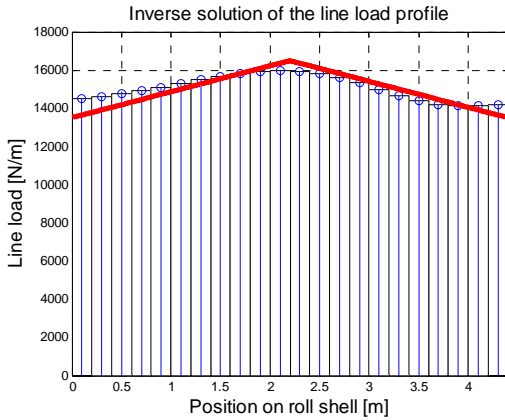
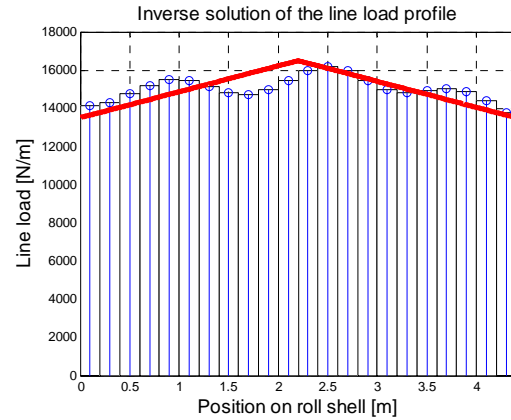


Figure 51.  $\delta = 10^{-7}$ ,  $Z_{5B}$ , Eq. (19).

Figure 52.  $\delta = 10^{-6}$ ,  $Z_{10A}$ , Eq. (19).Figure 53.  $\delta = 10^{-6}$ ,  $Z_{10B}$ , Eq. (19).Figure 54.  $\delta = 10^{-6}$ ,  $Z_{22A}$ , Eq. (19).Figure 55.  $\delta = 10^{-6}$ ,  $Z_{22B}$ , Eq. (19).

These figures can be regarded as illustrative examples of how different line load distribution profiles can be determined and described with the inverse procedure. The same tendency is obtained in the calculated load distributions and loading cases not presented here as well (see tables 9-11).

The difference between the two regularization equations used is that Eq. (19) is more sensitive, which can be seen in figures 50-55 as deviations in the inverse solution. This is also due to the fact that one uses a one decade smaller regularization parameter in order to retain the sensitivity. In this examination, Eq. (20) performs better, but in the case of a real measurement system, both of these regularization approaches could be considered.

There are no significant differences between the strain data choices of A (axial strain only) and B (axial and tangential strain). The detection of the line load profile is more exact with more strain data, since the number of point forces used to describe the profile is larger. The line load distribution is efficiently described with even five point forces of case I, which, on the other hand, is not enough for local detection of the line load distribution profile. The

best situation, but for practical measurements the most troublesome due to the number of sensors involved, situation is obviously that of case IV.

Next, the inverse load sensing method is tested in the case of a more difficult line load profile, as shown in figure 56, which has two humps at the ends. Eq. (20) was found to perform better, and accordingly, the inverse solutions are illustrated in figures 57-62.

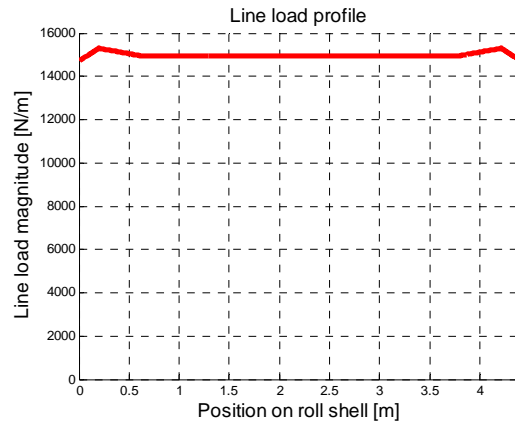


Figure 56. “Two humps” loading profile.

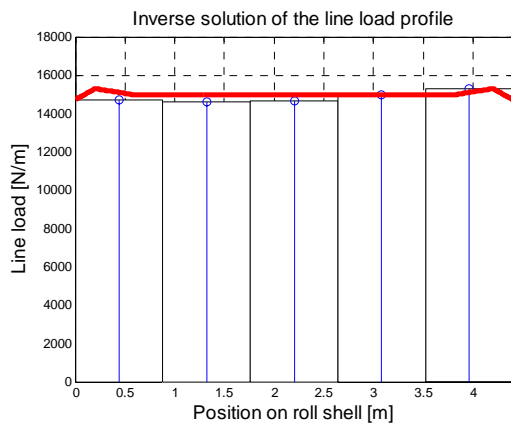


Figure 57.  $\delta = 10^{-7}$ ,  $Z_{5A}$ , error 1.89 %.

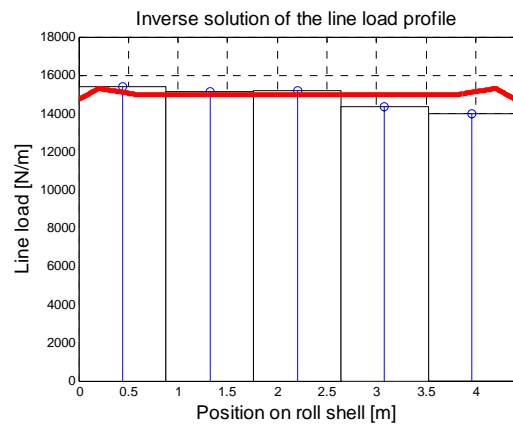


Figure 58.  $\delta = 10^{-6}$ ,  $Z_{5B}$ , error 2.74 %.

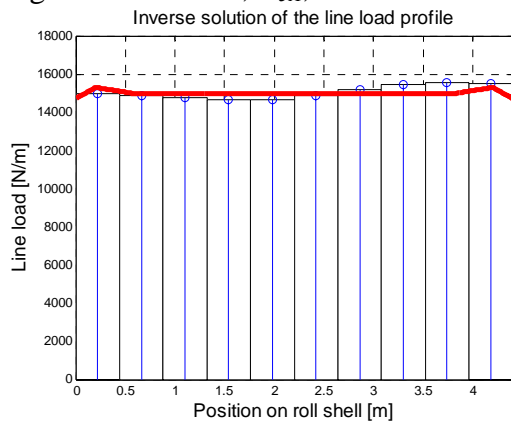


Figure 59.  $\delta = 10^{-6}$ ,  $Z_{10A}$ , error 2.10 %.

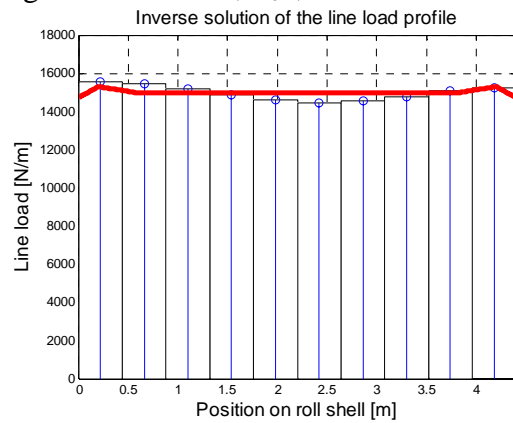


Figure 60.  $\delta = 10^{-6}$ ,  $Z_{10B}$ , error 4.03 %.

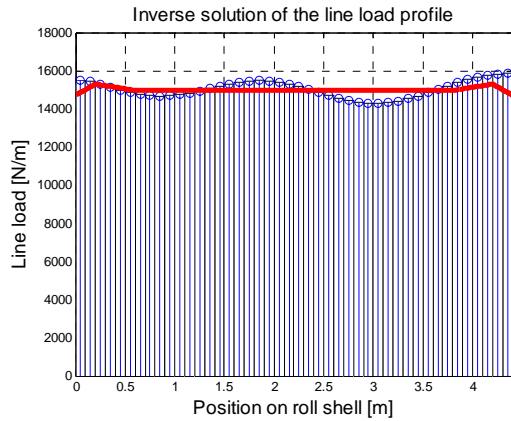


Figure 61.  $\delta = 10^{-5}$ ,  $\mathbf{Z}_{44A}$ , error 2.14%.

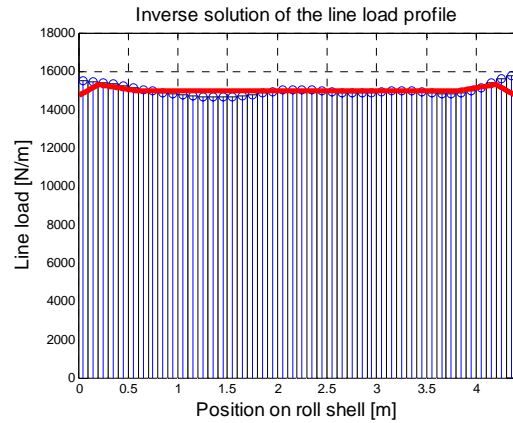


Figure 62.  $\delta = 10^{-5}$ ,  $\mathbf{Z}_{44B}$ , error 1.56 %.

The same conclusions as before apply to this case as well. Even this more difficult loading profile is nicely detected; the humps at the ends are noticeable in almost all of the solutions. Only the solutions of load case I, where five point forces describe the line load distribution, are a bit tricky to understand, but that is mainly because the line load dimension of the segments described by five point forces are large compared to the humps. Nevertheless, this unit point force approach is evidently a good and feasible method to measure line load distributions. The regularization approach and the parameters have to be carefully considered and their suitability is case-sensitive. Thus, the regularization approach of Eq. (20) and Eq. (19) will be used later in the case of utilizing real strain measurements of the pilot roll press.

### 6.2.2 Analysis of the method when unit loading function approach is used

The influence coefficient matrices are determined for four different load cases using 5, 10, 22 and 44 unit functional bases, respectively, of the simply-supported (SS) beam and free-free (FF) beam, as proposed in section 3.5.2. Otherwise, this analysis follows the same paths and conditions as the previous section 6.2.1.

The same FE model (figure 22) and the same measurement points (table 8) are used for the influence coefficients, while the same FE model (figure 37) and the same four loading distributions (figure 36) as used previously are used for the strain data as well. For each loading case, a normally distributed random error of 1 % of the maximum strain value of the measurement points is added.

Tikhonov regularization is used in accordance with the Eq. (20). The value of the suitable regularization parameter  $\delta$  is chosen based on Eq. (24), and the calculation of the L-curve. The approximations according to Morozov's principle are not applicable. In each case, three different values for  $\delta$  are used with the same principle as in section 6.2.1. This time, zeroth-order regularization according to  $\mathbf{D}_0$  from Eq. (29) is used, since no connection between the load vector values could be determined. The error norm percentage of each case is also calculated according to Eq. (83), as well as the condition number  $\chi$  of the respective system matrices for each  $\mathbf{Z}$  by Eq. (16).

The results of the inverse load sensing in the case of the two unit function approaches are collected in tables 12-15 for the four different loading cases of figure 36. The condition numbers of the matrices are also shown in tables 12 and 13 respectively.

Table 12. Inverse results using axial and tangential strain data in the case of CONSTANT loading and SS functional basis.

Influence coefficient matrix $\mathbf{Z}$ and cond. number $\chi$	Reg. parameter $\delta$	Error norm of the solution (%)	Influence coefficient matrix $\mathbf{Z}$ and cond. number $\chi$	Reg. parameter $\delta$	Error norm of the solution (%)
$\mathbf{Z}_{5A}$ $\chi_{5A} = 739$	$10^{-10}$	35.64	$\mathbf{Z}_{5B}$ $\chi_{5B} = 197$	$10^{-10}$	11.72
	$10^{-9}$	33.60		$10^{-9}$	25.01
	$10^{-8}$	31.76		$10^{-8}$	30.25
$\mathbf{Z}_{10A}$ $\chi_{10A} = 15000$	$10^{-9}$	59.87	$\mathbf{Z}_{10B}$ $\chi_{10B} = 710$	$10^{-9}$	33.09
	$10^{-8}$	23.77		$10^{-8}$	26.73
	$10^{-7}$	24.25		$10^{-7}$	23.10
$\mathbf{Z}_{22A}$ $\chi_{22A} = 2.4 \times 10^6$	$10^{-9}$	57.03	$\mathbf{Z}_{22B}$ $\chi_{22B} = 50800$	$10^{-9}$	36.14
	$10^{-8}$	24.09		$10^{-8}$	22.23
	$10^{-7}$	18.07		$10^{-7}$	19.76
$\mathbf{Z}_{44A}$ $\chi_{44A} = 2.2 \times 10^9$	$10^{-9}$	40.14	$\mathbf{Z}_{44B}$ $\chi_{44B} = 9.7 \times 10^8$	$10^{-9}$	49.01
	$10^{-8}$	17.96		$10^{-8}$	20.99
	$10^{-7}$	17.63		$10^{-7}$	17.57

Table 13. Inverse results using axial and tangential strain data in the case of CONSTANT loading and FF functional basis.

Influence coefficient matrix $\mathbf{Z}$ and cond. number $\chi$	Reg. parameter $\delta$	Error norm the solution (%)	Influence coefficient matrix $\mathbf{Z}$ and cond. number $\chi$	Reg. parameter $\delta$	Error norm the solution (%)
$\mathbf{Z}_{5A}$ $\chi_{5A} = 30$	$10^{-10}$	35.64	$\mathbf{Z}_{5B}$ $\chi_{5B} = 8.5$	$10^{-10}$	7.69
	$10^{-9}$	33.60		$10^{-9}$	7.60
	$10^{-8}$	31.76		$10^{-8}$	41.72
$\mathbf{Z}_{10A}$ $\chi_{10A} = 1970$	$10^{-9}$	59.87	$\mathbf{Z}_{10B}$ $\chi_{10B} = 44$	$10^{-10}$	42.20
	$10^{-8}$	23.77		$10^{-9}$	41.09
	$10^{-7}$	24.25		$10^{-8}$	67.34
$\mathbf{Z}_{22A}$ $\chi_{22A} = 20800$	$10^{-9}$	57.03	$\mathbf{Z}_{22B}$ $\chi_{22B} = 20800$	$10^{-8}$	130.62
	$10^{-8}$	24.09		$10^{-7}$	159.69
	$10^{-7}$	18.07		$10^{-6}$	178.78
$\mathbf{Z}_{44A}$ $\chi_{44A} = 2.8 \times 10^8$	$10^{-8}$	17.96	$\mathbf{Z}_{44B}$ $\chi_{44B} = 4.1 \times 10^7$	$10^{-8}$	127.34
	$10^{-7}$	17.63		$10^{-7}$	133.47
	$10^{-6}$	22.89		$10^{-6}$	171.19

Table 14. Inverse results using axial and tangential strain data in the case of various loadings and SS functional basis.

Influence coefficient matrix $\mathbf{Z}$	Reg. parameter $\delta$	Error norm the solution (%)	Influence coefficient matrix $\mathbf{Z}$	Reg. parameter $\delta$	Error norm the solution (%)
TRIANGLE loading					
$\mathbf{Z}_{5A}$	$10^{-10}$	27.08	$\mathbf{Z}_{5B}$	$10^{-10}$	12.65
	$10^{-9}$	30.09		$10^{-9}$	21.76
	$10^{-8}$	33.01		$10^{-8}$	26.04
$\mathbf{Z}_{10A}$	$10^{-9}$	36.23	$\mathbf{Z}_{10B}$	$10^{-9}$	30.87
	$10^{-8}$	22.99		$10^{-8}$	27.78
	$10^{-7}$	26.89		$10^{-7}$	25.45
$\mathbf{Z}_{22A}$	$10^{-8}$	21.26	$\mathbf{Z}_{22B}$	$10^{-9}$	35.95
	$10^{-7}$	21.51		$10^{-8}$	20.50
	$10^{-6}$	29.27		$10^{-7}$	19.05
$\mathbf{Z}_{44A}$	$10^{-8}$	18.28	$\mathbf{Z}_{44B}$	$10^{-8}$	19.10
	$10^{-7}$	18.06		$10^{-7}$	17.98
	$10^{-6}$	25.26		$10^{-6}$	23.94
SINE loading					
$\mathbf{Z}_{5A}$	$10^{-10}$	20.00	$\mathbf{Z}_{5B}$	$10^{-10}$	19.14
	$10^{-9}$	29.39		$10^{-9}$	25.22
	$10^{-8}$	28.86		$10^{-8}$	27.43
$\mathbf{Z}_{10A}$	$10^{-9}$	31.09	$\mathbf{Z}_{10B}$	$10^{-9}$	46.01
	$10^{-8}$	20.97		$10^{-8}$	29.33
	$10^{-7}$	22.01		$10^{-7}$	21.16
$\mathbf{Z}_{22A}$	$10^{-9}$	46.00	$\mathbf{Z}_{22B}$	$10^{-9}$	45.38
	$10^{-8}$	20.24		$10^{-8}$	25.27
	$10^{-7}$	16.36		$10^{-7}$	16.43
$\mathbf{Z}_{44A}$	$10^{-8}$	16.82	$\mathbf{Z}_{44B}$	$10^{-8}$	20.83
	$10^{-7}$	16.48		$10^{-7}$	16.76
	$10^{-6}$	20.61		$10^{-6}$	20.06
HAT loading					
$\mathbf{Z}_{5A}$	$10^{-10}$	28.38	$\mathbf{Z}_{5B}$	$10^{-10}$	5.53
	$10^{-9}$	31.51		$10^{-9}$	20.25
	$10^{-8}$	29.45		$10^{-8}$	26.20
$\mathbf{Z}_{10A}$	$10^{-9}$	46.75	$\mathbf{Z}_{10B}$	$10^{-9}$	28.70
	$10^{-8}$	27.19		$10^{-8}$	26.27
	$10^{-7}$	23.83		$10^{-7}$	21.66
$\mathbf{Z}_{22A}$	$10^{-9}$	41.45	$\mathbf{Z}_{22B}$	$10^{-9}$	53.90
	$10^{-8}$	19.63		$10^{-8}$	28.48
	$10^{-7}$	17.32		$10^{-7}$	16.80
$\mathbf{Z}_{44A}$	$10^{-8}$	23.29	$\mathbf{Z}_{44B}$	$10^{-8}$	20.21
	$10^{-7}$	17.94		$10^{-7}$	17.52
	$10^{-6}$	20.03		$10^{-6}$	19.01



Table 15. Inverse results using axial and tangential strain data in the case of various loadings and FF functional basis.

Influence coefficient matrix $\mathbf{Z}$	Reg. parameter $\delta$	Error norm the solution (%)	Influence coefficient matrix $\mathbf{Z}$	Reg. parameter $\delta$	Error norm the solution (%)
TRIANGLE loading					
$\mathbf{Z}_{5A}$	$10^{-11}$	25.16	$\mathbf{Z}_{5B}$	$10^{-10}$	57.17
	$10^{-10}$	28.93		$10^{-9}$	76.07
	$10^{-9}$	57.87		$10^{-8}$	38.84
$\mathbf{Z}_{10A}$	$10^{-9}$	47.02	$\mathbf{Z}_{10B}$	$10^{-10}$	37.63
	$10^{-8}$	89.30		$10^{-9}$	35.94
	$10^{-7}$	144.37		$10^{-8}$	56.31
$\mathbf{Z}_{22A}$	$10^{-9}$	130.26	$\mathbf{Z}_{22B}$	$10^{-9}$	186.66
	$10^{-8}$	109.34		$10^{-8}$	113.44
	$10^{-7}$	137.39		$10^{-7}$	141.93
$\mathbf{Z}_{44A}$	$10^{-9}$	131.35	$\mathbf{Z}_{44B}$	$10^{-9}$	124.58
	$10^{-8}$	111.99		$10^{-8}$	112.70
	$10^{-7}$	135.31		$10^{-7}$	117.72
SINE loading					
$\mathbf{Z}_{5A}$	$10^{-11}$	16.36	$\mathbf{Z}_{5B}$	$10^{-10}$	7.24
	$10^{-10}$	21.52		$10^{-9}$	11.35
	$10^{-9}$	58.14		$10^{-8}$	48.00
$\mathbf{Z}_{10A}$	$10^{-10}$	230.69	$\mathbf{Z}_{10B}$	$10^{-10}$	36.32
	$10^{-9}$	62.66		$10^{-9}$	31.28
	$10^{-8}$	114.10		$10^{-8}$	38.38
$\mathbf{Z}_{22A}$	$10^{-9}$	134.19	$\mathbf{Z}_{22B}$	$10^{-9}$	135.76
	$10^{-8}$	134.73		$10^{-8}$	131.48
	$10^{-7}$	161.90		$10^{-7}$	140.19
$\mathbf{Z}_{44A}$	$10^{-9}$	138.16	$\mathbf{Z}_{44B}$	$10^{-9}$	147.84
	$10^{-8}$	123.18		$10^{-8}$	125.80
	$10^{-7}$	150.17		$10^{-7}$	131.04
HAT loading					
$\mathbf{Z}_{5A}$	$10^{-11}$	61.72	$\mathbf{Z}_{5B}$	$10^{-10}$	11.60
	$10^{-10}$	54.94		$10^{-9}$	7.63
	$10^{-9}$	15.86		$10^{-8}$	35.34
$\mathbf{Z}_{10A}$	$10^{-10}$	343.42	$\mathbf{Z}_{10B}$	$10^{-10}$	54.88
	$10^{-9}$	80.14		$10^{-9}$	42.75
	$10^{-8}$	82.85		$10^{-8}$	40.04
$\mathbf{Z}_{22A}$	$10^{-9}$	130.32	$\mathbf{Z}_{22B}$	$10^{-9}$	146.59
	$10^{-8}$	126.35		$10^{-8}$	126.15
	$10^{-7}$	157.75		$10^{-7}$	139.35
$\mathbf{Z}_{44A}$	$10^{-9}$	130.95	$\mathbf{Z}_{44B}$	$10^{-9}$	128.12
	$10^{-8}$	121.49		$10^{-8}$	125.14
	$10^{-7}$	148.26		$10^{-7}$	132.81

The accuracy of the inverse solutions is distinctively weaker with the unit loading function approach than with the unit point force approach. This is independent of the functional bases used. The error norms are of the magnitude of tens of percents. The error is generated, because the inverse solutions tend to oscillate quite a lot around the known correct loading distribution. The phenomenon is the same as observed in section 5.2, and the reason for it is due to the same causes, namely from the coefficients of the basis functions that should have been zero or close to it. The same tendency was also noticed previously with the two case studies for which the inverse load sensing method was tested in the case of point forces. In those cases, the error in the elements, which should have been zero, was not as harmful since the interpretation of the solution was easier. Here, one has to rely solely on the outcome of the linear superposition of the functions, and, thereby, the errors in the elements that have zero or close-to-zero value also become very large.

The condition numbers of the system matrices of the unit function approach are notably higher than those of the unit point force approach. Use of regularization is therefore inevitable. The selection of the regularization parameter is done in the same manner as in the previous section. Equation (24) and the L-curve give reasonable estimates, based on which the approximation for the appropriate values is made as before. But in this case, one does not have a good *a priori* knowledge of the solution, and zeroth-order regularization has to be used. This also compounds the errors.

The only way that one would have more accurate results with this approach would be to decrease the magnitudes of the modelling and measurement errors, which are simulated here by adding random error to the strain data. Thus, one would have to have a more accurate model and measurements. Another way of getting better results with this approach would be to develop a better regularization technique, and have additional *a priori* knowledge. In any case, use of the technique of Eq. (19) would not help the outcome here.

In conclusion, it can be said that this unit loading function approach is not feasible enough to solve for the line load distributions, because of the erroneous presence of oscillations in the solutions. Figures 65-72 illustrate examples of the inverse solutions of the line load distributions in different cases, when suitable regularization parameters are chosen. The red line represents the known loading distribution, while the bars and blue lines represent the inverse solution. The oscillations can be observed very clearly.

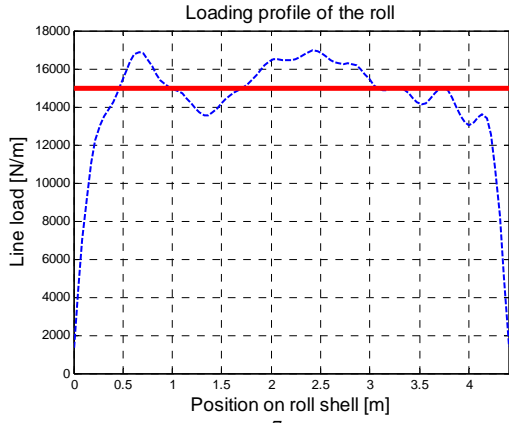


Figure 63. SS  $\delta = 10^{-7}$ ,  $\mathbf{Z}_{22B}$ .

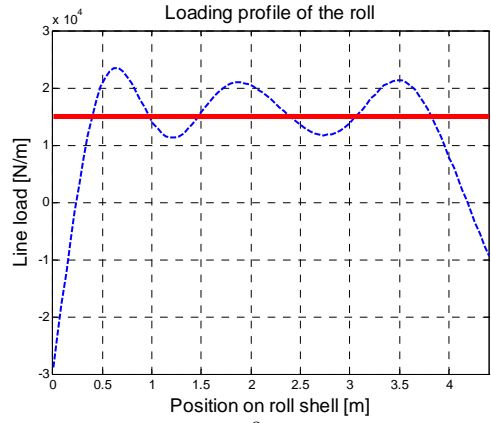


Figure 64. FF  $\delta = 10^{-8}$ ,  $\mathbf{Z}_{10B}$ .

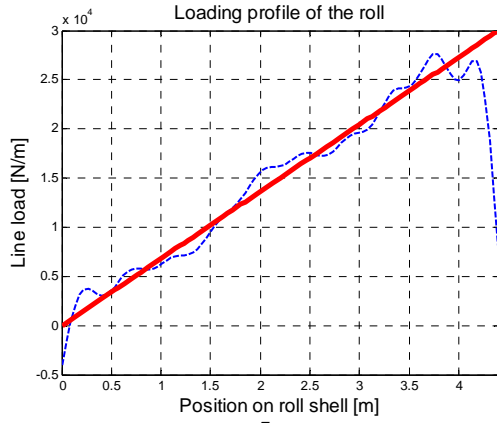


Figure 65. SS  $\delta = 10^{-7}$ ,  $\mathbf{Z}_{22B}$ .

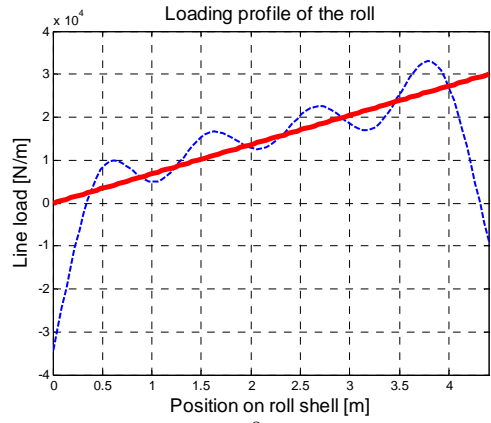


Figure 66. FF  $\delta = 10^{-8}$ ,  $\mathbf{Z}_{10B}$ .

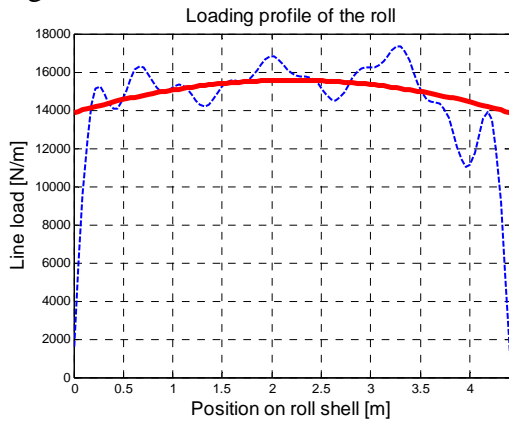


Figure 67. SS  $\delta = 10^{-7}$ ,  $\mathbf{Z}_{22B}$ .

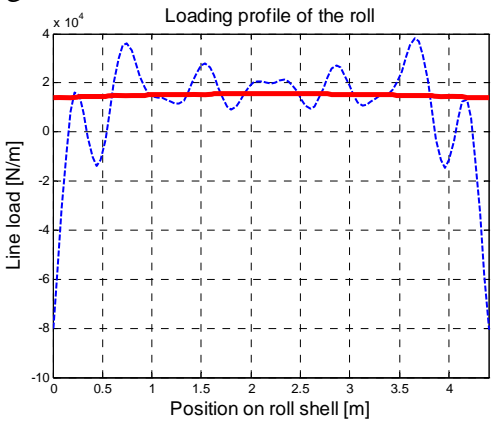


Figure 68. FF  $\delta = 10^{-7}$ ,  $\mathbf{Z}_{22B}$ .

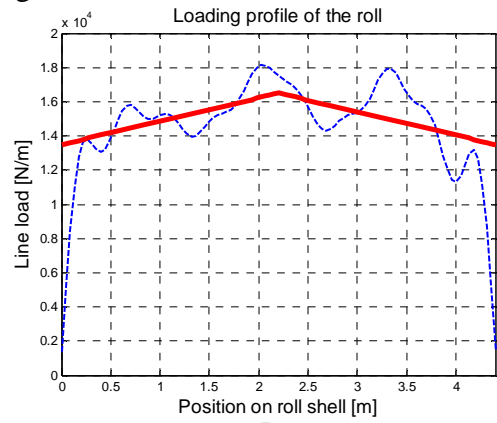


Figure 69. SS  $\delta = 10^{-7}$ ,  $\mathbf{Z}_{22B}$ .

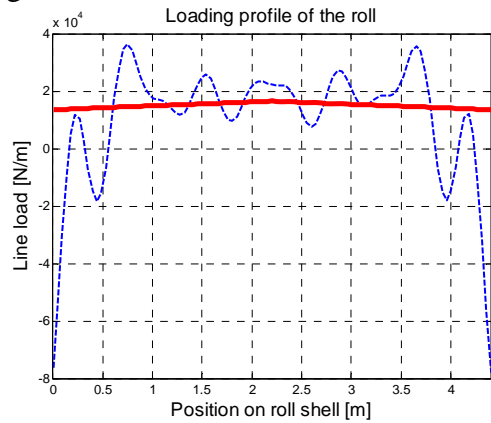


Figure 70. FF  $\delta = 10^{-7}$ ,  $\mathbf{Z}_{22B}$ .

## **7. Analysis of the inverse load sensing method in a dynamic case, case study: pilot roll press**

In this chapter, the feasibility of the inverse load sensing method is analyzed further in a dynamic environment, and a case study of a rotating paper machine roll is presented. The dynamic environment presents a challenge, because there are more forces acting on the rotating roll than there are in a static case. The influence coefficient matrices for the roll are determined, as previously with the unit point force approach in section 6.2.1, using the appropriate measurement points of the measurement system. The dynamic forces have to be accounted for in such a way that the quasi-static assumption is valid. This is done by measuring and treating the strain appropriately. Finally, the real strain measurements serve as an input for the different load solving routines proposed, and the loading distribution results thereby obtained can then be analyzed more carefully.

### **7.1 Strain measurements of the pilot roll press**

The strain measurement system of the lower roll was presented in section 2.2. Not all of the strain gages can be used at the same time, since there are four A/D converters. Nevertheless, it is found that 12 strain signals could be measured simultaneously using multiplexing, and their locations on the roll inner wall are represented in figure 71. In each location, both axial and tangential strains are measured. The measurement frequency used is 2 kHz.

#### **7.1.1 Dynamical considerations**

In contrast to the static cases, this time the operational environment is dynamical. On the other hand, the line load, which one is trying to measure, is assumed to behave quasi-statically. In order to use the proposed inverse load sensing method, one has to separate the quasi-static strain response of the line load. Thus, all the other significant responses originating from the other dynamic force components included in the directly measured strain data have to be taken into account for, before performing the final inverse calculation procedure. The direct strain measurements at a point including all strain responses under a 15 kN/m line load are illustrated in figure 72.

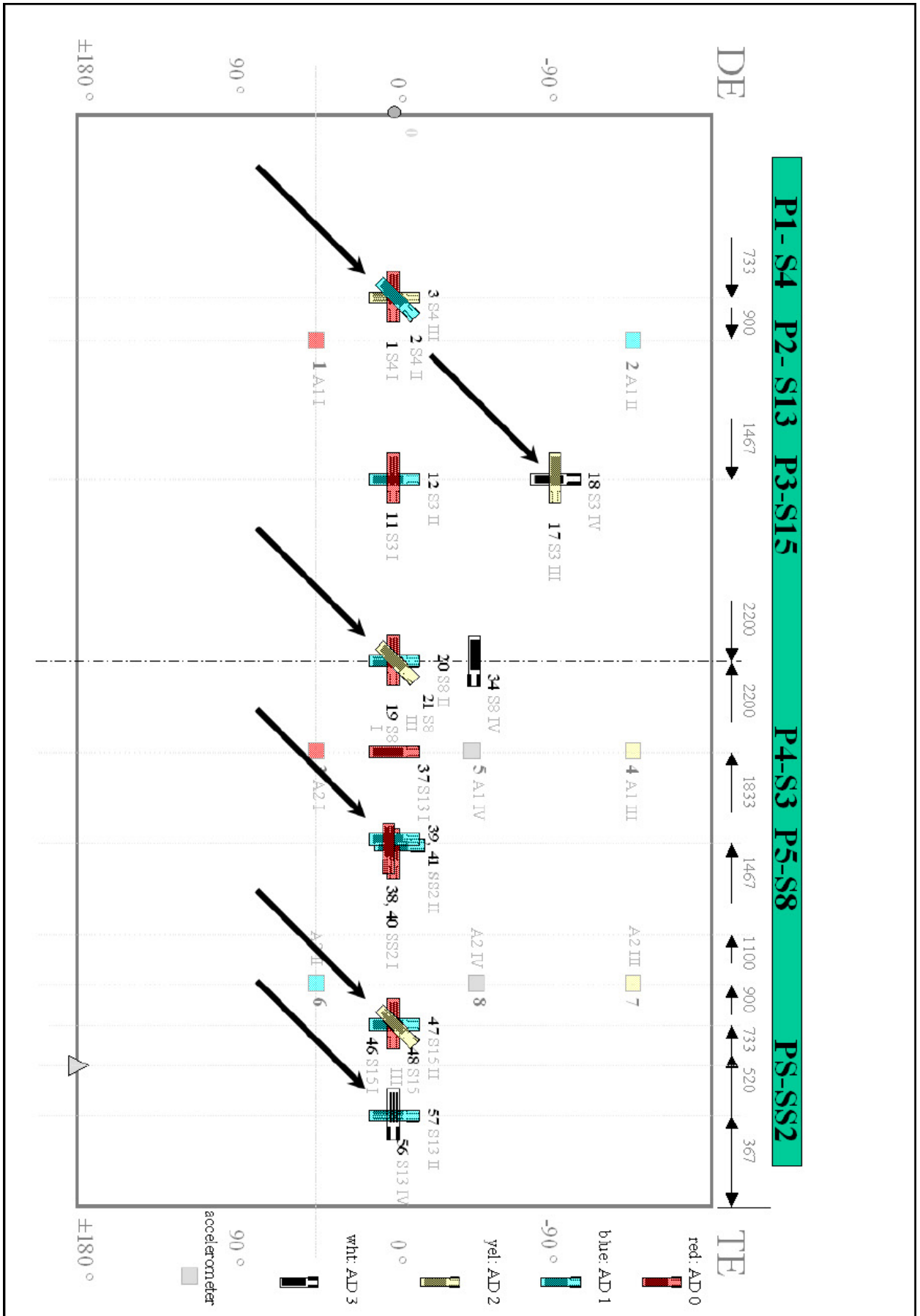


Figure 71. The strain gauges of the lower roll used in the measurements pointed out with arrows.

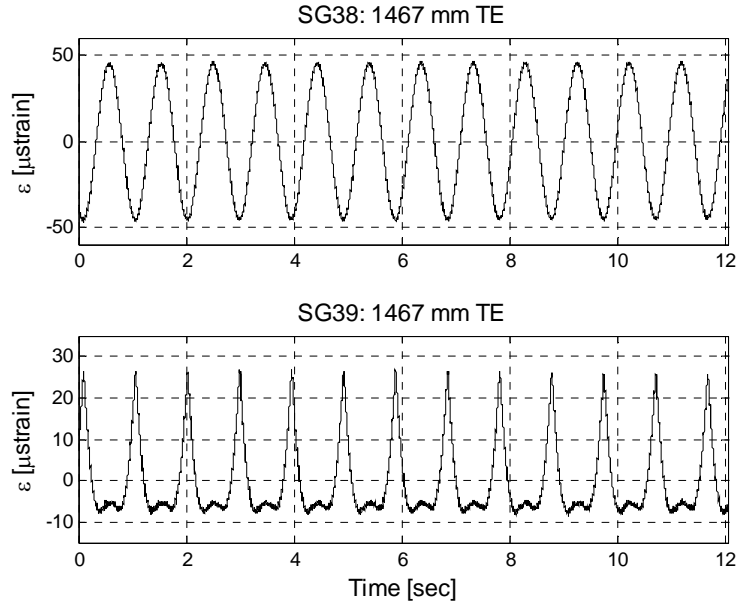


Figure 72. Axial (upper) and tangential (lower) strain responses at a measurement point.

The two significant loadings that have a noticeable influence on the strain response of the roll are the gravity and the centrifugal force. Fortunately, the strain response of these two force components can be measured, and then subtracted from the directly measured strain data to find out the sole strain response of the line load. When the nip is open, gravitational and centrifugal forces are the dominant force components, and their respective responses can be measured for desired rotational speeds. The axial and tangential strain data at a point, caused by gravity and centrifugal force, is presented in figure 73.

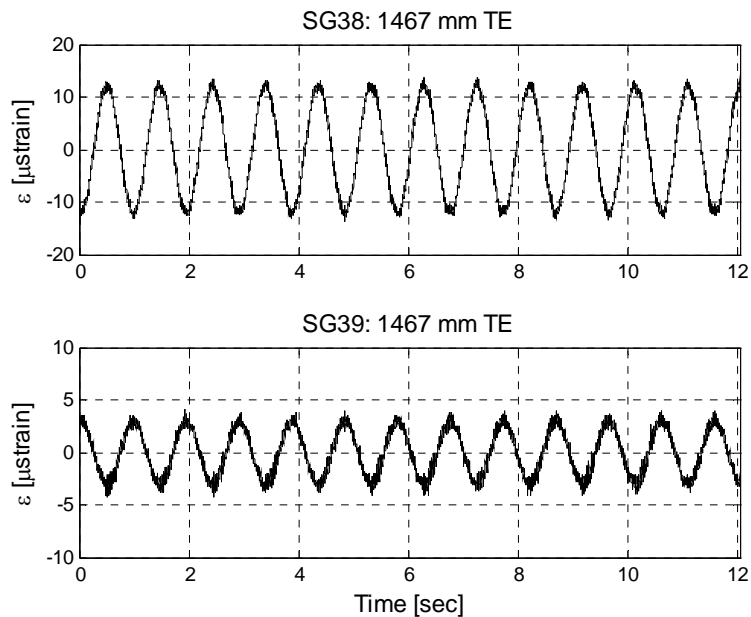


Figure 73. Axial (upper) and tangential (lower) strain responses of gravity and centrifugal forces at a measurement point.

When making the strain measurements, naturally, resonance situations should be avoided. In addition, the excitation caused by unbalance of the roll confuses the measurement data, and therefore has to be avoided.

### **7.1.2 Adapting the measurements**

Accordingly, the system matrices or the inverse load sensing method using the unit point force approach were determined in a position, where the strain measurements are done at the opposite side of the line load (“bottom” position). This means the strain data from the measurements has to be recorded accordingly.

The strain measurement procedure is performed as follows. First the strain data from all of the desired 12 measurement points is recorded for a suitable period of time that depends of the rotational speeds. For each speed, the minimum of 10 revolutions is recorded. These measurements are done with the nip closed, using the desired nip loads and speeds, and also with the nip open for the same corresponding speeds.

Then, the measurement signals are processed. The angular coordinate is determined on the basis of the local maximum values at the nip, and at the lowest point nip closed and nip open respectively. The raw measurement data is filtered with a low-pass Butterworth filter at a suitable frequency that depends on the rotational speeds. Also, the offset has to be removed, i.e., the zero-level of the strain signals is determined as a mean value from the full revolutions of the measurement signals.

Finally, the strain values at the desired angular measurement location are averaged over the whole measurement signal, nip closed and nip open respectively. Thus, the sole strain response of the line load at the measurement points is determined by subtracting the nip open value from the nip closed value.

Since one is dealing with real measurements, there is always some amount of disturbances in the measurement data, all of which can not be eliminated by filtering. Also, the definition of the zero level is somewhat difficult. Nevertheless, it can be said that the measurements and strain calculations with the FE model correspond quite well, even though the crowning shape of the roll is not included in the FE model.

## 7.2 Calculating the loading profile based on strain measurements

Finally, the strain values measured from the pilot roll press are used in the inverse load sensing procedure. Based on section 6.2.1, the unit point force approach with Tikhonov regularization is used. Then, the solutions are compared to reference line load measurements that were carried out with nip paper.

### 7.2.1 Results when unit point force approach is used

Two different unit point force cases, cases I and II from table 7, are used to describe the line load distributions with five and ten point forces, respectively. For determining the system matrices, the FE model of section 6.2 and all of the 12 measurable strains are used. The strains were measured under two different line loads, the nominal line load of 15 kN/m and the line load of 20 kN/m, and two different running speeds, 20 m/min and 200 m/min. The inverse solutions were calculated with a couple of different regularization parameters, and using both regularization approaches of Eqs. (20) and (19). The results for each run are plotted in figures 74-89, where TE is on the left (zero) and DE is on the right side.

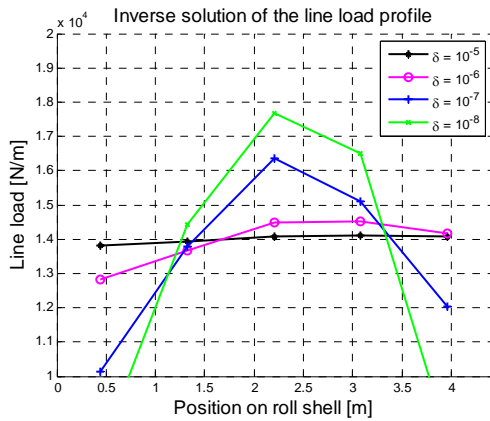


Figure 74. 15 kN/m, 20 m/min Eq. (20).

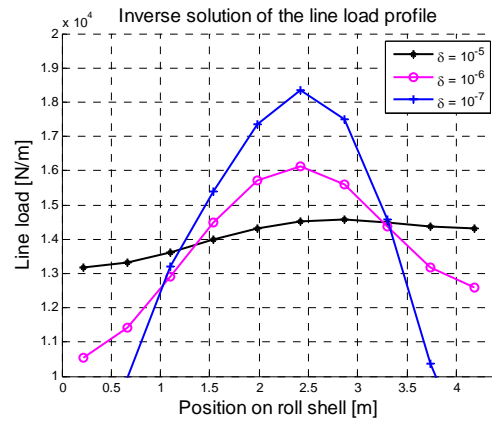


Figure 75. 15 kN/m, 20 m/min Eq. (20).

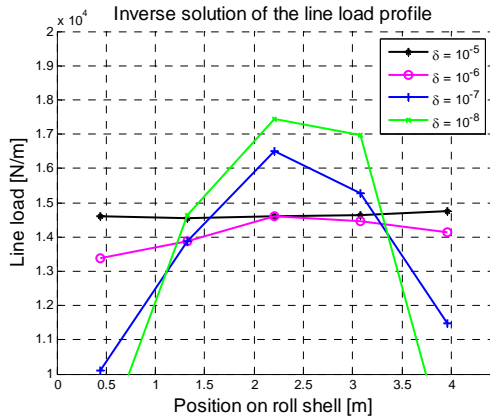


Figure 76. 15 kN/m, 20 m/min Eq. (19).

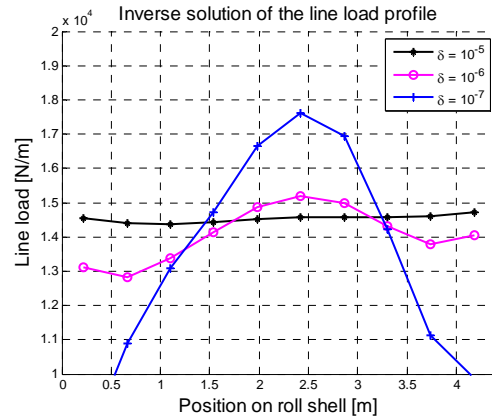


Figure 77. 15 kN/m, 20 m/min Eq. (19).



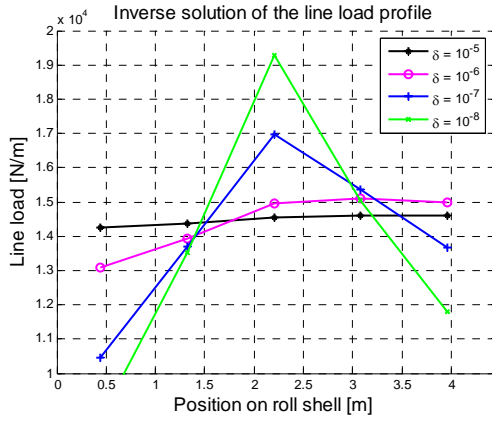


Figure 78. 15 kN/m, 200 m/min Eq. (20).

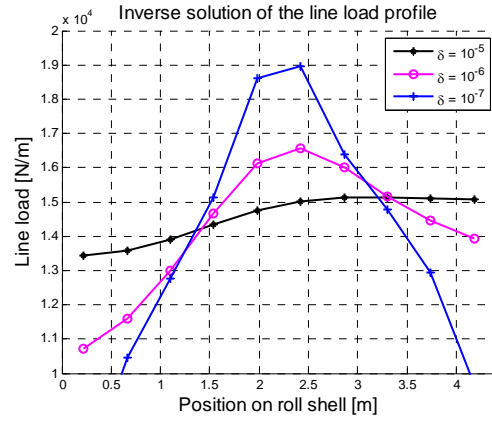


Figure 79. 15 kN/m, 200 m/min Eq. (20).

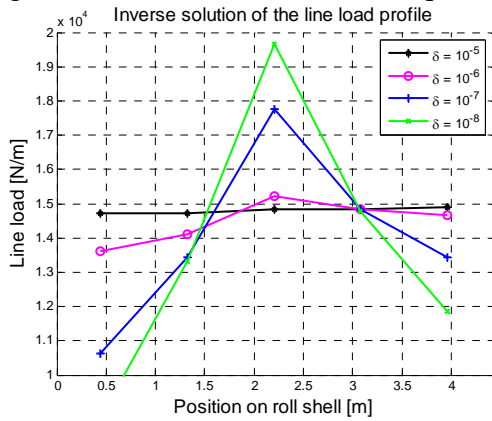


Figure 80. 15 kN/m, 200 m/min Eq. (19).

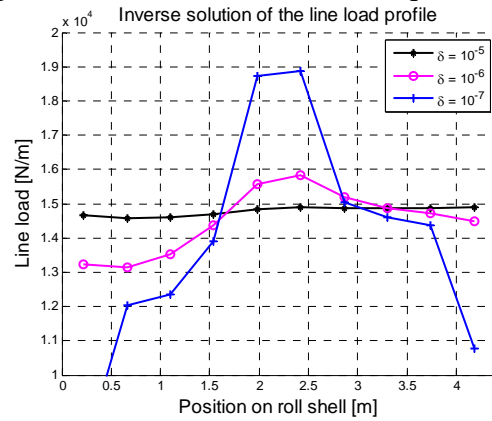


Figure 81. 15 kN/m, 200 m/min Eq. (19).

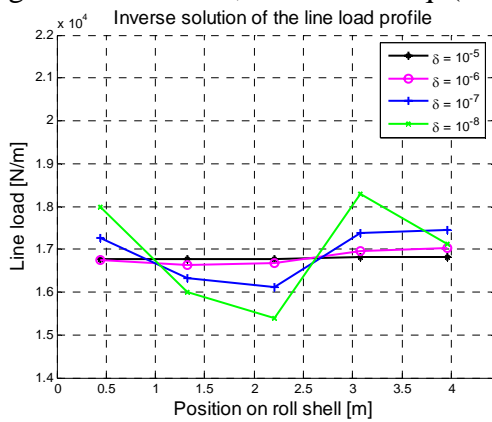


Figure 82. 20 kN/m, 20 m/min Eq. (20).

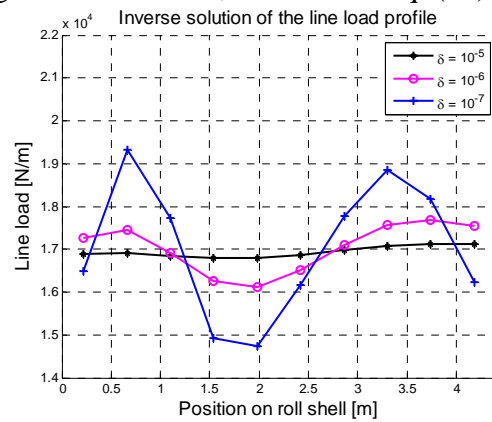


Figure 83. 20 kN/m, 20 m/min Eq. (20).

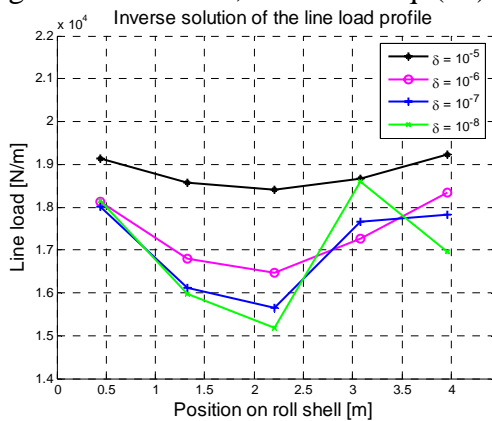


Figure 84. 20 kN/m, 20 m/min Eq. (19).

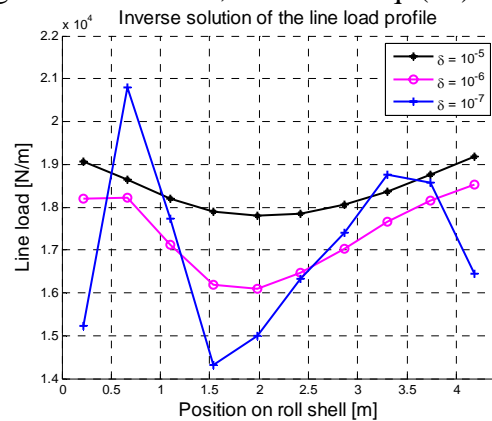


Figure 85. 20 kN/m, 20 m/min Eq. (19).

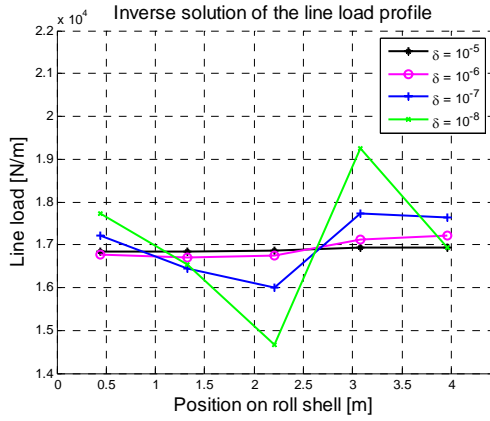


Figure 86. 20 kN/m, 20 m/min Eq. (20).

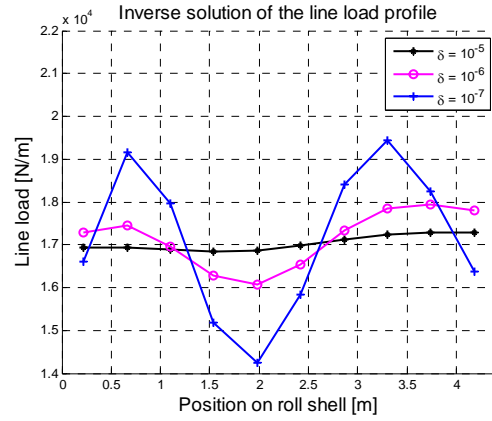


Figure 87. 20 kN/m, 20 m/min Eq. (20).

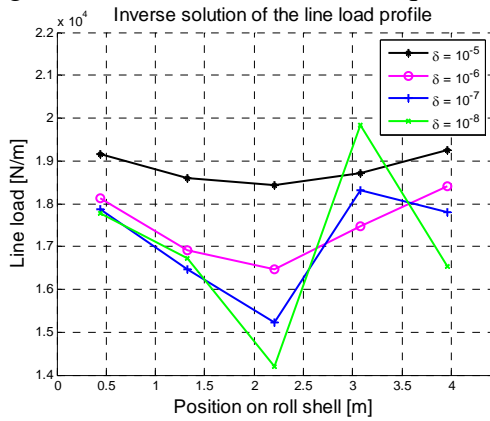


Figure 88. 20 kN/m, 200 m/min Eq. (19).

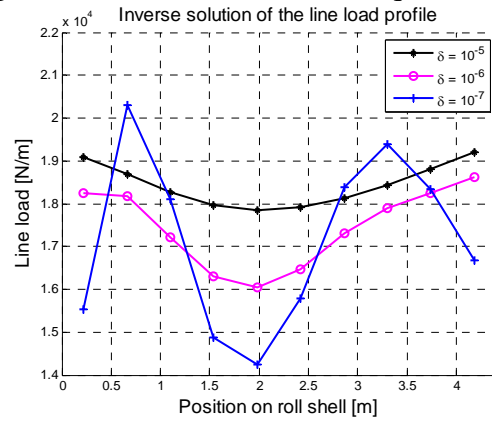


Figure 89. 20 kN/m, 200 m/min Eq. (19).

The results are interesting. First of all, the running speed does not have an effect on the results; the same type of results is obtained with both of the speeds. This merely verifies that the subtraction of the influences of gravity and of centrifugal forces is correct.

With the solutions according to Eq. (20), the level of the line loading seems to be lower than it should be, since with 15 kN/m it is about 14.5 kN/m and with 20 kN/m only about 17 kN/m. In comparison, the inverse solutions of Eq. (19) are closer to the real load level. For better examination, the inverse solutions with suitable regularization parameters are plotted and demonstrated in figures 90-97. Based on the results of figures 74-89, the suitable values for the regularization parameter  $\delta$  are  $10^{-6}$  for load case I and  $10^{-5}$  for load case II. Interestingly, the approximations of the L-curve of  $\delta$  are also just slightly larger than the chosen values, and the same type of over-regularization effect as in the analysis of section 6.2 did not occur with these real strain measurements of the roll. Since the running speed did not make any difference, 20 m/min is used.

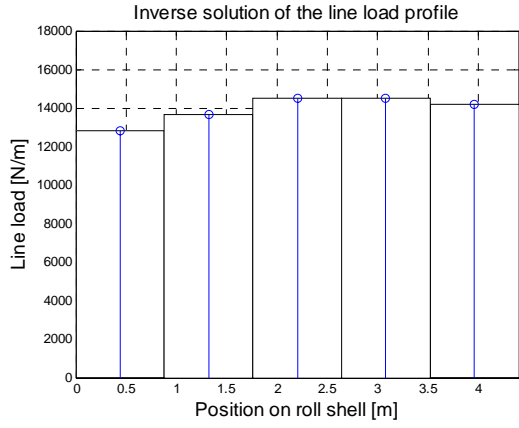


Figure 90. 15 kN/m, 20 m/min Eq. (20).

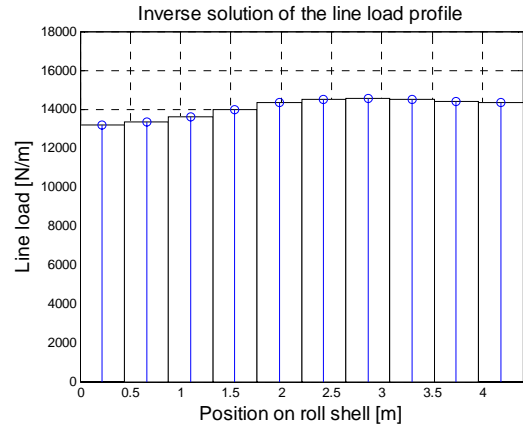


Figure 91. 15 kN/m, 20 m/min Eq. (20).

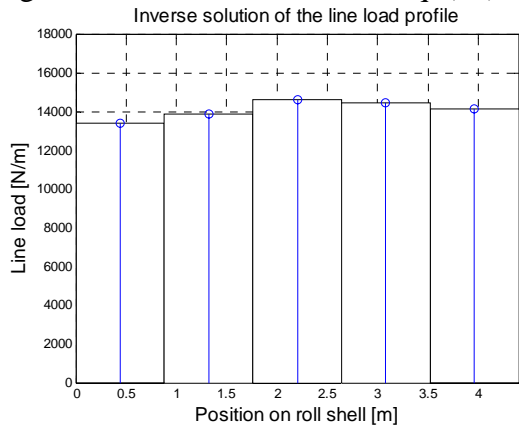


Figure 92. 15 kN/m, 20 m/min Eq. (19).

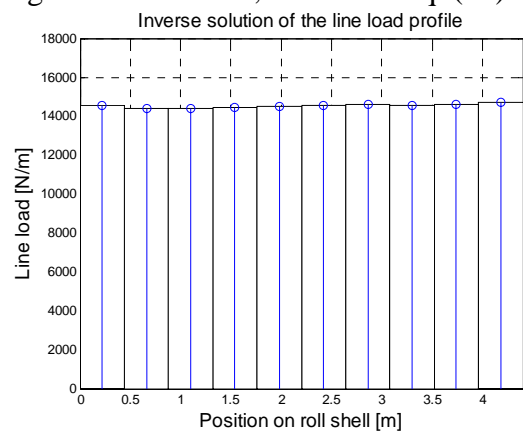


Figure 93. 15 kN/m, 20 m/min Eq. (19).

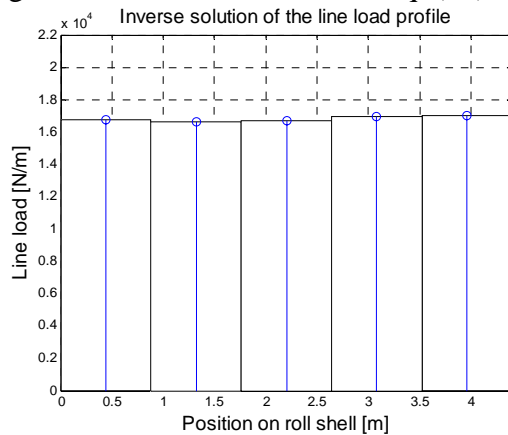


Figure 94. 20 kN/m, 20 m/min Eq. (20).

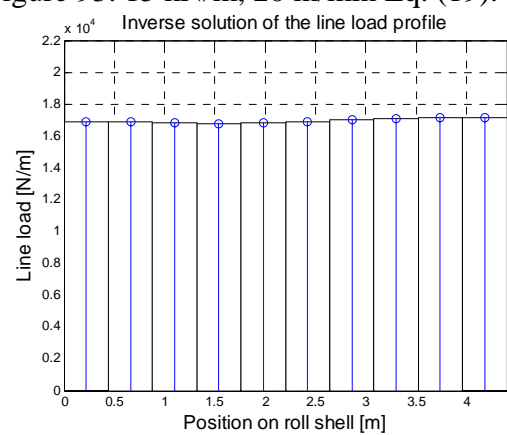


Figure 95. 20 kN/m, 20 m/min Eq. (20).

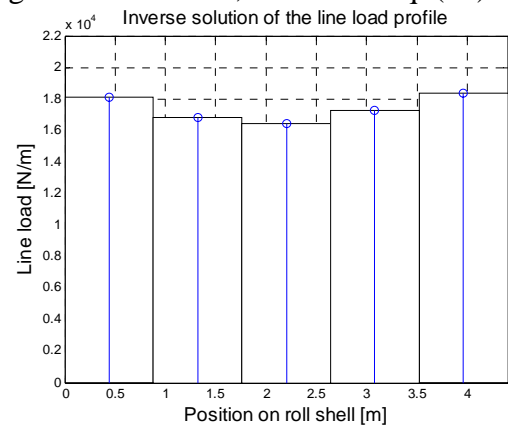


Figure 96. 20 kN/m, 20 m/min Eq. (19).

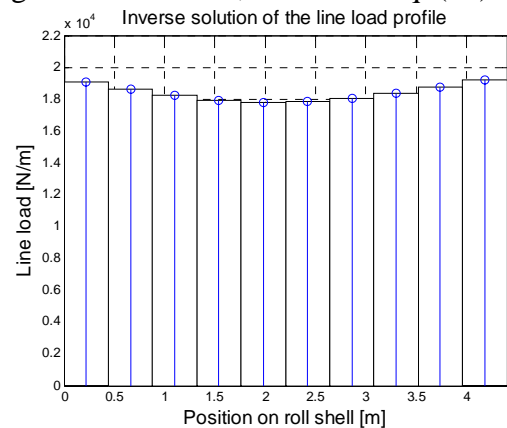


Figure 97. 20 kN/m, 20 m/min Eq. (19).

With the two different line load intensities (15 kN/m and 20 kN/m), the results from Eqs. (20) and (19) differ slightly. Based on Eq. (20), under 15 kN/m the line load profile is sine shaped with its maximum in the center, slightly on the DE, while Eq. (19) produces similar, but more constant, line load profiles. When there are more point forces describing the profile in figure 93, especially, the profile is almost even. Under 20 kN/m, the line load profile is slightly dented in the middle with maxima at the ends, the greater value at the DE once again. The distinction between Eqs. (20) and (19) is that with Eq. (19), the maxima at the ends are notably higher.

Moreover, the conclusions about the load level made previously apply here as well. The line load level of the inverse procedure might be caused by some faulty measurements of the strain itself since, for instance, the tangential strain values are relatively small and therefore susceptible to errors. Nevertheless, with Eq. (19), where the line load level and the probable shape is assumed to be known, the load level can also be more accurately interpreted. In fact, the conventional line load measurement system of load sensors at the ends of the rolls indicates the actual load level very accurately. Combined with this inverse load sensing method, information about the load distribution itself could be obtained.

These solutions obtained for the line load profiles can be considered reasonable, since 15 kN/m is the nominal load for which the crowning is designed, and therefore at 15 kN/m the line load profile should be even. At 20 kN/m, the maximum loads occur at the ends because of the bending of the roll. Thus, the inverse load sensing method is feasible. The comparison to reference measurements is made in the next section.

### **7.2.2 Reference results from the nip paper measurements**

As a reference, the line loading of the nip unit was measured with nip paper under line loads of 15 and 20 kN/m. The results of these nip profile measurements are presented in figures 98 and 99, where DE is on the right side, and TE on the left. The nip paper measurements were done with a very slow roll speed.

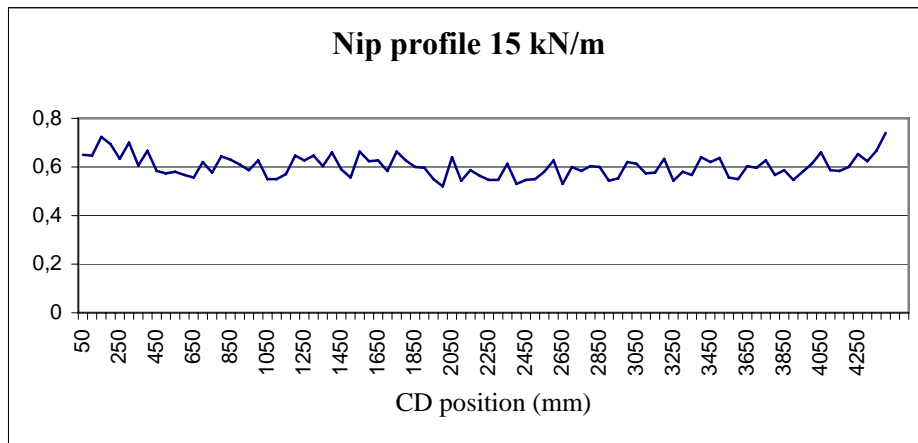


Figure 98. Nip profile under 15 kN/m loading measured with nip paper [Ainasoja 2008].

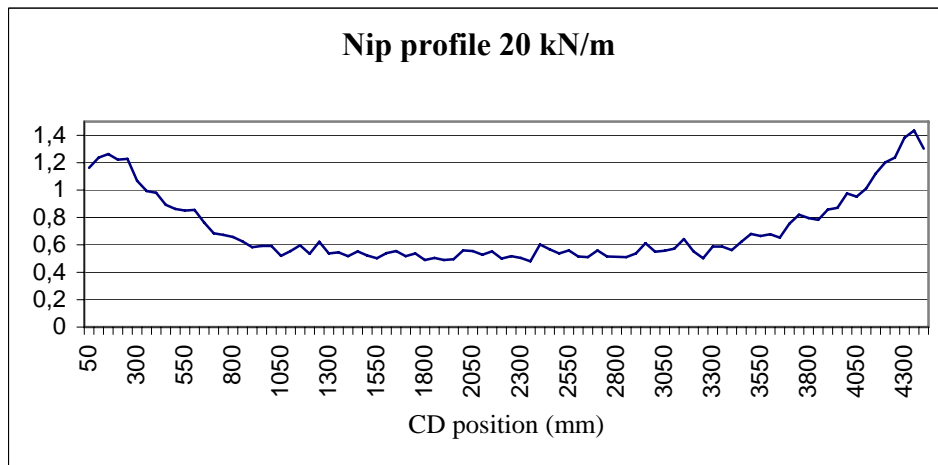


Figure 99. Nip profile under 20 kN/m loading measured with to nip paper [Ainasoja 2008].

In comparison to the results of the inverse load sensing method in figures 90-97, these results from the nip paper measurements are a bit different. The line load profile under 15 kN/m of figure 98, especially, is almost even, and has its peak values at the ends, as compared to figures 90-92 in which the profile was sine shaped and the maximum was at the centre. However, the inverse solution produced by Eq. (19) in figure 93 is very close to the even line load. Furthermore, with 20 kN/m, the nip paper measurements of figure 81 give stronger peak values at the ends, as compared to results of figures 94 and 95, but again, and now with fewer point forces moreover, the inverse solutions of Eq. (19) in figures 96 and 97 are fairly close to the reference profile. In addition, a slight DE tendency of the line load profile is noticeable in the reference measurements. All things considered, all of the compared results have their similarities, and the results of the inverse load sensing method can be considered feasible. Correspondingly, the interpretation of the different regularization approaches, and that of the parameters has to be made carefully.

## 8. Conclusions

A new method for measuring line load distributions of beam-like structures was proposed. The goal of this study was to develop and investigate the feasibility of the load sensing method. The main applications of this work are the unit processes of paper manufacturing, where line load is an important control parameter influencing the surface quality of the paper web such as surface sizing and calendering. In those processes, the paper web is compressed between rolls in a contact zone, where the line load distribution in the cross direction not only affects on the paper, but also the rotating beam-like roll structures. In the proposed method, the strain response of one of the roll structures is measured, and based on that, the governing line load input is calculated using an inverse formulation. In this study, the inverse method is called the inverse load sensing method.

The inverse load sensing method is based on a system matrix, which is composed of influence coefficients and describes the relation of the known strain data and the unknown line load distribution. These types of methods have been used in various applications of structural force identification studies, and even rotor balancing procedure is based on the same type of principle for example. The basic principle of the method is to use the known response data (strain) to calculate the unknown input (load) that caused it in the first place by utilizing a system matrix that relates the input to the response. Thus, the problem is inverse.

In many cases, as often occurs in inverse problems in general, the system equations tend to be ill-posed, which means that even the smallest disturbances in the measured data contribute to large errors in the solution. In order to eliminate or reduce these kinds of stability problems in the solutions, some kind of regularization technique has to be used. With appropriate regularization, one can improve the solution quality by taking into account additional *a priori* information in the procedure. In this case, Tikhonov regularization was used.

The strain-force relationship of a structure is described by a system matrix, which was first determined by a unit load procedure. Two different unit load approaches were considered; i.e., the system matrix was determined from 1) unit point forces, and 2) unit loading functions. The matrix can be constructed on either a purely computational basis, or a

purely experimental basis. In this work, the choice of method was based on what was appropriate for any given application.

The method was initially implemented for a static structure, but since the main application of a paper machine roll is a rotating rotor, rotor dynamics have to be considered. With appropriate handling of the data one could, in fact, use the static implementation of the method in the case of the rotating roll. The rate, at which the line load changes, is relatively slow, and a quasi-static approach is thereby justified.

The implementation of the method was first tested by two smaller static case studies, with which point force/forces were solved based on the strain measurements of the structures. These two beam-like case studies, a simply supported prismatic beam and a tubular roll structure, demonstrated the feasibility and applicability of the method to real structures and strain measurements. Point forces were efficiently solved and the ill-posed equations did not present harmful problems.

Then the method was analysed with a roll structure, which was affected by different line load distributions. This analysis was intended as a preliminary to the real measurement case of a pilot roll press, since the computational model and the roll share the same geometry and properties. Also, the influence of different measurement and load set-ups, as well as the response to disturbances in the measurement data, was to be analysed. These analyses were purely computational and involved calculating the measured strain data artificially by a FE model, and adding some random error to it. The system matrices themselves were also determined with FEM, but with a different FE model in case of 1) unit point forces and 2) unit loading functions. In case 1), *a priori* knowledge was utilized with two different regularization approaches, while in case 2), two different functional bases and elementary regularization were used.

The results in case 1) were excellent and that approach can therefore be considered as feasible with either of the regularization approaches used. The simulated line load profiles were efficiently detected with the inverse method even with a small number of measurement points. The depiction of the line load profiles was more distinctive when more measurement data, and consequently more specific load data, was attained. However, there were some differences between the outcome of the two regularization approaches and

one should always carefully consider which of them would perform better in a given application.

In case 2) the results were not as good, even though two different functional bases were utilized. The major problem with approach 2) was the presence of vigorous oscillations in the inverse results that originated from the errors in the strain data. Approach 2) was not feasible when the strain data was disturbed. Another important observation when the two approaches are compared is the lack of good *a priori* in approach 2) as compared to the efficient *a priori* knowledge of approach 1).

Finally, the feasibility of the inverse load sensing method was verified using measurements of a real pilot roll press, where the line load distribution was calculated based on the data of 12 strain signals. Approach 1), with unit point forces, was utilized, and both of the previously studied *a priori* approaches for regularization were investigated. The inverse results obtained were compared to reference results for the line load profile measured using nip paper. The correspondence of the inverse results to the nip paper measurements was not perfect, but the inverse load sensing method can nevertheless be regarded as feasible for line load determination. As before, there were slight differences between the inverse solutions of the two different regularization approaches; the other one was notably closer to the reference profiles. Moreover, the results obtained were more sensitive to changes in the measured strain data albeit stable. This only confirms the fact that one has to try out and evaluate different regularization approaches and parameters to find the most suitable one for the application at hand.

The results from the analyses of the roll structure, in the case of unit point force approach, were impressive, and the method also worked satisfactory in a real dynamic measurement application of the pilot roll press, even with a limited amount of measurement data.

In the future, the inverse load sensing method should be further investigated using real nip measurements, and the number of measurement points increased. An integrated control system that would use this method to measure and zone-controlled rolls to adjust the line load distribution of the nip could be designed and studied. In addition, the implementation of the strain measurement system could be developed to suit the rotating roll applications better. Moreover, other possible applications for the method could be considered.



## 9. References

Adams R. & Doyle J.F., 2002, Multiple Force Identification for Complex Structures, *Experimental Mechanics*, Vol. 42(1), pp. 25-36.

Ainasoja T., 2008, Iroll-tekniikan soveltuvuus analyysityökaluksi paperin jälkikäsitelyssä, MSc. Thesis, University of Oulu, 90 p.

Allen M.J. & Dibley R.P., 2003, Modelling Aircraft Wing Loads from Flight Data Using Neural Networks, NASA TM-2003-212032.

Bathe K-J., 1982, *Finite Element Procedures in Engineering Analysis*, Prentice-Hall Inc., New Jersey, USA, 735 p.

Bishop R.E.D. & Gladwell G.M.L., 1959, The Vibration and Balancing of an Unbalanced Flexible Rotor, *Journal of Mechanical Engineering Science*, Vol. 1(1), pp. 66-77.

Bisplinghoff R. L., 1955, *Aeroelasticity*, Dover publications, New York, USA, 860 p.

Busby H.R. & Trujillo D.M., 1987, Solution of an Inverse Dynamics Problem using an Eigenvalue Reduction Technique, *Computers & Structures*, Vol. 25(1), pp. 109-117.

Busby H.R. & Trujillo D.M., 1995, Optimal Regularization of an Inverse Dynamics Problem, *Computers & Structures*, Vol. 63 (2), pp. 234-248.

Chan T.H.T., Yu L., Law S.S. & Yung T.H., 2001a, Moving Force Identification Studies, I: Theory, *Journal of Sound and Vibration*, Vol. 247(1), pp. 59-76.

Chan T.H.T., Yu L., Law S.S. & Yung T.H., 2001b, Moving Force Identification Studies, II: Comparative Studies, *Journal of Sound and Vibration*, Vol. 247(1), pp. 77-95.

Chen, W.J. & Gunter, E.J., 2005, *Introduction to Dynamics of Rotor-Bearing Systems*, Trafford Publishing, Victoria, British Columbia, Canada, 481 p.

Choi H.G., Thite A.N. & Thompson D.J., 2007a, A Threshold for the Use of Tikhonov Regularization in Inverse Force Determination, *Applied Acoustics* 67, pp.700-719.

Choi H.G., Thite A.N. & Thompson D.J., 2007b, Comparison of Methods for Parameter Selection in Tikhonov Regularization with Application to Inverse Force Determination, *Journal of Sound and Vibration*, Vol. 304, pp. 894-917.

Dally J.F. & Riley W.F., 1991, *Experimental Stress Analysis*, 3<sup>rd</sup> ed., McGraw-Hill Inc., New York, USA, 639 p.

Doyle J.F., 2004, *Modern Experimental Stress Analysis*, John Wiley & Sons Ltd., Chichester, England, 424 p.

Ehrich Fredric F., 1992, *Handbook of Rotordynamics*. McGraw-Hill Inc., USA, 452 p.

Engl H.W., Hanke M. & Neubauer A., 1996, *Regularization of Inverse Problems*, Kluwer Academic Publishers, The Netherlands, 321 p.

Gobbi M., Gastinu G. & Giorgietta F., 2005, Sensors for Measuring Forces and Moments with Application to Ground Vehicle Design and Engineering, *Proceedings of IMECE2005 ASME International Mechanical Engineering Congress and Exposition*, November 5-11, Orlando, Florida, USA.

Goodman T.P.A., 1964, A Least-Squares Method for Computing Balance Corrections. *Journal of Engineering for Industry*, Transactions of ASME, Vol. 86(3), pp. 273-279.

Granger S. & Perotin L., 1999a, An Inverse Method for the Identification of a Distributed Random Excitation Acting on a Vibrating Structure Part 1: Theory, *Mechanical Systems and Signal Processing*, Vol. 13(1), pp. 53-65.

Granger S. & Perotin L., 1999b, An Inverse Method for the Identification of a Distributed Random Excitation Acting on a Vibrating Structure Part 2: Flow-induced Vibration Application, *Mechanical Systems and Signal Processing*, Vol. 13(1), pp. 67-81.

Hansen, P.C., 1992, Analysis of Discrete Ill-posed Problems by Means of the L-curve, SIAM Review, Vol. 34, pp.561-580.

Hollandsworth P.E. & Busby H.R., 1989, Impact Force Identification Using General Inverse Technique, International Journal of Impact Engineering, Vol. 8(4), pp. 315-322.

Hurty W.C. & Rubinstein M.F., 1964, Dynamics of Structures, Prentice-Hall, New Jersey, USA, 455 p.

ISO 11342:1998, 1998, Mechanical Vibration -- Methods and Criteria for the Mechanical Balancing of Flexible Rotors, 39 p.

Jacquelin E., Bennani A. & Hamelin P., 2003, Force Reconstruction: Analysis and Regularization of a Deconvolution Problem, Journal of Sound and Vibration, Vol. 265, pp. 81-107.

Järvenpää V-M., 2005, Numerical Modelling of a Roll Mechanism for Multi-Objective Dynamical Analyses, Phd. Thesis, Tampere University of Technology, Publications 569, 97 p.

Järvinen V., 2003, Analysis of Whirling Response by Internal Roll Sensing Method, Phd. Thesis, Tampere University of Technology, Publications 455, 99 p.

Jenkins J.M. & DeAngelis V.M., 1997, A Summary of Numerous Strain-Gage Load Calibrations on Aircraft Wings and Tails in a Technology Format, NASA TM 4804.

Jenkins J.M. & Kuhl A.E., 1977, A Study of the Effect of Radical Load Distributions on Calibrated Strain Gage Load Equations, NASA TM 56047.

Jokio M., 1999, Book 10: Papermaking, Part 3, Finishing, Fapet, Helsinki, Finland, 361 p.

Kaipio J. & Somersalo E., 2005, Statistical and Computational Inverse Problems, Springer Science+Business Media, New York, USA, 339 p.

Kaipio J. & Somersalo E., 2006, Statistical Inverse Problems: Discretization, Model Reduction and Inverse Crimes, *Journal of Computational and Applied Mathematics*, Vol. 198(2), pp. 493-504.

Kang Y., Chang Y-P., Tseng M-H., Tang P-H. & Chang Y-F., 2000, A Modified Approach on Influence Coefficient Method for Balancing Crank-Shafts, *Journal of Sound and Vibration*, Vol. 234(2), pp. 277-296.

Kang Y., Lin T-W., Chang Y-P., Wang Y-P. & Hsueh C-C., 2006, Study in Balancing Accuracy and Condition Number of Flexible Rotors, *Proceedings of the 25<sup>th</sup> IASTED International Conference of Modelling, Identification, and Control*, February 6-8, 2006, Lanzarote, Canary Islands, Spain.

Kang Y., Liu C-P. & Sheen G-J., 1996, A Modified Influence Coefficient Method for Balancing Unsymmetrical Rotor-Bearing Systems, *Journal of Sound and Vibration*, Vol. 194(2), pp. 199-218.

Kang Y., Sheen G-J. & Wang S-M., 1997, Development and Modification of a Unified Balancing Method for Unsymmetrical Rotor-Bearing Systems, *Journal of Sound and Vibration*, Vol. 199(3), pp. 349-368.

Kang Y., Tseng M-H., Wang S-H., Chiang C-P. & Wang C-C., 2003, An Accuracy Improvement for Balancing Crank Shafts, *Mechanism and Machine Theory*, Vol. 38, pp. 1449-1467.

Karlsson S.E.S., 1996, Identification of External Structural Loads from Measured Harmonic Responses, *Journal of Sound and Vibration*, Vol. 196(1), pp. 59-74.

Kellenberger W., 1972, Should a Flexible Rotor Be Balanced in  $N$  or  $(N+2)$  Planes?, *Journal of Engineering Industry, Transactions of ASME, Series B*, Vol. 94(2), pp. 548-560.

Keskinen E. & Kivinen J-M., 2002, Continuous balancing method for long flexible rotors, *Proceedings of IMAC-XX: A Conference on Structural Dynamics*, February 4-7, 2002, Los Angeles, California, USA, pp. 511-515.

Keskinen E., Järvinen V., Miettinen J. & Sundström K., 2002, Fatigue Monitoring of Paper Machine Rolls by Internal Strain Gage Measurements, Proceedings of 3rd Asia-Pacific Conference on Systems Integrity and Maintenance, September 25.-27, 2002, Cairns, Australia, pp. 184-189.

Keskiniva M., 1997, Simulation and Balancing of Flexible Rotors in Terms of Semidefinite Modal Coordinates, Phd. Thesis, Tampere University of Technology, Publications 220, 125 p.

Kivinen J-M., 2001, A Variable Parameter Facility for Dynamic Testing of Polymer Covered Paper Machine, Phd. Thesis, Tampere University of Technology, Publications 347, 95 p.

KnowPap, 2007, Knowpap Program 9.0 (11/2007).

Kolehmainen V., Siltanen S., Järvenpää S., Kaipio J.P., Koistinen P., Lassas M., Pirttilä J. & Somersalo E., 2003, Statistical Inversion for Medical X-ray Tomography with few Radiographs II: Application to Dental Radiology, Physics in Medicine and Biology, Vol. 48, pp. 1465-1490.

Law S.S., Bu J.Q., Zhu X.Q. & Chan S.L., 2004, Vehicle Axle Loads Identification Using Finite Element Method, Engineering Structures, Vol. 26(8), pp. 1143-1153.

Lehtinen E., 2000, Book 11: Pigment Coating and Surface Sizing of Paper, Fapet, Helsinki, Finland, 810 p.

Liu Y. & Shepard Jr., W.S., 2006, An Improved Method for the Reconstruction of a Distributed Force Acting on a Vibrating Structure, Journal of Sound and Vibration, Vol. 291, pp. 369-387.

Lokos W.A., 2004, Strain-Gage Loads Calibration Parametric Study, NASA TM-2004-212853.

Lund J.W. & Tonnesen, J., 1972, Analysis and Experiments on Multi-Plane Balancing of a Flexible Rotor, Journal of Engineering for Industry, Transactions of ASME, Vol. 94(1), pp. 233-242.

Maniatty A., Zabaraz N. & Stelson K., 1989, Finite Element Analysis of Some Inverse Elasticity Problems, Journal of Engineering Mechanics, Vol. 115(10), pp. 1303-1317.

Martin M.T. & Doyle J.F., 1996a, Impact Force Identification from Wave Propagation Responses, International Journal of Impact Engineering, Vol. 18 (1), pp. 65-77.

Martin M.T. & Doyle J.F., 1996b, Impact Force Location in Frame Structures, International Journal of Impact Engineering, Vol. 18 (1), pp. 79-97.

Metso Paper Product Catalogues, 2008, <http://www.metsopaper.com>.

MTS sensors, 2008, <http://www.mts.com> (cited 10.10.2008).

Nagakiri S. & Suzuki K., 1999, Finite Element Interval Analysis of External Loads Identified by Displacement Input with Uncertainty, Computer Methods in Applied Mechanics and Engineering, Vol. 168, pp. 63-72.

Neumaier A., 1998, Solving Ill-conditioned and Singular Linear Systems: A Tutorial on Regularization, SIAM Review, Vol. 40, pp. 636-666.

Outinen H. & Salmi T., 2004, Lujuusopin perusteet, Pressus Oy, Tampere, Finland, 464 p.

Pat. FI 110712 B, Laitteisto pyörivien telojen värähtelyn hallitsemiseksi, Keskinen E. & Kivinen J-M., Tampere, (Keskinen E. & Kivinen J-M.), Hak. nro FI 20010800, 19.4.2001, (14.3.2003), 6 p.

Pat. FI 114413 B, Menetelmä nippivoiman määrittämiseksi ja nippivoiman tasaamiseksi kahden pyörivän telan välillä, Keskinen E., Miettinen J. & Järvinen V., Tampere, (Keskinen E., Miettinen J. & Järvinen V.), Hak. nro FI 20020501, 18.3.2002, (15.10.2004), 9 p.

Paulapuro H., 2000, Book 8: Papermaking, Part 1, Stock Preparation and Wet End, Fapet, Helsinki, Finland, 461 p.

Perezat C. & Gyander J.L., 1995, Two Inverse Methods for Localization of External Sources Exciting a beam, *Acta Acustica* 3, pp. 1-10.

Perezat C. & Gyander J.L., 2000, Identification of Vibration Sources, *Applied Acoustics*, Vol. 61, pp. 309-324.

Press W.H., Teukolsky S.A. & Vetterling W.T. and Flannery B. P., 1992, *Numerical Recipes in C The Art of Scientific Computing*, 2<sup>nd</sup> ed., Cambridge University Press, New York, USA, 994 p.

Przemieniecki J. S., 1968, *Theory of Matrix Structural Analysis*, Dover Publications, New York, USA, 468 p.

Romppanen A-J., Keskinen E., Miettinen J. & Järvinen V., 2005, Line Load Determination of Press Rolls by Inverse Coefficient Method. *Proceedings of Society of Experimental Mechanics Annual Conference and Exposition on Experimental and Applied Mechanics*, June 7-9, 2005, Portland, Oregon, USA.

Salmenperä P., Järvinen V., Miettinen J. & Hirvonen M., 2002, Wireless Monitoring System for Rotating Rolls. *Proceedings of ICMA in conference on Human-friendly Reliable Mechatronics*, September 11-13, 2002, Tampere, Finland.

Shakespeare J., 2001, *Identification and Control of Cross-Machine Profiles in Paper Machines: A Functional Penalty Approach*, Phd. Thesis, Tampere University of Technology, Publications 352, p. 190.

Shen S., 1986, *Identification of Distributed Static Loadings on Beams*, MSc. Thesis, Florida Atlantic University, Boca Raton, Florida, 83 p.

Siltanen S., Kolehmainen V., Järvenpää S., Kaipio J.P., Koistinen P., Lassas M., Pirttilä J. & Somersalo E., 2003, Statistical Inversion for Medical X-ray Tomography with few Radiographs I: General theory, *Physics in Medicine and Biology*, Vol. 48, pp. 1437-1463.

Skopinski T.H., Aiken Jr. W.S. & Huston W.B., 1954, Calibration of Strain-Gage Installations in Aircraft Structures for the Measurement of Flight loads, NACA Report 1178.

Stevens K.K., 1987, Force Identification Problem – an Overview, Proceedings of SEM Spring Conference on Experimental Mechanics, Florida, USA, pp. 838-844.

Tan S.G. & Wang X.X., 1993, A Theoretical Introduction to Low Speed Balancing of Flexible Rotors: Unification and Development of the Modal Balancing and Influence Coefficient Techniques, *Journal of Sound and Vibration*, Vol. 168(3), pp. 385-394.

Tessarzik J.M., Badgley R.H. & Anderson, W.J., 1972, Flexible Rotor Balancing by the Exact Point-Speed Influence Coefficient Method, *Journal of Engineering for Industry, Transactions of ASME*, Vol. 96(1), pp. 148-158.

Thite A.N. & Thompson D.J., 2003a, The Quantification of Structure-borne Transmission Paths by Inverse Methods. Part 1: Improved Singular Value Rejection Methods, *Journal of Sound and Vibration*, Vol. 264, pp. 411-431.

Thite A.N. & Thompson D.J., 2003b, The Quantification of Structure-borne Transmission Paths by Inverse Methods. Part 2: Use of regularization Techniques, *Journal of Sound and Vibration*, Vol. 264, pp. 433-451.

Thite A.N. & Thompson D.J., 2006, Selection of Response Measurement Locations to Improve Inverse Force Determination, *Applied Acoustics* 67, pp. 797-818.

Turco E., 1998, Load Distribution Modelling for Pin-jointed Trusses by an Inverse Approach, *Computer Methods in Applied Mechanics and Engineering*, Vol. 165, pp. 291-306.



Turco E., 2005, A Strategy to Identify Exciting Forces Acting on Structures, *International Journal for Numerical Methods in Engineering*, Vol. 64, pp. 1483-1508.

Venemies J., 1999, Paperikoneen taipumakompensoidut telat ja teloihin liittyvä hydraulikka, *Kunnossapitolehti*, Vol. 6, pp. 36-43.

Wirgin A., 2004, The Inverse Crime, *Mathematical Physics*, [www.arxiv.org](http://www.arxiv.org), arXiv:math-ph/0401050v1, (Cited 10.10.2008).

Yamamoto T. & Ishida Y., 2001, *Linear and Nonlinear Rotordynamics*, John Wiley & Sons, Inc., New York, USA, 2001, 348 p.

Yu L. & Chan T.H.T., 2007, Recent Research on Identification of Moving Loads on Bridges, *Journal of Sound and Vibration*, Vol. 305, pp. 3-21.

Zhu X.Q. & Law S.S., 2002, Practical Aspects in Moving Load Identification, *Journal of Sound and Vibration*, Vol. 258(1), pp. 123-146.

Zienkiewicz O.C., Taylor R.L. & Zhu J.Z., 2005, *The Finite Element Method: Its Basis and Fundamentals*, 6<sup>th</sup> ed., Elsevier Butterworth-Heinemann, USA, 733 p.